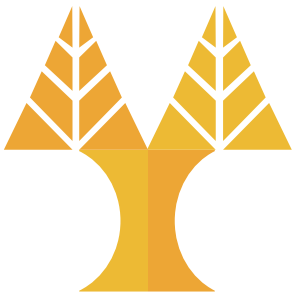

University of Cyprus

Department of Electrical and Computer Engineering

A Wearable, Multimodal, Vitals Acquisition Unit for Intelligent Field Triage

Christoph Beck

A dissertation submitted to the University of Cyprus in partial fulfillment of the requirements for the degree of Doctor of Philosophy

April 2016

Approval Page

Doctoral candidate: Christoph Beck

Dissertation title: A Wearable, Multimodal, Vitals Acquisition Unit for Intelligent Field Triage

The present doctoral dissertation was submitted in partial fulfillment of the requirements for the degree of Doctor of Philosophy at the Department of Electrical and Computer Engineering and was approved on April 22nd, 2016 by the members of the Examination Committee.

Committee Chair

Prof. Constantinos Pitris, University of Cyprus

Research Supervisor

Prof. Julius Georgiou, University of Cyprus

Committee Member

Prof. Constantinos Pitris, University of Cyprus

Committee Member

Prof. Chrysostomos Nicopoulos, University of Cyprus

Committee Member

Prof. Constantinos Pattichis, University of Cyprus

Committee Member

Dr. Pantelis Georgiou; Imperial College London

Declaration of Doctoral Candidate

The present doctoral dissertation was submitted in partial fulfillment of the requirements for the degree of Doctor of Philosophy of the University of Cyprus. It is a product of original work of my own, unless otherwise mentioned through references, notes, or any other statements.

……

……

Abstract

Natural or man-made disasters that result in large numbers of human casualties always pose difficult challenges. An analysis of the historical data since 1900 indicates that the probability of occurrence and degree of severity of mass casualty incidents (MCIs) have grown and shown a noticeable rise since 1985. Over the past four years, more than 400 thousand people have been killed and 676 million were affected by such incidents and the total damage is estimated to be more than USD 790 billion. The main challenge in these situations is to gain high quality information in order to develop a methodical approach for the assignment of the limited resources. In this context, this project focuses on the design and development of a body worn multimodal human vitals sign acquisition unit to continuously provide high quality medical information of each subject for intelligent field triage. This comprises ECG signals, blood oxygenation levels, body temperature and multichannel auscultation of heart and lung sounds. The proposed system also offers real-time analysis and transmission capabilities towards a wider network. It is the only known platform that transmits multichannel heart and lung sounds, in addition to standard emergency parameters to a wider network that is location-independent from the emergency site. Given that a comparable system does not yet exist, it might also serve as a research platform.

The wider network is simulated with a herein developed MATLAB® application. It is capable of receiving, analyzing and monitoring data, basic decision making and visualizing in real time. The application can be sourced with both on- and off-line data. Characterizing the acquisition unit in various experiments has shown promising results. Hardware modules, additional hardware functions, embedded software, MATLAB® application and data transfer performed as expected. The acquisition of human vital signs such as ECG signals, blood oxygenation levels, body temperature and up to eight-channel auscultation was successfully performed. The combination of ECG and heart sounds allowed the design of a low performance heart sound separation algorithm. A database containing the vital signs of ten healthy male subjects at rest and at an accelerated pulse rate of more than 100 beats per minute was created. The first generation of the wearable, multimodal, vitals acquisition unit for intelligent field triage has been completed.

Overview of the Chapters

Chapter 1 introduces the background and current state of the art and the need for a wearable, multimodal, vitals acquisition unit for intelligent field triage and provides background information on the related work in this area, triage, telemedicine and body sounds.

Chapter 2 introduces the proposed system's general architecture and develops the requirements and technology for the essential modules. It focuses on all of the acquisition paths and processing unit.

Chapter 3 describes the design, development and characterization of the wearable, multimodal, vitals acquisition unit for intelligent field triage with particular emphasis on experiments in the acquisition of human vital signs, automated alarming, sound source localization and the algorithm design to analyze heart sounds based on timing information from the ECG data.

Chapter 4 describes the contribution of this thesis to research and illustrates that the hardware platform, create as part of a single PhD Thesis, allows the acquisition of a new and unique data set by linking the various research areas.

Chapter 5 summarizes the work and the completion of the first generation of the wearable, multimodal, vitals acquisition unit for intelligent field triage. It further lists recommendations for future work to successfully develop the next generation of this project.

To my beloved family and children.

Acknowledgments

I am indebted to Professor Julius Georgiou for welcoming me in his lab team, sharing his knowledge and wisdom, and giving me the opportunity to pursue my research activities through a part-time position.

My deepest thanks also goes to the entire Holistic Electronic Lab team, namely Nicoletta Nicolaou, Charalambos Andreou, Guillaume Garreau, Panayiota Demosthenous, and Evripides Kyriakides. They always welcomed me wholeheartedly and provided their ongoing support and guidance in all aspects and with regard to the challenges that a PhD student abroad encounters. In addition, a special thanks is extended to Allison Watson for her endless help in proofreading.

I am also grateful to the Department of Electrical and Computer Engineering of the University of Cyprus for the opportunity to study in a gentle and supportive environment as well as for the possibility to attend the required seminars at the University of Freiburg, Germany.

I would like to express my deep gratitude to my parents Barbara and Clemens as well as to my sisters Nicola and Verena for their love and continuous support and encouragement. Without the strong support of my family this project would not have been possible.

Finally, I want to praise my beloved children Lorenz and Marlene for always accepting that their father has to work and in deep hope that this work will once inspire them to always be curious and strive for knowledge as those were my reasons for this project.

Content

1 Introduction 1

1.1 Related Work 6

1.2 Triage 13

1.3 Telemedicine 16

1.4 Body Sounds 16

2 System Design 19

2.1 General Architecture 21

2.2 ECG 22

2.3 Pulse Oximetry 24

2.4 Temperature Measurement 26

2.5 Blood Pressure 27

2.6 Auscultation 28

2.6.1 Heart Sounds 28

2.6.2 Lung Sounds 30

2.6.3 Signal Transduction 33

2.7 Acoustic Preconditions 34

2.7.1 Dimensions of the Body 35

2.7.2 Speed of Sound in the Body 36

2.7.3 Wavelength 37

2.8 Acquisition Path 38

2.8.1 Sampling Rate 38

2.8.2 Aliasing 39

2.8.3 Dynamic Range in the Analog Front End 39

2.8.4 Analog-to-Digital Conversion 40

2.8.5 Resolution 41

2.8.6 Data Rate and Storage 42

2.9 Processing Unit 44

2.10 System Feature Summary 48

3 Accident and Emergency Center Intelligent Acquisition Unit 49

3.1 Phase 1 – Definition 50

3.2 Phase 2 – Design and Implementation 51
3.2.1 Task 5 – Schematics and Component Selection 52
3.2.2 Task 6 – PCB Design 58
3.2.3 Task 7 – Manufacturing 59
3.2.4 Task 8 – Embedded Software Development 60
3.2.5 Task 9 – MATLAB® Processing and Analysis 73
3.3 Phase 3 – Characterization 78
3.3.1 Test – MCU Hardware 78
3.3.2 Test – Heart Sounds 92
3.3.3 Test – Lung Sounds 96
3.3.4 Test – ECG Acquisition 99
3.3.5 Test – Pulse Oximetry 103
3.4 Vital Signs Acquisition 106
3.5 Automated Alarm 110
3.6 Sound Source Localization 112
3.7 ECG Time-Based Heart Sound Analysis 119
4 Contributions 125
5 Conclusion 127
5.1 Future Work 128
6 References 131
7 Appendix A – Publications 137
8 Appendix B – Schematics 139

List of Figures

Figure 1: Main topics that immediately arise when an MCI occurs. 3

Figure 2: Each subject is monitored with a mobile unit (red hearts) that acquires human vital signs and transmits relevant data to a central node (computer below). 3

Figure 3: The START triage procedure in two phases. First to perform the 'Simple Triage' and then 'Rapid Treatment'. 15

Figure 4: Three-tier general architecture. 21

Figure 5: ECG board EMB3/6 by Corscience GmbH. 24

Figure 6: Pulse oximetry module by Corscience. GmbH 26

Figure 7: Time correlation of ECG and acoustic phenomena. [60] 29

Figure 8: a) 1, 4, 5 and 8 are the locations for auscultating the corresponding heart valves: aortic valve (2), tricuspid valve (3), pulmonary valve (6), and mitral valve (7). b) Anatomic projection of the valves: aortic valve (1), tricuspid valve (2), pulmonary valve (3) and mitral valve (4). *Erb's point. [60] 30

Figure 9: Sound source in the horizontal plane. [76] 31

Figure 10: Sound source in the vertical plane. [77] 31

Figure 11: Conventional and expanded lung sounds of normal and abnormal breathing. [78] 32

Figure 12: Acquisition of bronchial and vesicular lung sounds at the base of the lungs ..33

Figure 13: Cross-section of the thorax using a rectangle as a first approximation; the ratio of the square (w/h) is 10.0/7.5. [76] 35

Figure 14: Dynamic range of an analog system. [86] 39

Figure 15: Number of bits as stated in the data sheet versus sampling rate for different types of structures. [88] 41

Figure 16: System block diagram. 51

Figure 17: Block diagram of the mobile client unit. 52

Figure 18: Lithium ion charging behavior split into four stages: 1) constant current (CC), 2) constant voltage (CV), 3) self-discharge and 4) maintenance. [97] 54

Figure 19: Single cell lithium ion/lithium polymer battery charger and power path management device. 54

Figure 20: Power management unit (PMU) to supply the Xilinx Spartan-6 FPGA and peripherals. 55

Figure 21: Analog front end divided in three areas: 1) microphone (two assembly options), 2) differential amplifier and 3) differential tracks. 56

Figure 22: SN820X EZ Web Wizard Software Architecture Diagram. [100] 57

Figure 23: PCB (top view): 1) FPGA, 2) ADCs, 3) microSD card holder and 4) micro USB socket. 59

Figure 24: a) 3D representation before manufacturing; b) photo taken from real device. 59

Figure 25: (1) Baseboard with ECG and PulseOx module; (2) battery; (3) microSD card and card slot; (4) ECG leads; (5) PulseOx lead; (6) stethoscope leads 60

Figure 26: Block diagram of embedded software. 61

Figure 27: Block diagram for Xilinx ISE design flow. [104] 66

Figure 28: Flow chart for on-board data management. 68

Figure 29: Sensor-specific communication frame data rate defined as frames per second (FPS). 69

Figure 30: Data flow from top-level entity to server or MATLAB® application. 70

Figure 31: Finite state diagram of receive process of ChipOx module. 72

Figure 32: MATLAB® application with functional groups 1) *Recording*, 2) *Single Mic Analysis*, 3) *Multi Mic Analysis* and 4) *Log.* 74

Figure 33: Sensor overview figure: diagram (1) shows one of the three ECG channels, diagram (2) shows the plethysmogram along with an information box with pulse, blood oxygen and signal quality, and diagram (3) shows one of the eight preselected acoustic channels. 75

Figure 34: ASA overview figure showing sub-diagrams of the data streams of all the microphones along with basic statistical information for each channel. 76

Figure 35: Custom board to measure current and power consumption with a 0.142 Ohm resistor (1% tolerance) between lithium ion battery and PCB. 80

Figure 36: Custom board to measure current and power consumption with a 0.142 Ohm resistor (1% tolerance) between USB 2.0 port and PCB. 81

Figure 37: A) MCU and Opal Kelly board embedded in a robust housing; B) front side of the housing with self-explanatory labeling; C) left side with plugs for ECG and channels 5 to 7; D) right side with plugs for PulseOx and channels 1 to 3. 89

Figure 38: Schematic test setup to verify the MCU's acoustic performance. 91

Figure 39: MATLAB® plot of time difference between channel one and three in the sampling period steps recorded by the MCU. 91

Figure 40: Scope plot of time difference between channel one and three recorded in microseconds with a scope. 91

Figure 41: Block diagram of test setup for multichannel heart sound acquisition. 93

Figure 42: Stethoscope placement according to location definition. 94

Figure 43: Output of stethoscopes placed at described locations with the following microphone-to-channel mapping: Channel 1 -> Stethoscope B, Channel 2 -> Stethoscope C, Channel 3 -> Stethoscope D, Channel 5 -> Stethoscope A. 95

Figure 44: Block diagram of test setup for single channel lung sound acquisition. 97

Figure 45: Single-sided amplitude spectrum over a lung sound acquisition period of ten seconds: unfiltered (blue curve) and low-pass filtered (red curve). 98

Figure 46: Block diagram of test setup for MCU ECG verification. 99

Figure 47: 1) MCU test setup with electronic parts embedded in a robust, shock, dust and splash water resistant housing; 2) Corscience test setup with EMB3/6 development kit with USB 2.0® connection to PC, patient leads and self-adhesive pads. 100

Figure 48: Synchronous recording of ECG with both the Corscience development kit (blue) and MCU (red). 101

Figure 49: Synchronous recording of ECG with both Corscience development kit (blue) and MCU (red) after postprocessing with MATLAB® "detrend" function. 102

Figure 50: ECG tracing of a single cardiac cycle recorded with the Corscience EMB3/6 development kit (blue) and MCU (red).....103

Figure 51: Block diagram of test setup for MCU pulse oximeter verification. 104

Figure 52: 1) Electronic parts embedded in a robust, shock, dust and splash water resistant housing; 2) Corscience's ChipOx development kit with interface to PC, power supply and finger sensor. 105

Figure 53: Block diagram of test setup for human vital data acquisition. 107

Figure 54: Electronic parts embedded in a robust, shock, dust and splash water resistant housing. 107

Figure 55: Body locations for stethoscope heads A–D (chest) and E–F (back). 108

Figure 56: Alarm indication if heart rate deviates from defined margin of 50 to 210 BPM. 111

Figure 57: Simultaneous auscultation of the heart with channel one (top) to three (bottom). Clipping was experienced at channel two (middle) which is indicated in red. 112

Figure 58: Original spiking neuron model developed for the sand scorpion by Stürzl et al. [129] The eight command neurons are shown in black. For two of them, k = 3 and k = 7 = **3**, which corresponds to R3 and L2 respectively. The inhibitory partner neurons are shown in grey. The triad of R3 consists of L1, L2 and L3. 115

Figure 59: schematic setup with video and time surveillance and the speaker placed in the same horizontal plane as the microphones rotating counterclockwise. 116

Figure 60: sine wave recordings illustrated in diagrams, amplitude over time, where 1 shows the switch on behavior, 2 a recording with equal microphones to speaker distance and 3 a recording with varying microphones to speaker distance.....117

Figure 61: Plots of the speaker bearing angle (red), the estimated bearing angle (blue) and the estimation error (cyan). The average error reported was 6.34° ± 4.36°.....118

Figure 62: Plots of the speaker bearing angle (red), the estimated bearing angle (blue) and the estimation error (cyan). The average error reported was 4.05° ± 3.01°.....119

Figure 63: 1) Combined, synchronous and normalized ECG and auscultation over time; 2) A single heart cycle with prominent R-wave, S1 and S2.....123

Figure 64: Calculation of a mean S1 over the S1 vector with 30 entries for subject CPE at rest. 124

List of Tables

Table 1: Summarized data on complex, natural and technical disasters in the period from 2010 to 2014. [8] The large number of deaths in 2010 is attributable to the earthquake with epicenter near Port-au-Prince, Haiti. [9] The extensive damage in 2011 is attributable to the earthquake with epicenter near the east coast of Honshu, Japan. [10] 2

Table 2: Survey and comparison of wearable systems for human vital sign acquisition. .11

Table 3: Required technical specifications for the ECG module. 23

Table 4: Required technical specifications of a pulse oximeter module. 25

Table 5: Heart sounds and their frequency ranges. 30

Table 6: List of the major categories of respiratory sounds as postulated by Pasterkamp et al. [80] 32

Table 7: Overview of rapid technological development based on a comparison of Spartan-1 and Spartan-6 series product features. 46

Table 8: System Feature Summary 48

Table 9: Project definition and task description. 49

Table 10: Phase 1 – Definition. 50

Table 11: Phase 2 – design and implementation. 51

Table 12: The 7-layer OSI model. [106] 67

Table 13: Phase 3 of design and implementation 78

Table 14: Test objectives and results related to power supply and consumption 81

Table 15: Test protocol for verification of programming and configuration commands..82

Table 16: Test results for the Corscience and herein developed pulse oximetry systems. 106

Table 17: Monitored parameters that trigger an alarm if values deviate from the defined margin. 110

1 Introduction

Natural or man-made disasters that result in large numbers of human casualties have always posed a serious and difficult challenge. Overwhelming conditions, very limited medical resources and difficult ethical implications make them virtually impossible to handle.

A historical analysis of the data since 1900 indicates that the probability of occurrence and degree of severity of mass causality incidents (MCIs) have grown and shown a noticeable rise since 1985. [1] This widely known trend has attracted considerable attention from the European Union (EU), which maintains various active research programs with a budget of nearly EUR 100 million. [2] This shows that today's Western society is aware of the threats and challenges supporting the actuality and significance of the research field. As a result of experience and research, far-reaching emergency management systems have also been established and maintained [3] in addition to primary health care systems. [4]

If this trend continues, these emergency management systems will have to be expanded even further. *"Especially climate related disasters affected 217 million people each year since 1990."* [5] Furthermore, *"in the year 2011, natural disasters once again had a devastating impact on human society. Worldwide, 332 reported natural disasters caused the death of more than 30 770 people, made 244.7 million victims and caused a record amount of USD 366.1 billion of damages. A total of 101 countries were hit by these disasters."* [6] Also with respect to civil conflicts, *"about 300 million people now live amidst violent insecurity around the world."* [7]

The summary of the data on complex, natural and technical disasters worldwide over the past four years shown in Table 1 gives an even more devastating picture. More than 400 thousand people have been killed and 676 million affected by such incidents and the total damage is estimated to be more than USD 790 billion.

Table 1: Summarized data on complex, natural and technical disasters in the period from 2010 to 2014. [8] The large number of deaths in 2010 is attributable to the earthquake with epicenter near Port-au-Prince, Haiti. [9] The extensive damage in 2011 is attributable to the earthquake with epicenter near the east coast of Honshu, Japan. [10]

Year	Total disas-ters	Deaths	Affected	Injured	Homeless	Total Affected	Total Damage [mUSD]
2010	670	315,343	254,823,572	746,425	2,435,528	258,005,525	151,435
2011	604	40,722	210,726,795	56,127	2,004,452	212,787,374	363,991
2012	562	17,599	108,133,756	74,010	855,040	109,062,806	156,511
2013	544	29,505	96,090,914	129,002	339,954	96,559,870	118,416
Total	2,380	403,169	669,775,037	1,005,564	5,634,974	676,415,575	790,355
Mean	595	100,792	167,443,759	251,391	1,408,744	169,103,894	197,588

Since most natural disasters occur spontaneously, most people are often unprepared when they strike. When professional first responders arrive at a crisis scene, the initial activity is to perform triage, which is a stratification procedure for allocating limited medical resources in an emergency setting. The overall goal is to achieve the best solution for all involved, which implies that individual needs have lesser priority. [11] One of the most critical and most difficult steps is the initial categorization of the wounded. This decision has a direct and potentially severe impact on the victim's health or even life. [12] Prof. Dr. med. Domres, a professor at the University of Tübingen who has served as a medical professional in various combat zones, experienced the oppressive situation that can occur in any MCI in Cambodia when he had to take care of more than 100 wounded people with just one other colleague. [13]

Various triage methods for MCIs have been used for hundreds of years. One of the most well-known codes of conduct in this context, *Women and children first*, was mentioned as early as 1840 by the author S. A. Howland in his collection of steamboat disasters and railroad accidents. [14] However, the changing nature of MCIs and the progress in civilization and technology has always required and allowed for continuous improvement.

Today, obtaining fast, reliable and accurate information is a key element. Satellite pictures are the first step in helping to estimate the dimension and severity of the

situation on the ground. Area and street maps are also needed to identify routes to plan and manage the rescues. In essence, virtually any information is useful. As shown in Figure 1 the three main topics are listed that immediately arise when an MCI occurs.

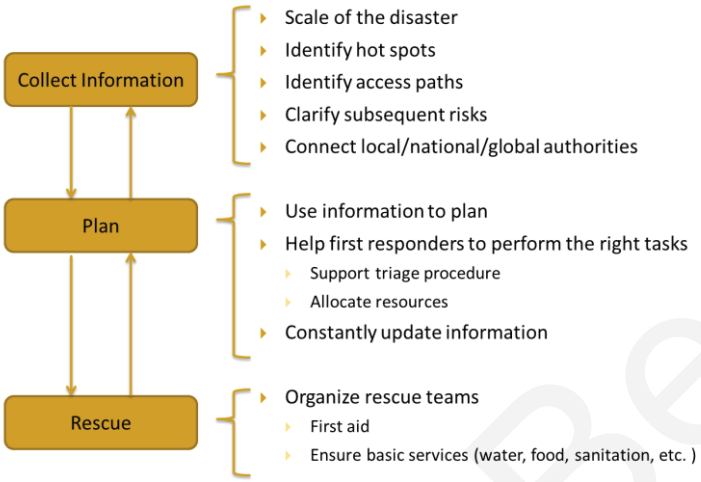

Figure 1: Main topics that immediately arise when an MCI occurs.

Another interesting recent worldwide trend is that of bringing healthcare services as close as possible to the patient through new technologies in telemedicine. [15] This can be applied in many scenarios, such as computer-aided assistance to the doctor and patient or to the first responder in an emergency setting. Real-time data on the location and condition of the physically injured would thus provide valuable information and greatly improve medical resource management.

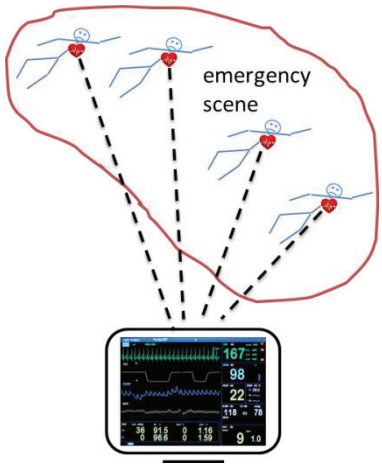

Figure 2: Each subject is monitored with a mobile unit (red hearts) that acquires human vital signs and transmits relevant data to a central node (computer below).

In order to ensure a holistic approach to dealing with mass casualty events, research in areas related to effective medical care in rural areas, [16] organizational issues with respect to rising costs, [17] and innovative new approaches in technology to improve or even solve key issues such as the automated analysis of vital signs, decision making or automatic heart sound analysis for telecardiac auscultation will also be taken into consideration in this project. [18]

The main objective of this project is to help first responders gain real-time information of multiple casualties and thus develop a more methodical approach to resource assignment. It emphasizes the design and development of a prototype system for the continuous acquisition of human vital signs, analysis in an emergency setting and transmission to a wider network which of a schematic representation can be found in Figure 2. The aim of this multidisciplinary project is to link a wide variety of research areas in order to provide a solid basis for further research, design and development.

The proposed thesis concerns the development of a body-worn human vital signs monitor prototype that acquires basic parameters in an emergency setting, such as: (1) electrical heart activity and pulse measured by an ECG; (2) blood oxygenation, perfusion and pulse measured by a pulse oximeter; (3) heart and lung sounds measured by multiple independent stethoscopes; and (4) body temperature measured by a temperature sensor. The prototype will (1) acquire, extract and transmit human vital signs; (2) synchronize data from the ECG, pulse oximeter, stethoscopes and temperature sensor for interchannel time-correlated analysis; (3) follow the design rules for a small and lightweight body-worn product; and (4) have a generic implementation strategy that easily allows subsequent extensions.

The unique ability to record ECG, blood oxygenation, heart and lung sounds, and temperature in this way allows further research activities in the automated diagnosis of traumata that is not possible with standard monitors. These may include the following (simplified):

- **Acute mitral insufficiency:** normal ECG; systolic murmur and possibly apical thrill
- **Pneumothorax** (or punctured lung): normal ECG; diminished breath sounds on the affected side
- **Blocked airways:** normal ECG; no breath sounds
- **Breathlessness:** normal ECG; flat breathing at a high rate

In addition, the synchronous acquisition modality opens up new analytical approaches by taking advantage of the time correlation between different vital signs. For example, heart sound segmentation requires comprehensive, high performance algorithms that

are very sensitive to ambient noise. This may be bypassed by using a robust ECG heart cycle detection algorithm and mapping the resulting time vector to the acoustic stream.

The synchronized recording also allows the utilization of redundancy to increase the robustness of the acquisition. In adverse environments, artifacts mainly occur in one domain. While ambient noise has no effect on the ECG, movement can affect the ECG and auscultation in different ways.

The main scientific objectives of this work are to: (1) provide a research platform for human vital sign acquisition; (2) prove basic methodologies for the analysis of vital signs; (3) provide verified data sets for subsequent research activities on a public data base; and (3) publish the results in related journals or conferences.

The specific technological objectives of this project are to: (1) design and develop a body-worn unit for vital sign acquisition; (2) demonstrate the merits of a system with synchronous acquisition; (3) minimize the system design with regard to size and weight in a way that suits the requirements of its intended use; (4) design digital algorithms for basic analysis and (5) decision making related to deteriorating changes in a patient's condition; (6) design a PC-based stand-alone application to receive raw data as well as to extract, analyze and display medical information.

The importance of this project lies in the combination of existing technologies to create a research platform and novel human vital sign acquisition modality to provide a new way of analyzing scene-oriented monitoring and automated diagnosis. The addition of multichannel auscultation as another source for analysis is an unprecedented approach. [19] Multiple independent channels also provide the capability of advanced processing related to acoustic pattern recognition or beam shaping especially with modern digital algorithms.

The added value of this work can therefore be described as (1) a first step towards a situation- and user-optimized mobile, lightweight and robust human vital sign monitor for an emergency setting that has (2) a novel acquisition setup.

This work may provide a solid base for future industrial applications such as (1) scene-oriented emergency monitoring, (2) a stand-alone surveillance monitor or (3) an extended acquisition unit for research and educational purposes.

1.1 Related Work

A search of the relevant academic research databases revealed that while a vast amount of knowledge on standard emergency parameter monitoring and auscultation exists, these two areas are treated separately. There are only a few publications that focus on the combination of standard emergency parameters and auscultation, but none that deal with standard emergency parameters together with multichannel auscultation. [20] This situation is corroborated by the lack of availability of such commercial products (e.g., emergency monitoring systems with single- or multichannel auscultation). [20] Current human vital sign monitors either focus on diagnosis and care with devices that have defibrillation capabilities or on smaller, more lightweight mobile devices with embedded telemedical concepts. There is currently no identifiable indication that industrial development is moving towards adding single- or multichannel auscultation. [20]

The annual number of publications in the IEEE Xplore database related to heart sounds has experienced a steady increase since 2007 [19], which indicates a growing interest in the field of body sound acquisition [21, 22] and pre/postprocessing and analysis. [23–25] One noticeable trend in this regard is the increasing importance of what is referred to as '"signal-to-noise separation," "characterization," "pattern detection" or "sound separation," i.e., the detection and analysis of specific sound patterns such as S1–S4.

This trend can most likely be explained by the accelerated research in digital algorithms as well as the continuous increase in (mobile) computing power, both of which are necessary for investigating the high structural complexity of sound patterns obtained from auscultation. Although auscultation provides additional and valuable diagnostic information, much research still remains to be done. [22]

No works on the merits of a multimodal system utilizing the redundancy of vital parameter acquisition technologies were found. For example, in a triage situation noise

is expected to be prominent in the acoustic domain. Instead of evaluating powerful signal-to-noise separation algorithms in general, as presented by A. K. Khan et al. [24] or using and analyzing data from an acoustic sensor array as done by Anita McKee [26–28] and Xuesong Ye [29], this work combines the data from auscultation with embedded ECG. For example, the R-wave detection method, which is the current state of technology, is well-known and robust. The first heart sound, S1, follows the R-wave. By synchronizing both recordings, S1 can be separated by using the time vector from the ECG.

Situations that need continuous multi-patient monitoring, such as emergency scenes, need very specific additional system requirements. Ongoing research, such as the BRIDGE project with a considerable budget of EUR 18 million [30], focuses on the "big picture," i.e., methods and tools that support runtime intra- and inter-agency collaboration, access to a broad range of incident-relevant data, simple and effortless exploration of high-quality information and consideration of organizational workflows and communication processes. [31] Human vital sign acquisition and analysis is not the focus here.

This system acquires human vital signs in order to provide continuous information on the health status of a subject. Previous research results offer a wide variety of strategies, systems and methods for doing this, but have proven that there is no "one-fits-all" approach. The individual environmental conditions force a generic approach. Plenty individually organized stakeholders add complexity to the organizational concept. And finally, on the device side result in often colliding design parameters such as sensor count vs. usability or data rate in wireless communication vs. power consumption. This requires a careful trade-off with respect to the intended use.

In recent years, several holistic research projects have presented new modalities and approaches for how to incorporate new technologies (e.g., wireless data transmission, ultra-low-power body sensors, geolocation, advanced information management and even drones) in existing concepts to create an advantage.

The collaborative project BRIDGE started in 2011 has an estimated duration of 48 months with a budget of EUR 18 million and follows a holistic approach. The consortium

consists of 14 partners located in the EU. The main objective is to *"increase the safety of citizens by developing technical and organizational solutions that significantly improve crisis and emergency management in the EU Member States. A BRIDGE platform will provide technical support for multi-agency collaboration in large-scale emergency relief efforts. The key to this is to ensure interoperability, harmonization and cooperation among stakeholders on the technical and organizational level."* [32] For human vital sign acquisition, they use a bracelet that wirelessly connects to vital sensors. *"The Triage Bracelet is a colored, reflective bracelet that snaps easily around a victim's limbs or neck. The bracelet incorporates a ZigBee radio node, a GPS sensor, and other microelectronics that allow it to become part of the Bridge MESH, where it reports the data from its sensors. Vital value sensors connect automatically to this bracelet. A local memory chip records all the measured values, so as to have a backup against network problems. The bracelet and tablet software work together to guarantee that a triaged victim will appear in the incident database as soon as possible, and no later than with the current process. No explicit interaction is required to start the data gathering and transmission."* [33] BRIDGE calls the process of initial medical attendance of the casualties in an MCI "eTRIAGE", but no specific information on sensor count, acquisition technology or performance was found.

Another holistic project called e-Triage was started in 2009, lasted 36 months and was coordinated by the German Aerospace Center as part of a comprehensive civil security initiative established by the German Federal Government. "*The objective of e-Triage is to create a system for the electronic registration of victims converting the previously paper based handling of data into a consistent overall concept. The goal is to provide a communication and database system for everyone involved in the rescue, transport and placement of victims in hospitals and temporary lodgings. [...] Apart from technical aspects, the degree to which emergency forces will accept the e-Triage system will depend primarily on psychological factors. These factors will be investigated as an integral part of the research project and made comprehensible through accompanying psychological research."* [34] Dr. Anton Donner, head of the project, further stated that "*Data Gathering in e-Triage should be more comprehensive than paper-based triage and registration systems for organizing MCIs. Although they are still state-of-the-art because*

they are robust and their usage is intuitive, the main drawback is that information about affected persons remains among the persons themselves, making disaster management considerably more difficult." [34]

The Advanced Health and Disaster Aid Network (AID-N) led by Dr. David White from the Johns Hopkins Physical Laboratory lasted from 2005 to 2007 and involved seven contributors. The AID-N team followed a holistic approach and derived their triage procedure from START. First responders started by acquiring vital signs and providing a proprietary low-power body-worn health monitor with wireless connectivity to a server. This was followed by grouping the subjects according to their degree of injury, which included first aid treatment. The third step involved organizing delivery to the neighboring health care centers. The health monitor includes ECG, pulse oximeter and blood pressure sensors in addition to geolocation, video surveillance and resource allocation functions. [35]

Besides holistic projects with research activities that focus on the big picture, there are smaller research groups that concentrate on wearable biosensor systems for health monitoring, which would be somewhat suitable in infrastructure networks used within the context of triage.

The work published by Pantelopoulos et al. *"attempts to review the current research and development on wearable biosensor systems for health monitoring [...] in an approach to identify the technological shortcomings of the current state-of-the-art in wearable biosensor solutions."* [36] The survey emphasizes multiparameter physiological sensing system designs aiming to *"serve as reference for researchers and developers."*

Pantelopoulos et al. stated in his conclusion that the monitors analyzed have *"the potential to revolutionize healthcare by providing low-cost solutions for ubiquitous, all-day, unobtrusive personal health-monitoring and are expected to enable early detection and better treatment of various medical conditions as well as disease prevention and better understanding and self-management of chronic diseases."* [36] However, they also indicated that many challenges still need to be resolved in order for wearable systems to become suitable for daily use.

The work published by Sakanushi et al. introduced a single sensor body-worn health monitoring system as a one-to-one replacement for paper triage tags. The authors highlighted its enhanced usability and easy application which takes just a few seconds. The monitor features an off-the-shelf pulse oximeter that is wirelessly connected to a triage server. Sakanushi et al. conclude that "*their proposed electronic triage system can save more lives than the paper triage tag during an MCI.*" [37]

Vishwanath et al. introduced a single-channel pre-amplified Bluetooth PCG to monitor the pulmonary, cardiovascular and intestinal status of patients in a clinical environment. The work included basic characterization of the system and shows the analysis results based on a Morlet Wavelet transformation. [38] The algorithm in particular could be of help in this context.

Bravo-Zanoguera et al. presented a three-channel PCG with synchronized ECG for educational purposes. *"This tool presents a visualization interface that assists in teaching of the cardiac cycle [...]."* The system is capable of displaying PCGs and ECG concurrently to facilitate understanding of the cardiac cycle. [39] Although the system is for educational purposes, design patterns can be interesting for this project.

None of the projects mentioned involved research on auscultation in an emergency setting or in the context of triage. Although phonocardiography (PCG) and data processing algorithms in this context have experienced increasing interest in research, there were no systems identified that provide the same human vital sign acquisition setting presented in this work. Table 2 lists all of the systems investigated as well as the projects focusing on human vital parameter monitoring and the accompanying devices.

Table 2: Survey and comparison of wearable systems for human vital sign acquisition.

Project Title (Institution)	Hardware Description	ECG	Pulse oximetry	Single-channel auscultation	Multichannel auscultation	Other
AID-N (N01-LM-3-3516) [35]	PDA, µC-board, server	x	x			x
Electronic Triage System (Osaka Univ., Japan) [37]	Sensor board		x			
Blue-stethsystem [38]	Custom stethoscope			x		
Multi-Site Phonocardiogram (Autonomous University of Baja California, Mexicali, Mexico) [39]	PC, commercial sensors (laboratory environment, educational purpose)	x			x	
Live Net (MIT, USA) [36]	PDA, µC-board	x				x
Health Care Information Infrastructure (Cheng Kung University, Tainan, Taiwan) [40]	Custom board, commercial sensors, PC	x		x		x
AMON (EU IST FP5 program) [36]	Wrist-worn device	x				x
LifeGuard (Stanford Univ., USA & NASA) [36]	Custom µC-based device & commercial biosensors	x				x
MyHeart (EU IST FP6 program) [36]	PDA, textile & electronic sensors on clothes & heart belt	x		x		x
WEALTHY (EU IST FP5 program) [36]	Textile & electronic sensors on jacket	x				x
MagIC (Univ. of Milan, Italy) [36]	Vest with textile sensors, custom electronic board, PDA	x				x
MERMOTH (EU IST FP6 program) [36]	Garment with knitted dry electrodes, PDA	x				x
Smart Vest (National Pr. on Smart Materials, India) [36]	Vest with woven sensors, µC	x	x			x
CodeBlue (Harvard Univ., USA) [36]	Sensor motes with custom processing boards	x				x
BAN (Valencia, Spain & Malta Univ. & Microvitae Tech) [36]	ZigBee-based motes & ZigBee-based custom base device	x				x
WSN u-Healthcare system (Dongseo Univ. Korea) [36]	Custom tiny motes, cell phone & commercial sensors	x				x
Human++ (IMTEC, Germany) [36]	Miniature low-power BAN nodes, energy scavenging	x				x
HealthGear, (Microsoft) [36]	Custom sensing board, commercial sensors and cell phone					x
HeartToGo (Univ. of Pittsburg, USA) [36]	Cell phone & commercially available Bluetooth biosensors	x				x
Personal Health Monitor (Univ. of Technology, Sydney, Australia) [36]	Cell phone & commercially available Bluetooth biosensors	x				x
Wearable ECG, arrhythmia detection (Eng. + Med. Depts., Norway) [36]	Microcontroller board, PDA	x				
AUDABE (Dept. of Med. Physics, Ioannina, Greece) [36]	Mask, glove, chest sensors	x				x
Lifeshirt (Vivometrics) [36]	Sensors embedded in vest, PDA	x				x
Bioharness (Zephyr Inc) [36]	Chest Belt	x				x
This System: MCU (Univ. of Cyprus, Cyprus)	Custom FPGA board, custom PCG, commercial sensors, PC, server, database	x	x		x	x

A key feature of this project is multichannel auscultation. Heart sounds usually have low amplitude and experience adverse signal-to-noise ratios (SNR), hence sophisticated strategies and powerful algorithms are necessary to extract the desired acoustic phenomena. The following paragraphs present some interesting approaches and recent work related to heart and lung sounds.

A survey on heart sound segmentation techniques was published by Bahekar et al. in 2014. Bahekar analyzed five approaches and concluded that *"phonocardiogram (PCG) segmentation using discrete wavelet transform (DWT) in conjunction with Shannon entropy provides a useful tool for phonocardiogram segmentation."* [41] Algorithms by Quiceno et al. [42] and Gupta et al. [43] achieved correct R-wave detection of over 90%.

Liang et al. describe the development of a segmentation algorithm of PCG signals based on the normalized average Shannon energy. The performance of the algorithm has been evaluated using 515 recordings from 37 patients, including normal and abnormal sound sources. The algorithm has achieved a correct ratio of 93%. [44]

Debbal and Bereksi-Reguig analyzed three different approaches to segregate the first (S1) and second (S2) cardiac sounds of a PCG signal and presented a comparison of the spectrogram, Wigner distribution and wavelet transform techniques. *"The continuous wavelet transform is found to be the most successful technique for the analysis based on the fact that the signals are characterized by transients and fast changes in frequency as time progresses."* [45]

Malarvili et al. was one of the first to present a different approach based on synchronous recordings of PCG and ECG. First, the algorithm detects the cardiac cycle by calculating the instantaneous energy of the ECG. Then the time vector is mirrored onto the PCG recordings to extract the first and second heart sound (S1 and S2). The algorithm was tested for 210 cardiac cycles based on normal and abnormal sources. Information on performance was not mentioned. [25]

Prof. Paul Erne from Kantonspital Luzern in Switzerland described the value of synchronous recordings in his review article *"Beyond auscultation – acoustic*

cardiography in the diagnosis and assessment of cardiac disease" as a new technology that offers a wide variety of both clinical and investigational applications. [46]

In reference to Prof. Erne's prediction, this work presents another investigational application called the mobile client unit (MCU), which introduces a body-worn human vital sign acquisition monitor that acts as a linking element for various research areas such as triage, digital algorithms and acoustic cardiography. This monitor will have the following unique features: (1) multichannel auscultation with up to eight channels; (2) highly synchronized ECG, pulse oximeter, multichannel auscultation and temperature sensor acquisition; (3) broad computational performance for onboard parallel processing; (4) high bandwidth and extended range interface for high-volume data transmission; (5) large onboard storage for offline processing; and (6) a three-tiered architecture that differs from the common approach described by [35] and [36], which forgoes ultra-low-power body area networks (BAN) and low data rate approaches in favor of high computational performance and fast data transmission.

1.2 Triage

In 1792, the French medical professional Dominique Jean Larrey developed the first classification models for amputation during the Napoleonic Wars and increased the survival rate of his patients. [47] The Russian surgeon Nikolai Iwanowitsch Pirogow first described the procedures for surgeries and classification of patients according to four categories based on the severity of injuries. [48] The medical professionals Spire and Lombardy further improved this method by defining triage as a procedure involving the following four steps: (1) diagnosis of the injuries; (2) priority of treatment (classification); (3) degree of transportability; and (4) specification of the destination. [49] With the founding of NATO, the categories were defined more precisely and continuously improved.

In modern healthcare systems, triage has expanded to include the following three phases: (1) prehospital triage in order to dispatch ambulance and prehospital care resources; (2) triage at the scene by first responders attending to casualties; and (3) triage on arrival at an emergency department or receiving hospital. [47]

For each of the phases mentioned, various specialized concepts exist today, which address the individual challenges of the nature of disasters, whether they be biological, chemical or natural. All triage algorithms describe categories or patient groups according to severity of injury, which serves as the basis for determining the priority of care, degree of medical treatment and transport.

For triage at the scene, which is the focus of this project, “Simple Triage and Rapid Treatment” (START) [12] or “Sort, Assess, Lifesaving Interventions, Treatment/Transport” (SALT) [50] are widely used concepts, especially in the USA. A graphical illustration is given in Figure 3 where the ‘Simple Triage’ is indicated with a pen and paper and the ‘Rapid Treatment’ is indicated with a medical first aid suitcatse. START and SALT are performed by first responders, who may have just rudimentary medical professional skills and therefore focus on fast and easy-to-use methods. Their initial task is to sort or categorize all the casualties. This decision-making process is dependent on the concept used but should usually not require more than 60 seconds per case. [51] This generates immense psychological pressure, as stated by Dr. Bubser during an interview: “*In many cases it is hard to decide which category a patient corresponds to, but as triage is a continuous process a correction can be made any time.”* [13] Of course retriage is also necessary in order to detect changes in vital conditions, which also ties up medical resources. A monitoring system that continuously acquires human vital signs would take both the immense psychological pressure off the first responder in order to arrive at the “correct” decision and allow specific retriage without necessarily having to attend to the casualty again.

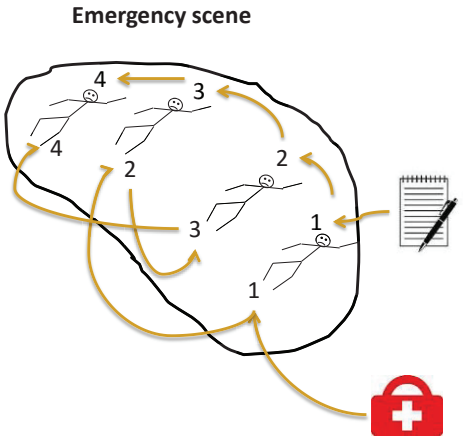

Figure 3: The START triage procedure in two phases. First to perform the 'Simple Triage' and then 'Rapid Treatment'.

Advanced triage is performed by medical professionals in sick bays, wards or hospitals, and is based on more sophisticated and complex decision models such as the Manchester Triage System [52].

This application may be the first step towards a solid system for continuous evaluation of the human vital signs of multiple casualties in real time and provide new modalities on how to approach MCIs.

Besides the organizational aspect, the results of individual actions also have to be considered for a holistic approach. This is accompanied by ethical implications with respect to the decision of who to help first. By treating a heavily wounded victim with little chance of survival, resources are tied up, thereby depriving others who may have a greater chance of survival with immediate care and little chance of survival if left untreated. This decision is sometimes solved by cultural rules, e.g., according to the maritime principle of "*women and children first"* and "*the captain leaves last*," but has to be addressed in a more systematic and individual manner during MCIs. In addition to these moral codes, holistic concepts also serve to guide and justify the actions of individuals. Furthermore, they help to protect mental health by freeing individuals of the burden of having to question their actions.

1.3 Telemedicine

Advances in telecommunication technologies have created new opportunities to provide telemedical diagnosis and care as an adjunct to classical medical management. Although the discipline of “telemedicine” is only ten years old, it already offers a huge variety of products and services around the world. [53] Driven by the motivation to improve the patient’s quality of life, [54,55] advance organizational aspects and reduce costs, [56] new products and services are continuously being introduced. One recent trend is to bring healthcare services as close as possible to the patient.

In a triage situation, telemedical systems allow new approaches such as embedding new technologies or methodologies in existing systems or concepts. Since triage is also an organizational challenge, telemedical systems can be of great help in retrieving, analyzing and providing the necessary information to related parties, so that the allocation of resources is optimized.

In this application, human vital signs are acquired at the patient’s body. Telemedical concepts now allow transmission to a host in real time which, in turn, provides acquired information to systems that are next in line.

A conceivable real-world scenario can be described as follows: First responders at the MCI follow the triage procedure and equip all casualties of certain categories with a mobile monitor. The monitors acquire and transmit human vital signs to a host, which receives, stores, and analyzes the incoming data to extract medical information. In turn, the host provides selected information to other parties. If, for example, a person’s physical condition deteriorates to the point where immediate attention or retriage is necessary, automated alarms are triggered.

1.4 Body Sounds

Today, auscultation is still one of the most popular means of examination. [21] The examiner uses a stethoscope to listen to body sounds, which provide important information for the evaluation of vital signs. This is especially useful in an emergency setting, where there is a lack of medical resources. While ECGs allow diagnosis and provide a reliable measurement of a wide range of heart conditions in addition to being mobile and robust, heart sounds in particular are still a valuable source of information

for determining cardiac insufficiency. [57] Ultrasonic devices, which are capable of diagnosing heart abnormalities, still have a large format, have difficult handling properties and limited mobility.

Unobtrusive respiration, another important check when attending to a patient in an emergency setting, is confirmed most quickly by visual inspection and listening to the breath sounds. This is most effective when accompanied by auscultation of the lungs. A common examination with a stethoscope takes 30 to 300 seconds depending on indication and the examiner. [58] Automated monitoring of respiration usually is done indirectly either by using the blood oxygen saturation as a surrogate marker or, at most, by monitoring the breathing rate and end tidal CO_2 as well. However, a host of emergency situations, such as pneumothorax or blocked airways, cannot be identified using blood oxygenation or CO_2 alone.

Although auscultation offers greater capabilities, is fast and requires minimum equipment, it greatly depends on the skill, experience, ambient noise and hearing ability of the examiner. [59] In addition, the interest of many physicians is focused on the increasing use of device-based treatment. [60]

Since digital stethoscopes have become available, some improvements have found their way into industrial products; however, research is still being done on relatively fundamental issues. This can be explained by the fact that acoustic data is intrinsically very complex and analysis needs highly sophisticated and exhaustive algorithms for rather basic tasks from an application point of view (e.g., noise cancelling, sound separation and segmentation). In general, there is very little related research activity, which is evident from the limited search results of just 78 publications for the term *"heart sound segmentation"* and 53 for the term *"heart sound separation"* in the IEEE Xplore database. [61]

Nevertheless, for automated and unattended monitoring at an emergency setting with a mobile and lightweight monitor, adding auscultatory capabilities is a significant set forward. Once the acquired data is transmitted to a powerful host, extensive real-time analysis can extract information and add a valuable source to automated vital sign monitoring and perhaps even diagnosing.

2 System Design

An accident and emergency center intelligent acquisition unit that provides the ability to monitor human vital parameters in a triage situation is of great benefit to first responders. The following chapter discusses the architecture, design parameters, implementation strategies and subsystems of such a unit.

Field triage in an emergency setting is performed in two phases as mentioned in chapter 1.2, which are: Simple Triage or Sort and Assess and Rapid Treatment or Lifesaving Intervention and Transport. Main drawback of the mentioned procedures is that with the triage or retriage only a snapshot of the physical conditions is available. To improve this situation a continuous collection of vital signs with a wearable monitor is proposed. This gives the first responders great advantages, such as the remote status in real-time, history, changes and trends. To accomplish this, the Field triage procedure will be slightly adapted. The trigger point is the contact between first responders and subject:

1. New: determine name, gender, age and location
   If the subject is responsive. Otherwise skip name and determine age group.
2. New: take a picture
3. From START: initial medical assessment
4. From START: categorization according to outcome
5. New: application with body-worn monitor for continuous assessment
6. New: pair monitor with subject file record

As a result the first responders will have the medical information of the initial and continuous assessment what gives a continuously updated picture of the subject's physical condition.

To determine the required human vital signs to draw a comprehensive picture of a subject's physical condition many emergency case protocols have been evaluated. Two examples are:

1. ABC (airway breathing circulation)
   A very general and simple emergency case protocol for lay and semi-professional

persons. ABC basically asks three questions: can the subject breathe? Does the subject breathe? And has the subject a pulse rate.

2. DIVI – hospital emergency case protocol
    - Neurologic condition according to Glasgow Coma Scale
    - Cardiovascular system (Blood oxygen, Blood pressure, ECG)
    - Respiratory system
    - Body temperature and pain
    - Psychological condition

Both protocols show great differences that result from different application areas. Whereas the ABC procedure is a very easy and simple first assessment, the DIVI protocol is a more sophisticated protocol for use in hospitals.

To evaluate the physical condition in an emergency setting based on automated analysis the following acquisition modalities are necessary:

1. ECG to determine the cardiac cycle
2. Pulse oximetry to determine the blood oxygen
3. Temperature to determine the body temperature and evaluate thermoregulation
4. Blood pressure (optional)

In addition to the abovementioned classic acquisition modalities this project intends to add auscultation for automated diagnoses of e.g. pneumothorax, punctured lungs or heart valve rupture due to a blunt impact, what is not possible when solely using the abovementioned acquisition modalities. With a stethoscope, those diagnoses can be determined. Beside the intended evaluation of the mentioned injuries is auscultation a comprehensive generic discipline of assessing a huge variety of malfunctions, injuries and diseases. This might become a great advantage to this project but in any case is a great added value to the generic approach.

An important objective is to keep the time correlation between all acquisition paths. This opens up new opportunities in the analysis of the medical information. Analysis of acoustic signals is very complex and the power consumption is high when compared to

ECG analysis algorithms. Keeping the correlation allows transferring the ECG time vector to the acoustic signal for heart sound segmentation, to mention just one example.

2.1 General Architecture

In order to put this work in a wider context, this chapter describes the general architecture in which this project is embedded.

The accident and emergency center intelligent monitoring system is organized according to a three-tier architecture as depicted in Figure 4. Layer 1 is located at the emergency site and involves as many body-worn MCUs as necessary to acquire and transmit the vital signs of all patients. Layer 2 is located close to the emergency site and involves mobile nodes that collect, analyze and display the selected information to provide a bigger picture of the scenario. Layer 3 is located in hospitals or sick bays and involves standard computers with internet access. Medical personnel receive real-time information of selected patients in preparation for their treatment.

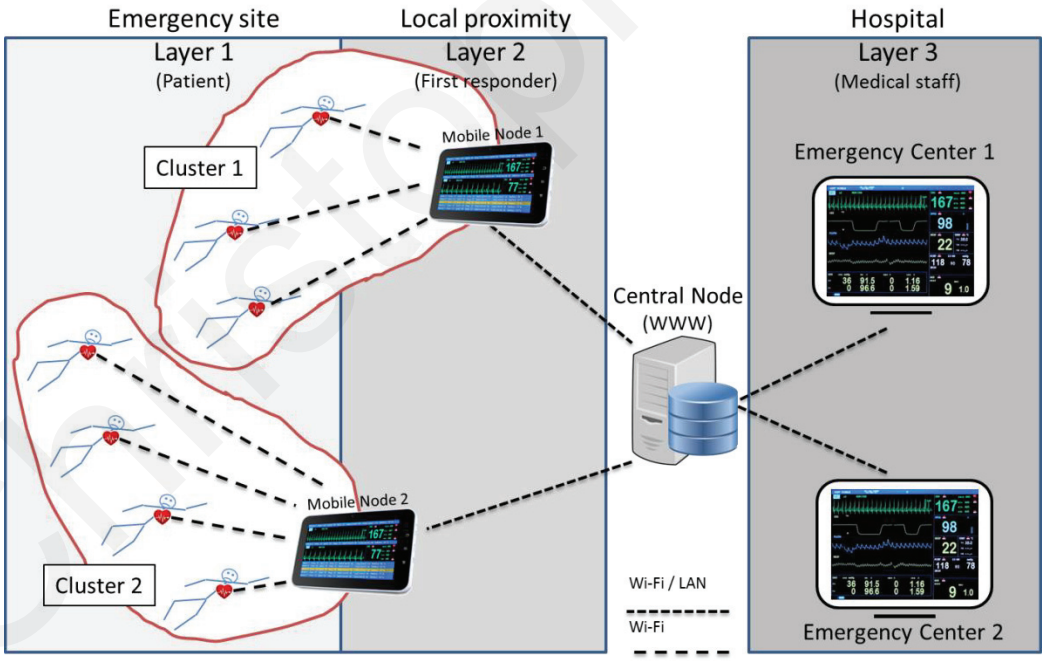

Figure 4: Three-tier general architecture.

All MCUs acquire the patients' physiological conditions, and then preprocess and transmit the vital information to dedicated mobile nodes via standard wireless interface technology. The mobile nodes establish clusters by connecting nearby MCUs. Today's

wireless technologies such as Wi-Fi (802.11) even allow for overlapping operations with respect to their reception area. Neither the patients nor mobile nodes are stationary, thus it is likely a use case. In a subsequent project phase, an additional feature will be implemented, in which the mobile nodes access a central node using standard interfacing technologies such as LAN, Wi-Fi or mobile phone networks to collect the vital signs of all the patients. The central node hosts a database server in order to store the incoming data and provides web services to emergency centers.

This project focuses on the design and development of the MCU and corresponding MATLAB® research application representing a mobile node. The MCU is intended to be a body-worn application, therefore some basic safety features were implemented in order to protect subjects from being harmed in the event of failure.

The MCU (1) is battery driven to ensure safety against electrical shock from the main power source and improve handling properties; (2) has basic overcurrent and overvoltage circuits to protect the patient and circuit; (3) is equipped with an external battery charger which is certified for the safe charging of medical applications while worn by the subject; (4) monitors system and (5) subsystem status.

Besides the aspects mentioned above, the following chapters discuss the subsystems for vital sign acquisition technologies.

2.2 ECG

The heart's electrical system controls all the events that occur during a heart cycle and includes the sinoatrial (SA) node, atrioventricular (AV) node and His-Purkinje system. In a healthy organ, every contraction is initiated by an electrical activation at the SA node. As it travels, the signal causes the heart to contract and pump blood. This is divided into the diastole and systole cycles and includes the opening and closing of the inlet and outlet valves of the right and left ventricles. This repetitive cycle adapts to the body's situation, so it accelerates the heart rate with increased activities and slows it down at rest. [62] The electrical characteristics correlate with the physical condition of the heart, thus significant medical information is identifiable by observing the electrical activity. [63]

In today's emergency medicine, the electrocardiogram (ECG) belongs to the basic diagnostic technologies available in commercial monitors. It is a fast, non-invasive, easily applied and reliable means of extracting vital information. In addition, there are strong algorithms to improve signal quality such as filters to eliminate artifacts caused by movement, electrical interfaces, muscle tremors, or electrode contact changes to mention just a few examples. Continuous 12-channel ECG monitoring is the standard examination and is available as an add-in in most stationary monitors, but has not spread in daily use except in very specific cases. [64] In conclusion, a 3/6-channel ECG with the specifications shown in Table 3 is deemed to be sufficient for the purpose of this project.

Table 3: Required technical specifications for the ECG module.

Technical specifications	
Number of channels, single ended	3 or 6
Input	AC coupled
Input dynamic range	DC: ±300 mV DC AC: 10 mV p-p AC
ECG signal slew rate	320 mV/s maximum
Input impedance	>2.5 MΩ at 100 Hz
Frequency response	DC – 40 Hz (0.0 ± 0.25 dB) and 40 – 150 Hz (0.0 ± 1 dB)
Line filter (60 Hz)	present
Channel-to-channel signal noise	30 µV p-v maximum
Multichannel crosstalk	≤ 0.5% maximum
ECG signal gain	1–1000 ± 0.01 V/V measured at 10 Hz
Channel-to-channel gain difference	0.1% maximum at DC – 150 Hz
DC offset (any channel)	± 5 mV maximum

ECG technology is well-known and widely used. Many industrial products exist, therefore developing a device for this project would not be new or innovative. [65] An off-the-shelf original equipment manufacturer (OEM) module with the following features has been implemented:

- Three to six channels
- R-wave trigger

- CE approved
- Algorithms for artifact detection
- Device status and error information
- Low-power consumption
- Small form factor

The ECG daughterboard EMB3/6 by Corscience GmbH shown in Figure 5 provides a complete technological basis for continuous 3/6-channel ECG measurement. Compared to alternative OEM products it consumes the least power, has the smallest form factor by fulfilling all requirements such as the R-wave trigger. The board is especially designed for use in mobile devices and optimized with regard to size and power consumption. It supports four patient leads for the left arm, right arm, left leg and right leg. In addition, it provides heart rate calculation, pacemaker detection, R-wave trigger and offline electrode contact measurement. The integrated R-wave trigger is delivered via a hard- and software interface, which offers low-performance modalities for multi-parameter synchronization in real time. [66] The device's communication interface is based on a versatile universal asynchronous receiver/transmitter (UART) protocol and is especially suitable for onboard communication.

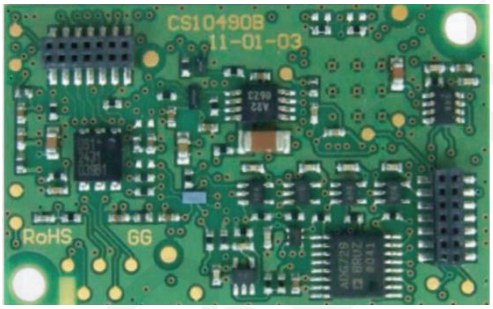

Figure 5: ECG board EMB3/6 by Corscience GmbH.

2.3 Pulse Oximetry

Pulse oximetry was introduced in 1983 as a non-invasive method of monitoring the arterial oxygen saturation of a patient's blood. Today, it is widely used in intensive care, operating rooms, emergencies and monitoring to name just a few areas of application. The advantages of pulse oximetry include non-invasiveness, ease of use, portability and patient comfort. [67] "*The pulse oximeter analyzes the light absorption at two wavelengths of only the pulse-added volume of oxygenated arterial blood.*" [68] It measures the ratio of transmitted red and infrared light intensities with wavelengths of approximately 660 nm and 905 nm, and compares this to a look-up table of empirical oxygen saturation values. In general, most of today's implementations are based on the

use of absorption spectrophotometry. [67] The probe of a pulse oximeter accordingly consists of two LEDs at the respective wavelengths and a detector. A transmittance probe has two LEDs on one side and a detector on the other. A reflectance probe on the other hand has the LEDs and detector on the same side. Finger and earlobe clips as well as sticky pads are widely used. This sensor should have the specifications shown in Table 4.

Table 4: Required technical specifications of a pulse oximeter module.

Technical specifications	
Oxygen Saturation (SpO2)	Range: 0–100 SpO2% Resolution: 1 SpO2%
SpO2 accuracy	±0.5 SpO2%, 70–100 SpO2% ±1 SpO2%, 50–69 SpO2%
Pulse Rate Range	20–300 BPM
Pulse Rate Resolution	1 BPM
Pulse Rate Accuracy	±1 BPM, 20–199 BPM ±2 BPM, 200–300 BPM
Patient Lead Components	Red LED IR LED Photo diode circuits
Measurement Wavelengths and Output Power	Red: 660 nanometers @ 0.8 mw maximum average Infrared: 910 nanometers @ 1.2 mw maximum average

Today, pulse oximetry technology is well-known and widely used. Many industrial products exist, therefore developing a device for this project would not be new or innovative. An off-the-shelf OEM module with the following features has been used:

- Continuous measurement of heart rate, SpO_2, plethysmogram
- Continuous measurement of signal quality
- CE approved
- Device status and error information
- Low-power consumption
- Small form factor
- Multiple sensor types

ChipOx shown in Figure 6 is a low-power small size OEM module provided by Corscience GmbH. Compared to alternative products it consumes the least power and has the smallest form factor by corresponding to all requirements and offering a complete solution. The module is described as a "*[…] pulse oximeter module for the non-invasive determination of the functional oxygen saturation in human arterial blood (SpO_2) and for measuring the pulse frequency.*" [69] According to the manufacturer, it is particularly suitable for battery-operated devices, mobile applications and multi-parameter monitors. It also provides remarkable features for research purposes such as raw plethysmogram, signal and error reporting and offers a wide range of sensor types, including finger clip, ear clip, arm wrap and a self-adhesive pad sensor. [69] The device's communication interface is based on a versatile UART protocol and is especially suitable for onboard communication.

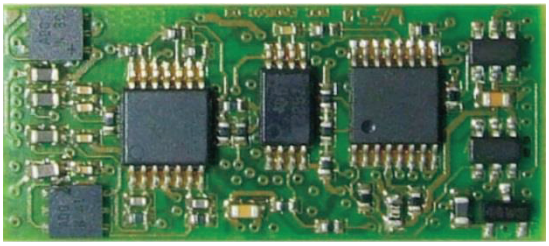

Figure 6: Pulse oximetry module by Corscience. GmbH

2.4 Temperature Measurement

Human body temperature control – thermoregulation – is part of a homeostatic mechanism that keeps the organism at optimum operating temperature. The 37 °C benchmark was established by Dr. Carl Wunderlich, a 19th century German physician who collected and analyzed over a million armpit temperatures of 25,000 patients. [70] There are many reasons for changes in human body temperature and slight variations throughout the day or during increased activity are considered to be normal. Values that deviate from the standard range or quick changes such as sudden drops indicate an abnormal condition or even grave danger. Checking body temperature is part of the first responder protocol and it is important to monitor it continuously. Many different technologies, such as thermocouples, thermistors or radiation thermometry [68] as well as body locations are suitable for measuring temperature, each of which has specific advantages and drawbacks. [71] For this application, an easily accessible location is preferable (e.g., the armpit, forehead or throat above the carotid artery). A medical grade digital temperature sensor is embedded in a medium-sized self-adhesive pad. The

device's communication interface is based on a proprietary UART protocol suitable for cable bound communication.

2.5 Blood Pressure

Non-invasive blood pressure measurement is a simple and inexpensive method of providing information about the condition of the cardiovascular system. Blood pressure is part of many multi-parameter monitors and belongs to the medical standard of cardiovascular diagnostics. [72] In contrast to the conventional method of manual blood measurement with a pressure cuff and stethoscope, automatic measuring devices are increasing in popularity. These are usually based on the oscillometric measuring method using a wrist or upper arm cuff. The main challenge in embedding a blood pressure module in mobile devices as realized in this project is their large size and immense power consumption. The smallest module inspected measures 80 x 60 x 25 mm (length, width, height) and consumes up to 750 mA at 5 V. [72] These input requirements greatly exceed the current allowable capacity.

A compromise-ridden but straightforward approach would involve an arm cuff-based stand-alone off-the-shelf pressure monitor that comes with a wireless communication interface. While this could be integrated in the wireless network used in this project, the added value is estimated to be negligible due to the fact that this monitoring principle has a slow response rate and therefore does not justify the implementation effort. This project aims to provide beat-to-beat monitoring together with synchronized acquisition.

Another interesting approach that should be considered for next generation devices was recently published by PR Newswire, which announced that the U.S. Food and Drug Administration (FDA) has cleared Sotera Wireless's patented continuous non-invasive blood pressure (cNIBP) technology. Since this new modality measures beat-to-beat blood pressure without the use of a catheter or blood pressure cuff, it would be the ideal fit for this project. [73] The technology uses ECG, pulse oximeter and extracted timing parameters to evaluate arterial blood pressure.

2.6 Auscultation

Auscultation gives the practitioner valuable information about the functional integrity of the examined organ. Various physical examinations are commonly practiced in daily routine, however, electronical acquisition with automated analysis is still at an early research stage and by far not suitable for everyday use. Including auscultation in a multi-parameter monitor requires new techniques, such as acquisition, noise cancelling, segmentation, phenomena separation, and parameter extraction to mention just a few examples. This project focusses on heart and lung sounds with six external acquisition channels: four for each propagation path of the heart valves on the chest and two for each lung on the back. Two additional channels shall be added to record ambient noise and speech.

The following chapters explain the corresponding acoustic phenomena used to derive the basic implementation parameters.

2.6.1 Heart Sounds

According to Joseph Wartak, the cardiac cycle can be divided into individual heart sounds the same way that ECG recordings can be divided into individual electrical events. [59] The **first heart sound** S1 is associated with the movement of blood during ventricular systole. As the ventricles contract, blood shifts toward the atria, closing the atrioventricular valves with a consequential oscillation of blood. It originates from oscillations of blood between the descending root of the aorta and ventricle and from vibrations due to blood turbulence at the aortic and pulmonary valves. Splitting of the first heart sound is defined as an asynchronous closure of the tricuspid and mitral valves. This first heart sound is aligned with the R-to-S wave transition of the ECG.

The **second heart sound** is a low frequency vibration associated with the deceleration and reversal of flow in the aorta and pulmonary artery and with the closure of the semilunar valves (the valves situated between the ventricles and the aorta or the pulmonary trunk). This second heart sound is coincident with the completion of the T-wave of the ECG.

The **third heart sound** is attributed to the sudden termination of the rapid filling phase of the ventricles from the atria and the associated vibration of the ventricular muscle walls, which are relaxed. This low-amplitude, low-frequency vibration is audible in children and in some healthy adults.

The **fourth or atrial heart sound** occurs when the atria contracts and propels blood into the ventricles. This sound is not audible by the human ear with a standard mechanical stethoscope, but can be acquired by electronic devices with built-in amplification.

Figure 8 shows the time correlation of ECG and acoustic phenomena. The two prominent heart sounds S1 and S2 are aligned with the R-to-S wave transition and completion of the T-wave accordingly.

Figure 7: Time correlation of ECG and acoustic phenomena. [60]

Figure 8 shows the specific locations for auscultating each heart valve and the corresponding acoustic propagation of the sound waves in the thorax. As depicted in the figure in order to inspect all valves it requires four acquisition paths.

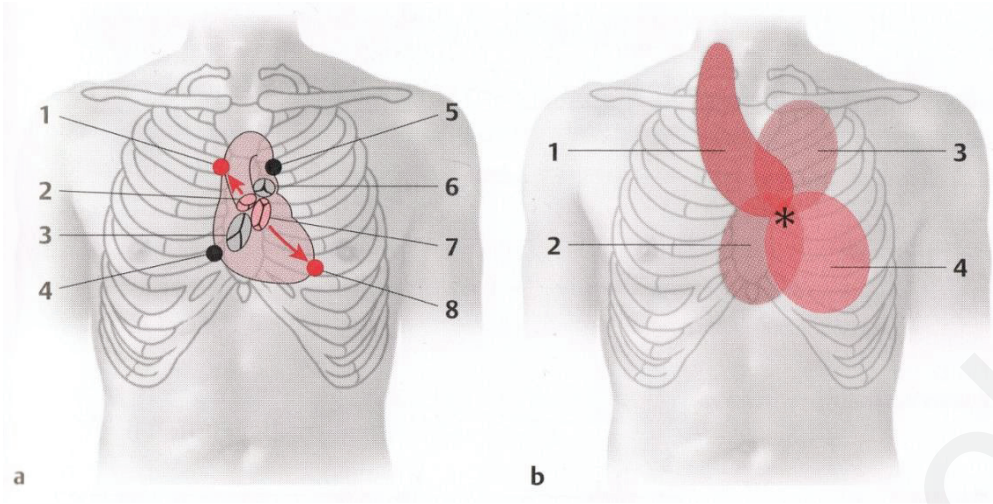

Figure 8: a) 1, 4, 5 and 8 are the locations for auscultating the corresponding heart valves: aortic valve (2), tricuspid valve (3), pulmonary valve (6), and mitral valve (7). b) Anatomic projection of the valves: aortic valve (1), tricuspid valve (2), pulmonary valve (3) and mitral valve (4). *Erb's point. [60]

A healthy heart sound is characterized by a clear acoustic phenomenon of short duration, whereas pathological heart sounds, such as murmurs, generally last longer. [60]

The relevant acoustic bandwidth for heart sounds is well-known and well-defined in the literature. Various papers and books exist that describe the acoustic phenomena and mention similar frequency ranges. Table 5 lists the frequency ranges of heart sounds and different heart valve disorders. [74]

Table 5: Heart sounds and their frequency ranges.

Acoustic Phenomenon	Frequency Range
S1 and S2	20–200 Hz
Aortic stenosis (AS) and mitral regurgitation (MR)	120–450 Hz
Aortic regurgitation (AR) and mitral regurgitation (MR)	150–700 Hz

2.6.2 Lung Sounds

Lung sounds include normal breath sounds and adventitious sounds, such as crepitations, wheezes, pleural rubs and stridor sounds. Breath sounds are produced in

the major airways, i.e., the trachea and major bronchi of which a schematic representation is given in Figure 9 and Figure 10. The bronchial breath sounds produced in the major airways propagate across the tissues to reach the body surface from where they are auscultated. While they are being transmitted through these tissues, higher frequencies are attenuated and the character of the sound changes. The velocity of air in the alveoli is not significant enough to produce turbulence or audible sounds. [75]

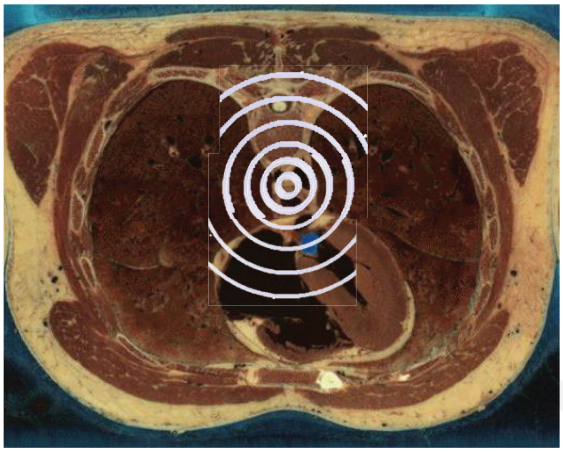

Figure 9: Sound source in the horizontal plane. [76]

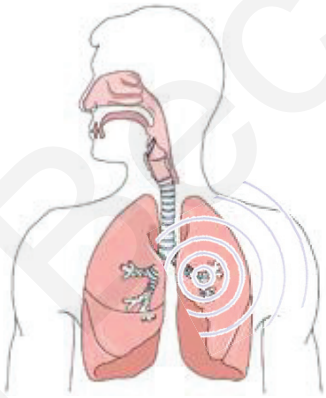

Figure 10: Sound source in the vertical plane. [77]

Bronchial or tracheal sounds are heard on the chest at sites that are close to the large airways. In contrast to vesicular sounds, they are relatively louder in expiration than inspiration. They have a tubular or blowing quality similar to air being blown through a tube. In the time amplitude plot, an apparently random undulating pattern is again seen. It has greater amplitude in expiration than inspiration. This type of breath sound is heard best over the trachea. Bronchial sounds are also heard on the back between the scapulae and at the lung apices especially on the right. They may also be heard in the axillae. When they are heard in locations at a distance from large airways they signify consolidation. This is believed to be due to better transmission of the centrally generated lung sound through the consolidated lung. This is more likely to occur during the expiratory phase because it has a more central origin than the inspiratory phase. [78] Some exemplary acoustic diagrams of conventional and expanded lung sounds of normal and abnormal breathing are shown in Figure 11.

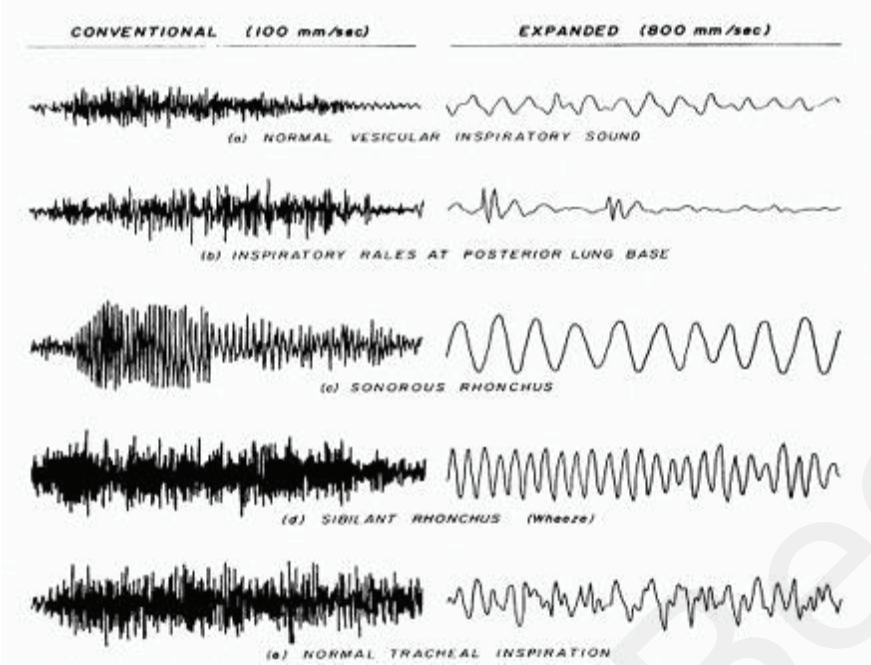

Figure 11: Conventional and expanded lung sounds of normal and abnormal breathing. [78]

The relevant acoustic bandwidth for lung sounds is well-known and well-defined in the literature. Various papers and books exist that describe the acoustic phenomena mention similar frequency ranges. Gavriely et al. carried out an objective, accurate measurement and characterization of breath sounds picked up over the chest wall of ten healthy subjects. [79] Table 6 lists the major categories of respiratory sounds as postulated by Pasterkamp et al. [80]

Table 6: List of the major categories of respiratory sounds as postulated by Pasterkamp et al. [80]

Respiratory sound	Mechanism	Acoustics
Normal lung sound	Turbulent flow vortices	Low-pass filtered noise range < 100 to > 1,000 Hz
Normal tracheal sound	Turbulent flow impinging on airway walls	Noise with resonances range < 100 to > 3,000 Hz
Wheeze	Airway wall flutter	Sinusoid range ~100 to > 1,000 Hz duration typically < 80 ms
Rhonchus	Rupture on fluid films	Series of rapid dampened sinusoids range typically < 300 Hz duration < 100 ms
Crackle	Airway wall stress-relaxation	Rapid dampened wave deflection duration typically < 20 ms

To identify the best location to acquire lung sounds, a questionnaire was prepared and given to medical specialists. Various different location patterns were reported, each of which related to the expected diagnosis. The two locations shown in Figure 12 were present in all reports and shall serve as acquisition location for the first experiments. [58]

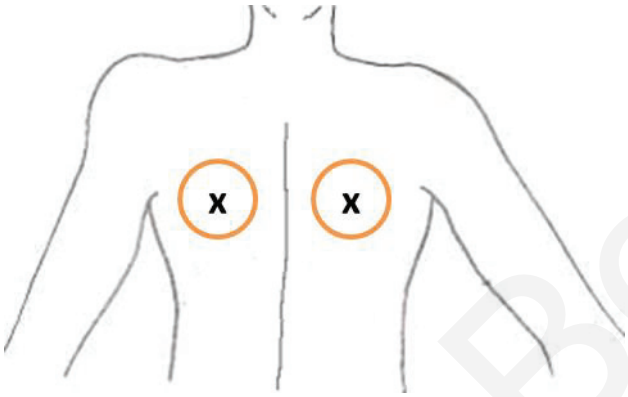

Figure 12: Acquisition of bronchial and vesicular lung sounds at the base of the lungs

Conclusively, in order to monitor both lungs it requires at least one acquisition path on each lung.

2.6.3 Signal Transduction

The Littmann 3200 electronic stethoscope defines three modes, which are equivalent to the frequency ranges described in Table 6. [81]

- Bell mode: 20–1000 Hz with emphasis on 20–200 Hz
- Diaphragm mode: 20–2000 Hz with emphasis on 100–500 Hz
- Extended range mode: 20–2000 Hz with emphasis on 50–500 Hz

Consequently, the frequency ranges from 20–2000 Hz. With respect to the novel approach of this project the widest possible frequency range with reasonable technical effort is defined:

- Minimum frequency: $f_{(min)}$ = 20 Hz
- Maximum frequency: $f_{(max)}$ = 5000 Hz
- Acoustic bandwidth: 4980 Hz

2.7 Acoustic Preconditions

The acoustic phenomena to be recorded with this system are not completely known yet, however, the basic acoustic phenomena have been identified in the previous chapters. There is a wide diversity of opinion concerning the theories that attempt to explain the origin of heart sounds and murmurs. For example, more than 40 different mechanisms have been proposed to explain the first heart sound. [60] Therefore, the system to be used for this project will have powerful recording potential. The parameters, such as sampling rate, accuracy and dynamic range, have been defined with a generous safety margin. At the recent project status the signal processing such as digital filtering will be carried out in software on the computer in order to ensure the greatest flexibility.

Many unforeseeable challenges can be expected to arise with respect to design, implementation and characterization because certain basic information is not yet known and cannot be determined through prior research without hardware. Following is a list of the issues that need to be addressed:

- Sound propagation in the body and reflections because the body consists of tissue and organs (bones, heart, lung, etc.) with highly diverse densities.
- The measured sound pressure level of different organs at different locations can be estimated in relation to each other and quantification with a common stethoscope is possible, however, it may not be quantifiable with respect to the system and ambient noise.
- A static system is not expected once all the microphones are attached to the patient's body because the degree of variation in acoustic properties created by the patient due to breathing or movement is not yet known.
- The required microphone count cannot be determined based on the available data. An alternative approach would be to identify the digital algorithms for postprocessing, such as independent component analysis or relevant folding techniques, and use their input requirements as a reference.
- The design of acoustic high-fidelity circuits is very complex and depends on many factors, each of which is capable of destroying the final signal quality. Therefore,

problems related to noise, nonlinearities, clocking or other unforeseeable issues can be expected.

The following chapters develop parameters, such as body dimension, propagation speed and wavelength, for determining the basic requirements.

2.7.1 Dimensions of the Body

Figure 13 shows a cross-section of a human thorax. The white rectangle depicts the first approximation of a width-to-height ratio of 10.0 to 7.5.

Figure 13: Cross-section of the thorax using a rectangle as a first approximation; the ratio of the square (w/h) is 10.0/7.5. [76]

According to the international standard EN 13402 for clothes sizes, the circumference of the thorax is based on the underbust girth for women and chest girth for men, respectively, as the "*horizontal girth of the body measured just below the breasts"* and the "*[...] maximum horizontal girth measured during normal breathing with the subject standing erect and the tape-measure passed over the shoulder blades (scapulae), under the armpits (axillae), and across the chest*." [82] According to EN 13402, the underbust girth for women ranges from 60 to 125 cm and chest girth for men from 84 to 144 cm. Adding a margin of 10% results in the following:

- Minimum circumference: 54 cm
- Maximum circumference: 158 cm

According to the width-to-height ratio, the dimensions are:

$$\frac{Width}{Height} = \frac{10}{7.5}$$

Equation 1: Width-to-height ratio according to first approximation.

$$2a + 2b = chest\ girth$$

Equation 2: Width and height as a function of chest girth.

Resulting in: $W_{(54cm)}$ = 15.5 cm

$H_{(54cm)}$ = 11.5 cm

$W_{(158cm)}$ = 45.13 cm

$H_{(158cm)}$ =33.85 cm

2.7.2 Speed of Sound in the Body

For the purpose of this study, the body is considered as a homogeneous medium comparable to salty water. A common approach for estimating the speed of sound in salty water is the following equation by Coppens: [83]

$$c(D,S,t) = c(0,S,t) + (16.23 + 0.253t)D + (0.213 - 0.1t)D2 + [0.016 + 0.0002(S\text{-}35)](S - 35)tD$$

Equation 3: Speed of sound in seawater according to Coppens.

$$c(0,S,t) = 1449.05 + 45.7t - 5.21t^2 + 0.23t^3 + (1.333 - 0.126t + 0.009t^2)(S - 35)$$

With: *t = T/10 where T = temperature in degrees Celsius*

S = salinity in parts per thousand

D = depth in kilometers; speed of sound is a function of the hydrostatic pressure, which proportional to depth.

Valid ranges: temperature 0 to 35 °C, salinity 0 to 45 parts per thousand, depth 0 to 4000 m

Equation 3 shows that the speed of sound is a function of temperature, salinity and depth. Body temperature (37 °C), maximum salinity (45‰) and no depth (0 km) are considered. The propagation speed according to Coppens can be evaluated as:

$$c(0\ \text{km}, 45‰, 37\ °\text{C}) = 1568.35\ \text{m/s}$$

Equation 4: Propagation for temperature 35 °C, salinity 45‰ and depth 0 m.

With: c(0 km,45‰,35 °C) = 1565.06 m/s

deviation 37 °C against 35 °C: 3.03 m/s =0.21%; to be neglected)

temperature 35 °C,

salinity 45‰ and

depth 1 m

2.7.3 Wavelength

As depicted in Equation 5, wavelength is a function of speed of sound and frequency. Assuming the body consists of a homogeneous medium, sound waves propagate linearly and the speed of sound can be considered a constant.

$$\lambda = \frac{c}{f}$$

Equation 5: Wavelength as a function of speed of sound and frequency.

$$\lambda_{(5{,}000\ Hz)} = \frac{1520\ ^{m}/_{s}}{5000\ Hz} = 0.304\ \text{m}$$

$$\lambda_{(20\ Hz)} = \frac{1520\ ^{m}/_{s}}{20\ Hz} = 76.000\ \text{m}$$

With: *λ = wavelength*

c = propagation speed

f = frequency

The resulting wavelengths are:

- Minimum wavelength: $\lambda_{(5{,}000\ Hz)}$ = 0.304 m
- Maximum wavelength: $\lambda_{(20\ Hz)}$ = 76.000 m

2.8 Acquisition Path

"Digital audio is a highly sophisticated technology. It pushes the envelope of many diverse engineering and manufacturing disciplines. Although the underlying concepts were well understood in the 1920s, commercialization of digital audio did not begin until the 1970s because theory had to wait 50 years for technology to catch up." [84] The digital techniques entail concepts that are foreign to analog audio methods, therefore they will be considered individually in the following chapters. First, the analog design parameters were determined according to the preconditions developed in chapter 2.7, which was then followed by the selection of an adequate transducer. Finally, the digital domain is focused.

2.8.1 Sampling Rate

Any sampling system is bound to the sampling theorem. In order to regain frequencies of up to 5000 Hz, the Nyquist sampling theorem has to be considered: *If a function x(t) contains no frequencies higher than B hertz, it is completely determined by giving its ordinates at a series of points spaced 1/(2B) seconds apart.* [85] The lowest sampling rate according to the theorem and the derived maximum frequency in chapter 2.7 is

10,000 samples per second (SPS). Commercially available ADCs usually provide a much higher rate with no additional effort, thus an adjustable sampling rate would add great value to this system.

2.8.2 Aliasing

Aliasing is a consequence of violating the Nyquist theorem mentioned in the previous chapter. These erroneous signals appear within the audio bandwidth and are impossible to distinguish from legitimate signals. It is vital that such distortion is prevented from ever occurring. The most important mitigation measure is bandlimiting the input with a low-pass filter. [84]

2.8.3 Dynamic Range in the Analog Front End

Acoustic dynamic range, measured as the range from noise floor to peak level, is an important parameter describing a system's performance. [86] In theory, the maximum achievable dynamic range is calculated as the ratio of the largest sine wave root mean square (RMS) to the largest noise RMS. [87] The largest sine wave is achieved when the microphone's output reaches the maximum level at full stimulation, which is the analog supply voltage (AVcc). In the absence of sound, the RMS of the microphone's voltage level is used as the noise level. Figure 14 shows the relationship of the signal-to-noise ratio and dynamic range.

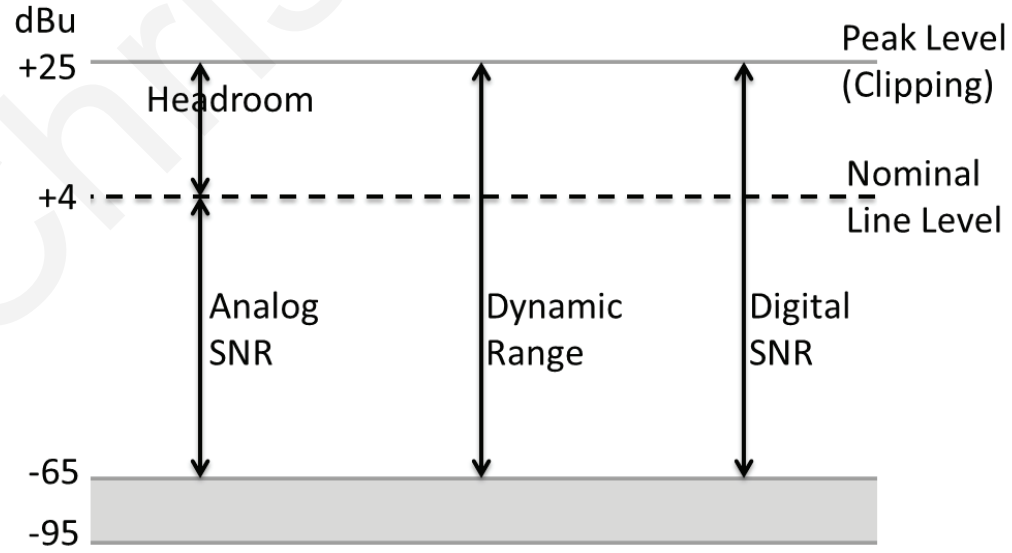

Figure 14: Dynamic range of an analog system. [86]

Equation 6 derives the dynamic range taking the 3.3 volts given for the system's supply voltage and estimating the achievable noise level to be 10 µV.

$$Dynamic\ Range\ (dB) = 20 * \log\left(\frac{V_{max}}{V_{min}}\right)$$

$$= 20 * \log\left(\frac{3.3V}{10\mu V}\right) = 110.4\ dB$$

Equation 6: Dynamic range of analog front end as function of voltage range.

With: *Vmax = peak voltage*

Vmin = RMS of noise level

2.8.4 Analog-to-Digital Conversion

The analog-to-digital converter is the central component on the encoding side. It is probably the most important element in the entire signal chain. The conversion principle and technology introduces desired or disadvantageous characteristics to the system, thus selecting the right converter is vital to ensure good performance. Bin Le et al. describe resolution, sampling rate, distortion and power dissipation as the general parameters to be considered in selecting the right technology. [88] The four types of structures considered for implementation were flash, successive approximation register (SAR), pipelined and sigma-delta. The pipelined structures are best suited for applications with high performance requirements such as wireless transceiver applications and military use. SAR ADCs have widely ranging sampling rates and are popular for their range of speeds and resolutions as well as their low cost and power dissipation. Sigma-delta ADCs have the highest resolution with relatively low sampling rates from kilosamples per second to megasamples per second, while flash ADCs have the highest sampling rates up to gigasamples per second due to their parallel structure, but with a limited resolution due to nonlinearity. [88]

Figure 15 illustrates the comprehensive technology review performed by Bin Le et al. in 2005. It clearly shows the merits of sigma-delta converters with respect to resolution at the expense of speed.

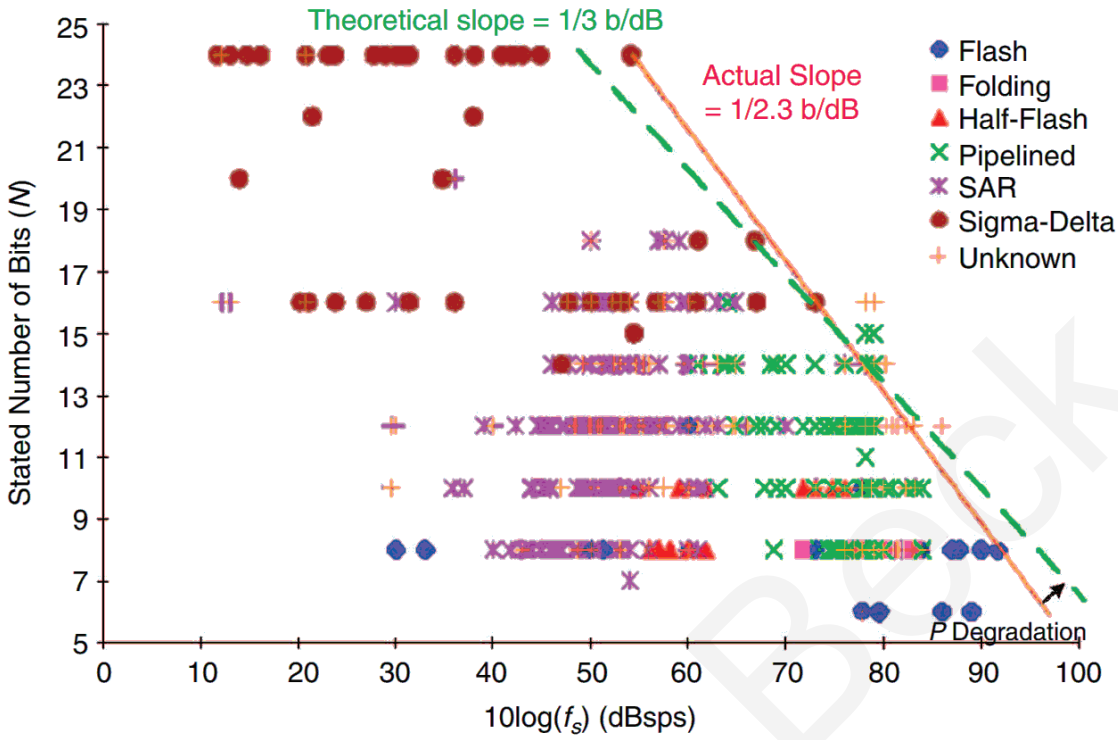

Figure 15: Number of bits as stated in the data sheet versus sampling rate for different types of structures. [88]

In this application, the input is an audio signal, thus it can be considered a very low frequency system with high resolution and SNR requirements. Consequently, a sigma-delta type of structure ensures the best performance. According to José de la Rosa [89], this type of structure is well-known for its low-noise recovery and beneficial noise shaping characteristics, where noise is reduced at lower frequencies by shifting to higher frequencies.

Additional parameters that are not necessarily related to the type of structure but important for a proper design are PCB space consumption, differential analog input, synchronized clocking features and the availability of standard communication interfaces.

2.8.5 Resolution

The number of bits (NOBs) in digital audio systems is directly related to the dynamic range derived in chapter 2.8.3, thus the resolution of the digital part has to at least meet a level of 110.4 dB. According to the *6 dB rule*, defining the relationship between quality and NOBs, each bit adds a dynamic range of 6 dB to digital audio systems. [86]

$$Dynamic\ Range\ (dB) = 20 * log_{10}\left(\frac{2^n}{1}\right) = 6.02 * n\ dB$$

Equation 7: Dynamic range as a function of number of bits according to the approximated 6 dB rule described in [86].

$$110.4\ dB = 20 * log_{10}\left(\frac{2^n}{1}\right) => \mathrm{n} = 18.34 => 19$$

$$144\ dB = 20 * log_{10}(\frac{2^n}{1}) => \mathrm{n} = 24$$

With: n = number of bits (NOBs)

A level of 110 dB would result in 19 NOBs; however, there are no commercially available devices with this specification. State-of-the-art ADCs offer a wide variety of NOBs, however, they generally use 12, 16 or 24 bits. With respect to the required sigma-delta technology, most devices come with a 24-bit resolution.

2.8.6 Data Rate and Storage

The requirements for transmission and storage of the data acquired are basically dependent on microphone count, resolution, sampling rate and recording time.

Current settings define microphone arrays with up to eight microphones, a 24-bit resolution, a sampling rate of 20 kHz and a recording time of at least one hour. The following formulation derives the basic raw data rate and storage, which does not yet include overhead.

Single microphone data rate:

Equation 8: Data rate of a single microphone.

$$v_{s_{mic}} = resolution * sampling\ rate$$

$$v_{s_{mic}} = 24\ bit * 20\ kHz = 480\ \frac{kBbit}{sec}$$
$$= 60\ \frac{kByte}{sec}$$

Array data rate:

Equation 9: Data rate of a microphone array.

$$v_{s_{array}} = v_{s_{mic}} * microphone\ count =$$

$$v_{s_{array}} = 60\ \frac{kByte}{sec} * 8 = 480\ \frac{kByte}{sec}$$

With: v_s: *data rate*

Single microphone storage:

Equation 10: Required storage per microphone.

$$S_{mic} = v_{s_{mic}} * T$$

$$S_{mic}(1sec) = 60\frac{kByte}{sec} * 1sec = 60\ kByte$$

$$S_{mic}(1min) = 60\frac{kByte}{sec} * 60sec = 3600\ kByte$$

$$S_{mic}(1h) = 60\frac{kByte}{sec} * 3600sec$$
$$= 210.94\ MByte$$

Microphone array storage:

Equation 11: Required system storage.

$$S_{array} = S_{mic} * n$$

$$S_{array}(1sec) = 480\ kByte$$

$$S_{array}(1min) = 28.13\ MByte$$

$$S_{array}(1h) = 1.69\ GByte$$

With: *S: storage*

v_s: data rate

T: period

n: microphone count

2.9 Processing Unit

Today's processing technologies offer comprehensive, powerful and complex architectures for processing units for embedded systems. Various technologies are commercially available and are employed in a plurality of products. The most common of these are microcontrollers (µC), field programmable gate arrays (FPGA), digital signal processors (DSP) and application specific integrated circuits (ASIC). [90] The main criteria for embedded systems when it comes to selecting a technology are performance, power consumption, complexity, cost per unit and non-recurring engineering costs.

This project requires a flexible, scalable and power optimized implementation for a prototype series. The processing unit will link, configure and control the hardware components, perform advanced arithmetic processing and hold the application logic.

Microcontrollers are general-purpose devices that cover a variety of applications. They are based on a serial architecture, thus performance is directly related to the clock frequency. They are best used for complex application logic. Typical applications include mobile devices, kitchenware and remote controls. [91] However, microcontrollers are

weak when it comes to parallelism such as multi-input real-time image/video and audio editing using algorithms with extensive performance requirements.

FPGAs are described as configurable hardware and can be programmed to the desired application or functionality. They are based on a true parallel architecture, thus performance is directly related to the implementation space or transistor count. FPGAs are best used for high data input/output (I/O) and processing. Typical applications require massive parallelism, such as Gigabit Ethernet, single- or multi-input real-time image/video and audio editing. [92] FPGAs are weak when it comes to the implementation of complex user logic, such as user interfaces or serial protocols.

While ASICs are highly optimized for very specific applications produced in large quantities, they exceed the budget for this project. DSPs, on the other hand, are within budget but lack scalability and the flexibility required for embedding application logic.

Even medium-sized 32-bit microcontrollers, such as Microchip's PIC32MZ family, would probably experience performance issues and lack potential real-time constraints or require complex and comprehensive optimization for the following tasks computed in parallel:

- Acquisition of eight acoustic channels, ECG, pulse oximetry
- Processing heart sounds in real time
- Processing lung sounds in real time
- Maintaining communication and data transfer to a host

In contrast, higher complexity in developing communication and user logic is more likely with FPGAs compared to microcontrollers. All FPGA-based communication interfaces (Ethernet, UART, SPI, I2C, etc.) require very accurate VHDL state machines, whereas microcontroller-based C implementations are comparatively simple, well tested and a wide variety are available through open source projects.

In conclusion, microcontrollers as well as FPGAs represent a potential approach. However, the focus of this project is the real-time acquisition, processing and transmission of data in parallel. In considering the technological merits and drawbacks of the architectures presented, FPGAs enable the design to embed extensive algorithms

by performing comprehensive audio editing in parallel on each input stream with inter-channel correlation in real time while maintaining reasonable complexity, power consumption, flexibility and scalability.

The market leader for FPGAs is Xilinx Inc., which had annual turnover of about USD 600 million in 2014. Xilinx's growth is largely driven by the following successful product lines: Virtex Ultrascale, Kintex Ultrascale, Virtex-7, Artix-7, Kintex-7 and Zynq-7000 as well as the Virtex-6 and Spartan-6 series. [93] The Xilinx Spartan family (FPGA) was introduced in 1998 and continuously developed until generation 6 was introduced in 2011.

Table 7: Overview of rapid technological development based on a comparison of Spartan-1 and Spartan-6 series product features.

Product Feature	Spartan-1 (1998): XCS40	Spartan-6 (2011): XC6SI150T
Logic Cells	1,862	147,443
System Gates	40,000	184,000
Max. IOs	224	540
Max. RAM [Kb]	25	1,355 DRAM +4,824 BRAM
Supply Voltage [V]	5	1.2
Process [nm]	500	45

Table 7 illustrates the rapid technological development between the basic product features of the Spartan-1 and Spartan-6 series. [94,95]

The Spartan®-6 family provides leading system integration capabilities. The thirteen-member family delivers expanded densities ranging from 3,840 to 147,443 logic cells with half the power consumption of previous Spartan families. It is faster, built on a mature 45 nm low-power copper process technology and provides many few features, such as a new, more efficient dual register 6-input lookup table with 18 Kb (2 x 9 Kb) block RAMs, second generation DSP48A1 slices, SDRAM memory controllers, enhanced mixed-mode clock management blocks, advanced system-level power management modes, and auto detect configuration options. According to Xilinx, the Spartan®-6 family offers the best solution for logic designs, consumer-oriented DSP designs and cost-

sensitive embedded applications. [95] In addition, with regard to the selection criteria, it also offered the following:

- Easy availability from any distributor
- Free comprehensive design tools
- High-quality documentation
- Extensive accompanying material, such as white papers, design guidelines, design examples and development kits

An important factor in choosing a device that is part of an extended product family is the possibility of easy upgrade to higher performance members with the same footprint.

2.10 System Feature Summary

The following table summarizes the system features derived in this chapter.

Table 8: System Feature Summary

System Specification Parameter	
Application	mobile emergency monitor
Acquisition Modalities	ECG, blood oxygen, body temp., 8-channel auscultation 1-4: each heart valve 5,6: each lung 7: ambient noise 8: undefined, maybe speech
Size	small (wearable)
Weight	< 200 g
Interfaces	USB, Wi-Fi (optional)
On-board processing	Capabilities for parallel acoustic processing
On-board storage	> 8 GB
ADC technology	Sigma-Delta principle
Data rate	+3.2Mbit
Memory	+14.4 GByte (one hour)

3 Accident and Emergency Center Intelligent Acquisition Unit

The design and development of this project follows the basic organizational methodologies required for industrial medical projects according to EN ISO 13485. The standard proposes an organizational procedure such as the waterfall model for defining consecutive phases. The following phases and tasks were defined for this project:

Table 9: Project definition and task description.

Phase		Task	Description
Phase 1 Definition	1	Description of the idea	Short abstract describing the basic idea.
	2	System requirements definition	Compendium of all requirements from all disciplines.
	3	System design	Extensive and detailed description of the system and all components.
	4	Modularization	Dividing the system into parts with an interface definition to create a block diagram. The aim is to decrease complexity and allow parallel implementation.
Phase 2 Prototype and Implementation	5	Schematics and component selection	Elaborate the electrical circuit, including component selection and simulation if applicable.
	6	PCB design	Layout and routing, including 3D design and the generation of manufacturing data.
	7	Manufacturing	Outsourced process, including PCB manufacturing, component purchasing and population.
	8	Embedded software development	Development of the FPGA VHDL implementation starting with a development kit and followed with the manufactured PCB.
	9	Processing and analysis	Programming a MATLAB@-based application for vital signs data set compilation, analysis and display.
Phase 3 Test	10	Verification	Approve appropriate behavior of each function or functionality, e.g., charge current, ADC sampling, storage, etc.

	11	Characterization	Measure the specific characteristics of the system that are essential for the mode of operation, e.g., jitter frequency of the ADC samples, SNR of acoustic front end, transmission speed of wireless interface, etc.
	12	Validation	Compare final system against requirements document to ensure that all requirements have been fulfilled.

3.1 Phase 1 – Definition

Phase I describes the basic idea, derives the fundamental requirements, and defines the modules, components and implementation strategies. Table 10 gives an outline of the respective tasks and status of the definition phase.

Table 10: Phase 1 – Definition.

Phase		Task	Status	
Phase 1 Definition	1	Description of the idea	High-level project description completed. Please refer to part 1.	**100%**
	2	System requirements definition	High-level requirements definition completed. Please refer to part 2.	**100%**
	3	System design	High-level specification definition completed. Please refer to part 3.	**100%**
	4	Modularization	Modularization of thesis project accomplished based on definition of several block diagrams. Please refer to part 3.	**100%**

Figure 16 shows the system block diagram with mobile unit and host application. The mobile unit acquires human vital signs and fulfills processing tasks in order to provide the data to a host application properly and securely via either a wireless or wired interface. Strict modularization is kept throughout the development and is defined as part of the design methodology. This decreases complexity and allows partial implementation and testing.

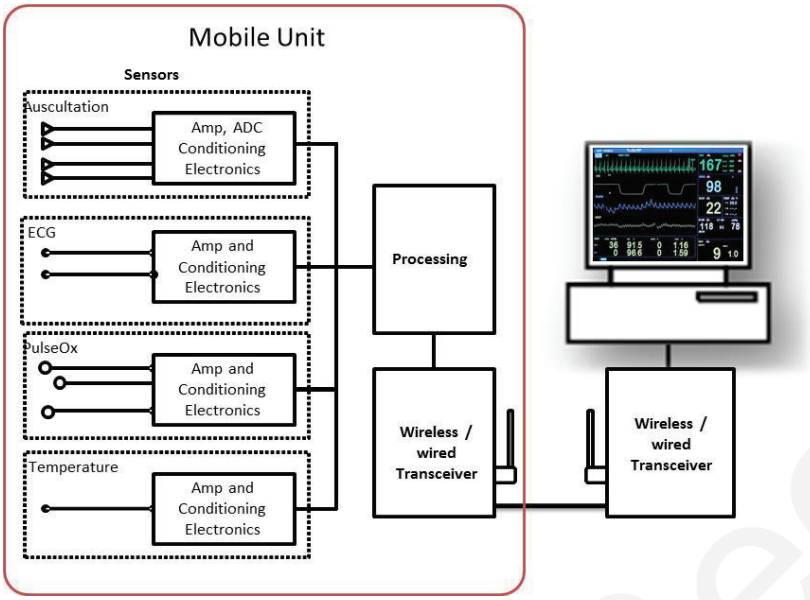

Figure 16: System block diagram.

3.2 Phase 2 – Design and Implementation

Table 11 defines the implementation tasks and shows the status of completion. The hardware design and manufacturing is complete. Five prototypes are available, four of which are in use.

Table 11: Phase 2 – design and implementation.

Phase		Task	Status	
Phase 2 Prototype and Implementation	5	Schematics and component selection	Schematics and component selection completed according to the specifications document, which follows the block diagram of the mobile unit. Please refer to Appendix B.	**100%**
	6	PCB design	PCB design completed following the basic implementation methodologies, by developing a 4-layer board with two signal planes (i.e., the power and ground planes).	**100%**
	7	Manufacturing	Manufacturing was outsourced to Evotronic GmbH, a company highly specialized in prototype and small series PCB manufacturing and population.	**100%**
	8	Embedded software development	Architecture and programming of embedded software completed.	**100%**
	9	Processing and analysis	Acoustic front end processing completed.	**100%**

3.2.1 Task 5 – Schematics and Component Selection

Figure 17 shows the block diagram of the mobile unit and represents the fundamental hardware architecture. The implementation follows a strict separation in order to achieve a high degree of independence. Each module contains a dedicated set of functions or functionality and is connected to the system via a well-defined interface.

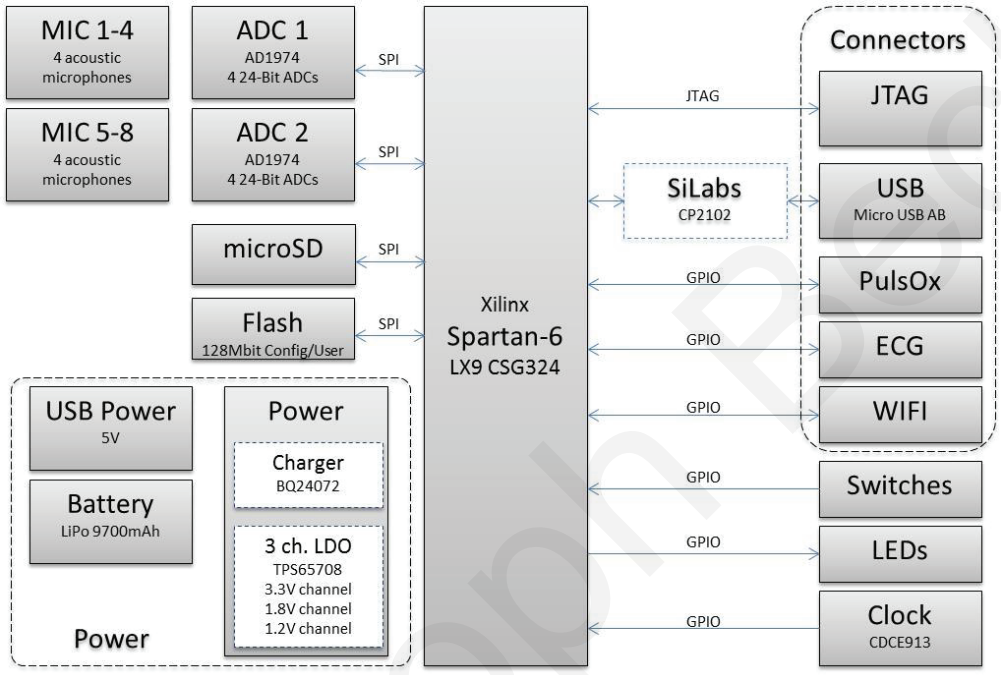

Figure 17: Block diagram of the mobile client unit.

Toolchain: Altium Designer® Summer 2013 was used for the hardware development. The design process involved the schematic design, component selection, PCB design, placement, layout, routing, purchasing and export for manufacturing.

FPGA: The core of the MCU is a powerful Xilinx Spartan-6® XC6LX9 FPGA in a CSG324 package providing 200 GPIOs. The selected device was already equipped with a generous safety margin with regard to computing power, speed and pin count at the expense of power consumption, implementation space and complexity. In case the margin is not sufficient, there are three more powerful family members (XC6LX16, XC6LX25, XC6LX45) in the same CSG324 package but with 218 to 232 I/O pins. The Spartan-6 XC6LX9 FPGA has 9,152 logic cells, whereas XC6LX45 has 43,661.

Flash: In order to permanently store the configuration and basic application setup, a 128 Mbit flash memory device was chosen. It is seamlessly integrated and can be used

throughout the whole development process of the embedded application without additional effort.

Memory: As shown in chapter 2.8.6, it is necessary to provide non-volatile storage of 14.4 GBytes per hour for raw data recording at a write cycle of 4 MBytes. Therefore, the microSD card technology was chosen because it meets the requirements of this project with regard to power consumption, implementation space, pin-count, complexity and ease of use. In addition, it offers high capacity to meet growing storage needs in a small format, is non-volatile and has sufficient write and read cycles. The fact that most of today's smartphones are equipped with a microSD card also supported this decision.

PMU: The power circuit is based on Texas Instrument's bq24072 single cell lithium ion and lithium polymer battery charger, and TPS65708 Power Management Unit (PMU). The bq24072 is a single cell integrated lithium ion/lithium polymer charger and power path management device. It operates either from a USB port or AC adapter and supports charge currents of up to 1.5 A. The bq24072 features dynamic power path management that powers the system while simultaneously and independently charging the battery. *"The circuit reduces the charge current when the input current limit causes the system output to fall below a threshold, thus, supplying the system load at all times while monitoring the charge current separately."* [96] The charging procedure is done in two stages as illustrated in Figure 18. The first stage is performed at a constant current and the second stage at a constant voltage. During the constant current phase, the charger applies a constant current to the battery. Thus, the voltage increases until the voltage limit is reached. During the constant voltage phase, the charger applies a constant voltage equal to the maximum cell voltage. Thus, the current decreases as the charging level increases. The bq72024 terminates charging once the charge current drops below 3% of the maximum. Stages three and four describe the self-discharge level, which is very low and the maintenance required for long storage is less relevant for this design. Additional information on this can be found in reference [97].

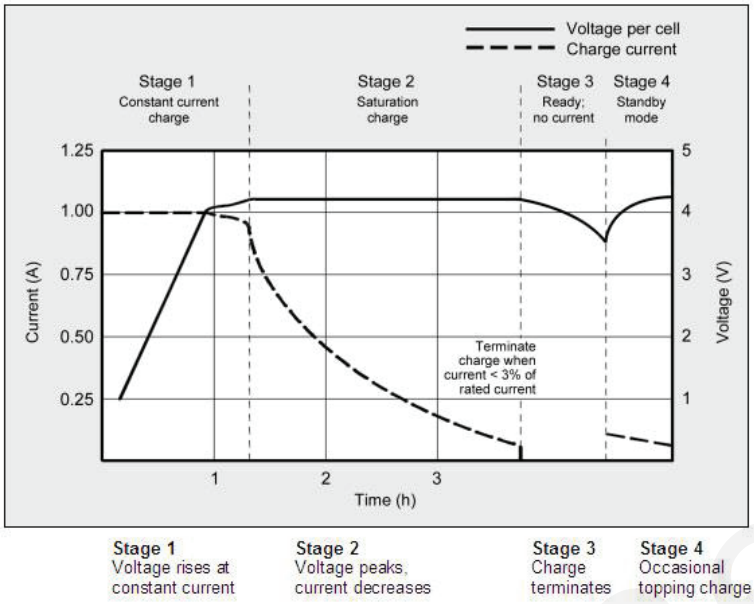

Figure 18: Lithium ion charging behavior split into four stages: 1) constant current (CC), 2) constant voltage (CV), 3) self-discharge and 4) maintenance. [97]

The schematic representation is shown in Figure 19. The system is either supplied by +5 V from a USB source or +3.6 V to +4.2 V from a lithium polymer battery. The charging configuration is defined by the logic state of certain pins. The default configuration is set by the hardware by means of either pull-up or pull-down resistors, but may be changed during runtime by the embedded application.

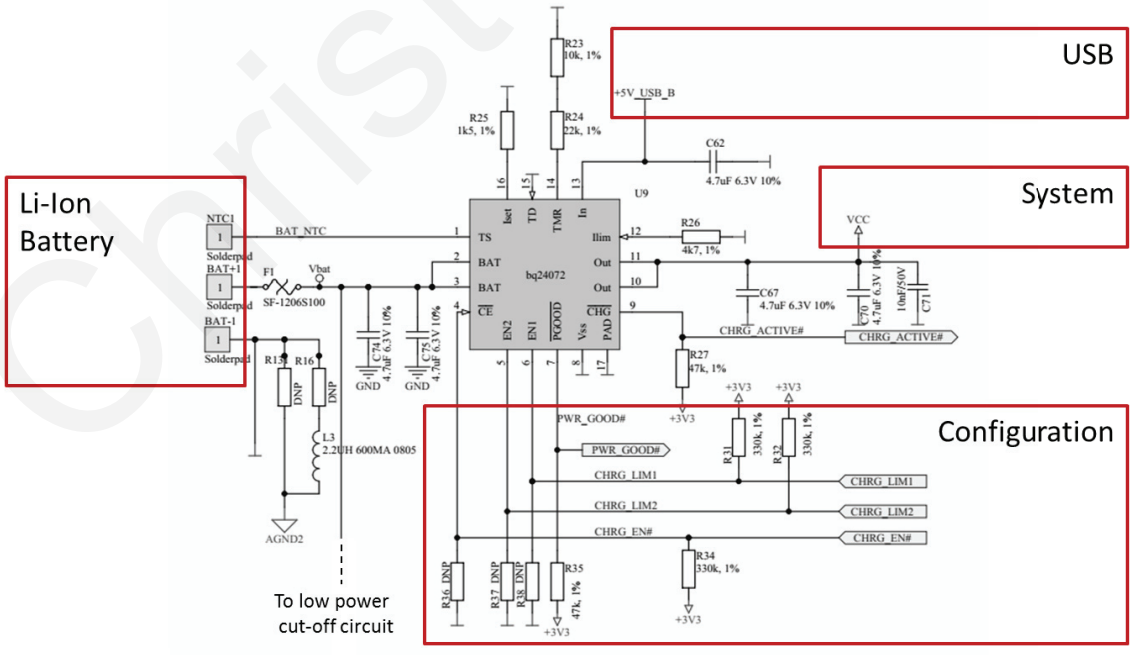

Figure 19: Single cell lithium ion/lithium polymer battery charger and power path management device.

The maximum current is either defined with a voltage divider at pin 12 (ILIM) [96] or set to a USB 2.0 default value with a combination of pin 6 and pin 5 (EN1, EN2). [96] In order to maintain the highest degree of flexibility, the default maximum current is set to 500 mA as defined in the standard; however, the setting can be manipulated by the embedded application because all the necessary pins are also connected to dedicated GPIOs.

The TPS65708 is a power management unit designed for embedded modules or other portable low-power consumer end equipment. It contains two high-efficiency step-down converters, two low-dropout linear regulators, and a 7.5 mA current sink for driving an LED. The device allows the use of small inductors and capacitors in order to obtain a small size implementation. [98] Figure 20 shows the schematic representation in detail and illustrates how the TPS65708 provides four different voltage potentials to supply the Xilinx Spartan-6 FPGA and peripherals.

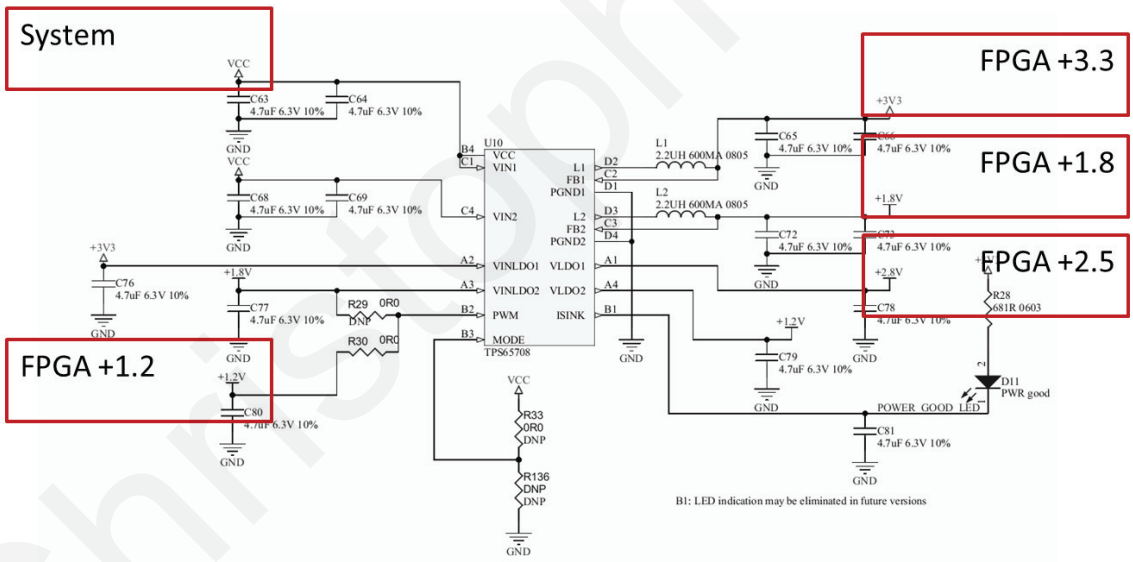

Figure 20: Power management unit (PMU) to supply the Xilinx Spartan-6 FPGA and peripherals.

Analog Front End: Sound acquisition is realized using eight Knowles® SPM0408HE5H MEMS microphones. They are pre-amplified and have a sensitivity of −22 dB at 1 kHz. Current consumption is as low as 200 µA at a 4.7 mm by 3.7 mm form factor. A second stage differential amplifier placed close to the microphone further increases the input signal with a fixed gain, filters and forwards the differential signal to the ADC. The schematic representation is shown in Figure 21.

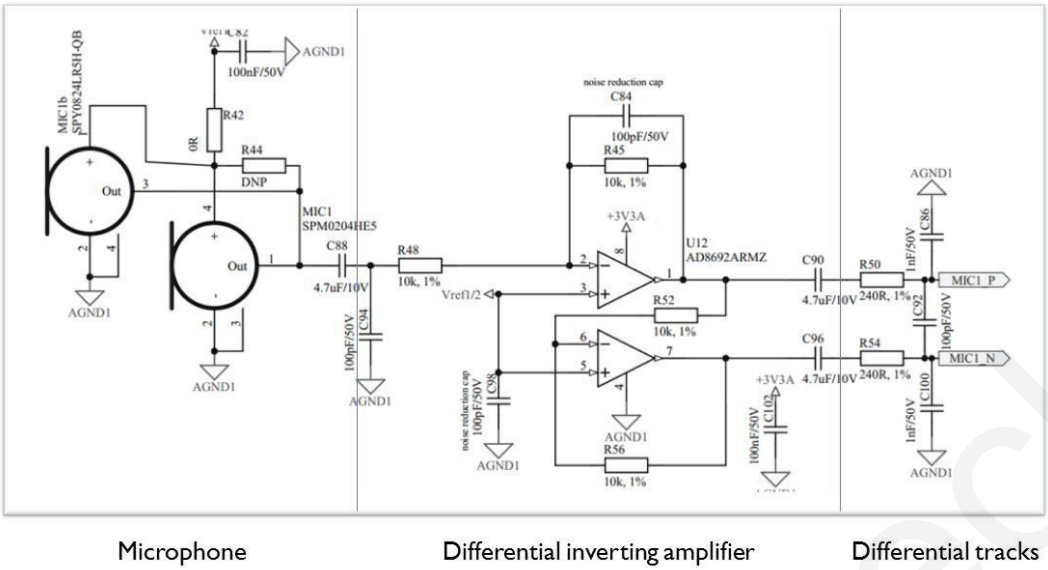

Figure 21: Analog front end divided in three areas: 1) microphone (two assembly options), 2) differential amplifier and 3) differential tracks.

ADC: Analog-to-digital conversion is done by two Analog Devices AD1974® four channel ADCs based on a multibit sigma-delta conversion architecture. Both ADCs are configured and synchronized by the FPGA for the lowest jitter. Each is connected to four microphones, sampled at 48 kHz with 24 bits.

External Modules: Pulse oximetry (ChipOx®), ECG (EMB3/6®) and Wi-Fi (muRata SN8200®) are powered by the PMU and are connected to the Spartan-6 via GPIOs. Communication is based on various protocols, such as UART, SPI or a proprietary implementation.

USB Interface: A micro USB plug provides charging capabilities and a data interface to configure the mobile unit using serial commands at a data rate of up to 1 Mbit per second. It is shielded to minimize induced noise and protected against overvoltage (ESD) with TE Connectivity PESD0402 ESD diodes at each signal line.

Wireless Interface: The muRata SN8200 module is a “low power, self-contained, embedded wireless module solution that addresses the connectivity demands of M2M applications. It integrates a microcontroller, a Wi-Fi BB/MAC/RF IC, an RF front end and two clocks into a small form factor” [99] measuring as little as 30.5 x 19.4 x 2.8 mm.

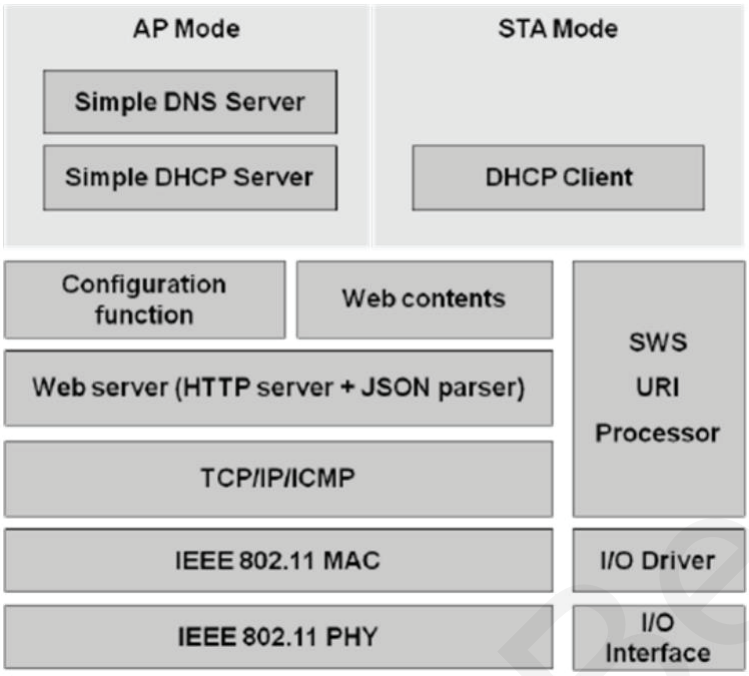

Figure 22: SN820X EZ Web Wizard Software Architecture Diagram. [100]

Wireless communication at a high data rate can be established via the STA mode at which the module acts like a common client and is perfectly suitable for the transmission of vital signs data while worn by the patient. In addition, it features an on-board web server that is compatible with Broadcom's WICED® SDK and is especially dedicated for configuration purposes, status indication and sensor data transmission via the AP mode (but at a low rate). The latter feature could be interesting for additional capabilities such as geolocation or device status information in standby mode. The SN820X EZ Web Wizard Software Architecture Diagram as shown in Figure 22 illustrates the communication stack with the mentioned options AP and STA mode.

Data/Debug Interface: A 17-bit parallel GPIO connector interfaces with either an Opal Kelly XEM6002® board with MATLAB® integration to stream raw data with additional debug information in real time or an MSO with real-time on-board debugging capabilities. Both modalities are meant to provide advanced access options during development and verification. In order to reduce the radiated electromagnetic noise caused by high-frequency transients, each signal line is equipped with a series resistor. In addition, the pin driving strength was set to a minimum in the FPGA's user constraints file.

Device User Interface: The mobile unit has four LEDs, which display basic status

information. Functionality varies with each setup and is currently implemented as follows: LED 1 – charging (ON = charging); LED2 – recording (ON = recording); LED3 – low battery (ON = battery low); LED4 – no function (OFF). Four dip switches are used to control the basic settings, which currently do not have functionality. The circuit can be reset externally by means of a push-button. The complete schematics can be found in Appendix 1 – ASArevA_SCHEMATICS. [101]

3.2.2 Task 6 – PCB Design

The design of the PCB complies with the general rules for analog and digital design. In order to ensure optimal handling, a circular PCB with a diameter of 87 mm was created. This shape was inspired by the diaphragm part of a stethoscope. Eight omnidirectional MEMS microphones are equally spaced at the outside edge at right angles to the array planes. The PCB consists of four layers, which are defined in the layer stack manager as follows:

- The **top layer** contains all the components except for the microphones and horizontal/vertical signal traces moving away from the FPGA.
- The **power plane** separates the different supply nets and spreads them to their destination. The analog supply nets are uncoupled from all the digital nets to reduce noise as much as possible. Special components such as RC filters or ferrite beads ensure proper filtering from the digital domain.
- The **ground plane** separates the different ground planes and spreads them to their destination. The analog ground nets are uncoupled in the same way as their corresponding supply nets.
- The **bottom layer** contains only the signal traces and microphones in order to ensure unobstructed propagation of the sound in case they are surface mounted.

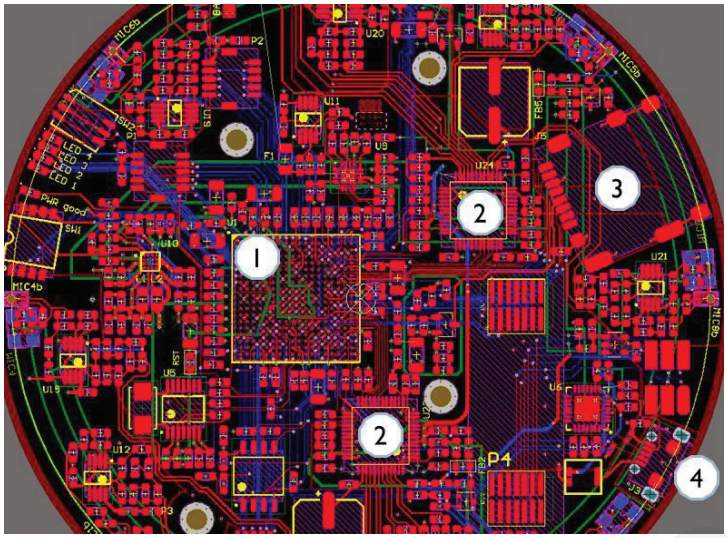

Figure 23: PCB (top view): 1) FPGA, 2) ADCs, 3) microSD card holder and 4) micro USB socket.

Figure 23 shows the center top view of the completed PCB design with some of the main features marked. The red components and traces are placed on the top layer and the blue components and traces on the bottom layer.

3.2.3 Task 7 – Manufacturing

The described hardware has approximately 430 components. Of these, 13 are equipped with a QFN or BGA package, which have pins facing the PCB and cannot be soldered by hand. Since five prototypes are needed, manufacturing and assembling was outsourced to Evotronic GmbH, a company highly specialized in prototyping and small series production.

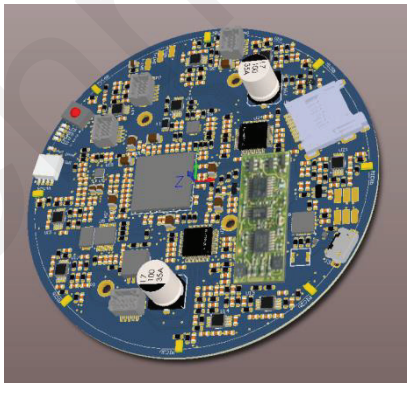
a)

b)

Figure 24: a) 3D representation before manufacturing; b) photo taken from real device.

Figure 24 shows the 3D representation of the completed PCB before manufacturing and a photo taken after delivery of the prototypes. Both show the ChipOx® daughterboard.

The EMB3/6® and Wi-Fi modules are not shown in order to ensure proper representation of the PCB.

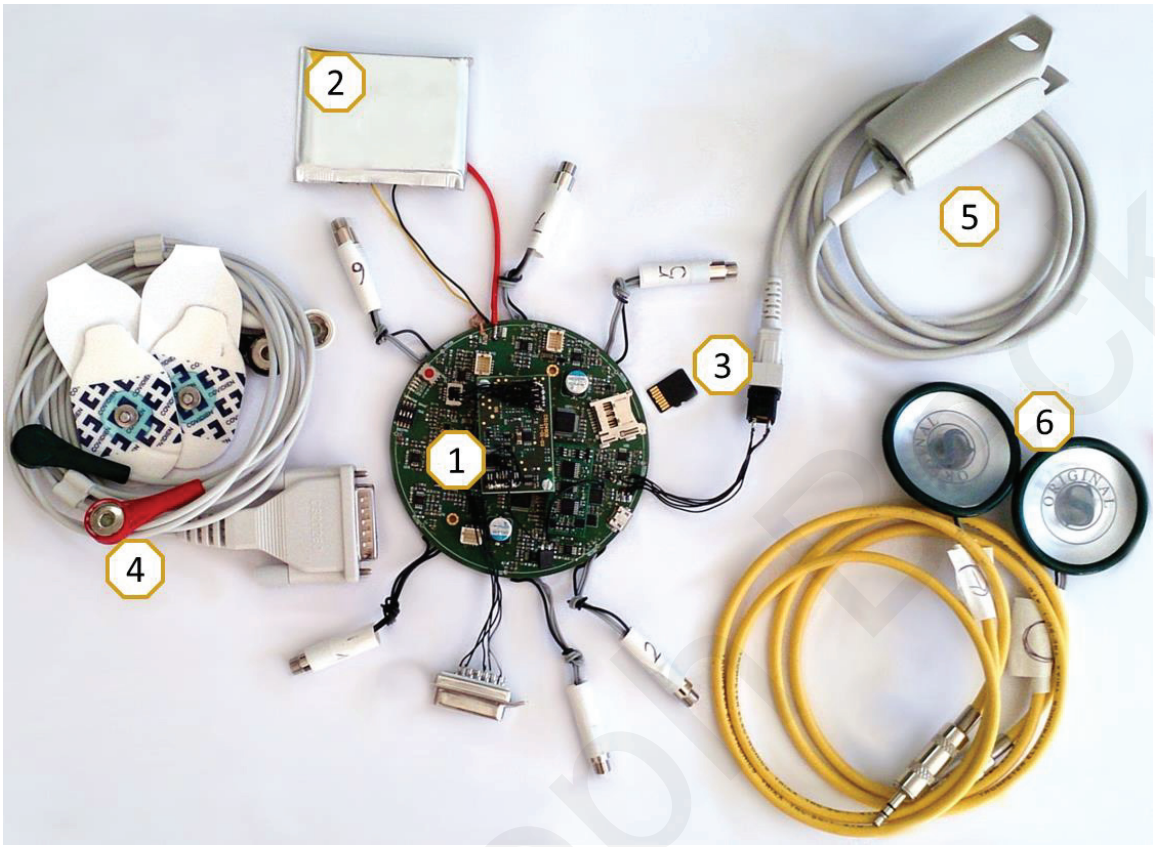

Figure 25: (1) Baseboard with ECG and PulseOx module; (2) battery; (3) microSD card and card slot; (4) ECG leads; (5) PulseOx lead; (6) stethoscope leads

Figure 25 illustrates the mobile monitor with all patient leads as designed and developed in this project and used in the experiments (case not depicted).

3.2.4 Task 8 – Embedded Software Development

A strictly modular architecture is followed for describing the FPGA's behavior. Each module mirrors a set of functions or functionality following the structure provided by the hardware and is kept independent up to the sub-level entity if appropriate. Well-defined module interconnections and a strong focus on well-known design patterns ensure independence, reduced complexity and increased reliability of the embedded application. In the block diagram in Figure 26, the modules closest to the hardware are represented in the lower part of the diagram.

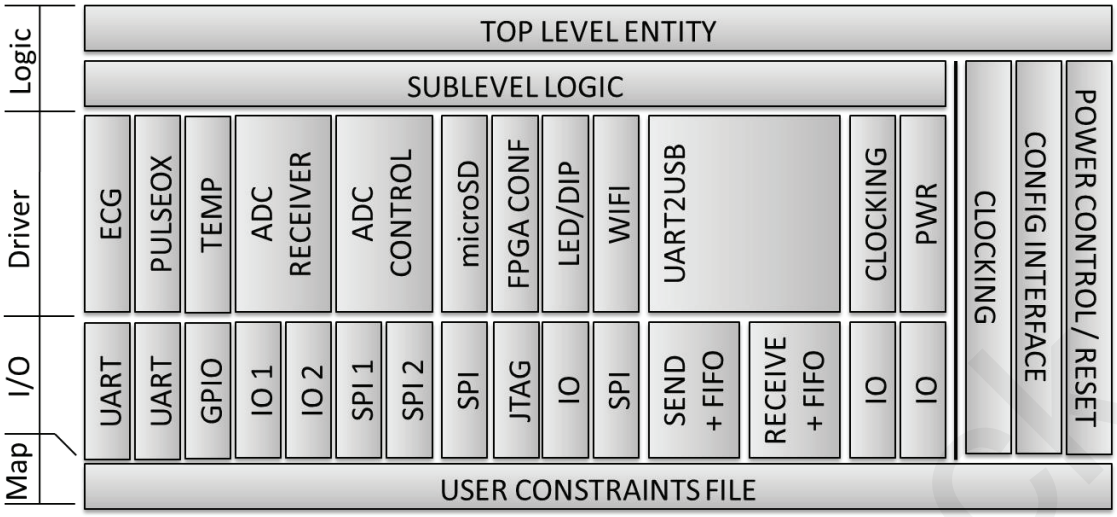

Figure 26: Block diagram of embedded software.

Top-Level Entity: Initialization, configuration and top-level data management are organized in the top-level entity and define the main logic. All processes run independently due to the concurrent nature of the FPGA's architecture.

Sub-Level Logic: A second layer involves task-specific logic and generic routines. This layer was introduced to reduce the size and complexity of the top-level entity.

Driver Layer: The hardware implementation groups the functionality in modules if appropriate. The embedded application reflects the grouping and groups corresponding to the functionality in the stand-alone drivers. Each of these provides module-specific functions with respect to the sub-level logic, such as "switch on," "switch off," "set default configuration" or "read status." In addition, these may also include more specific functions, such as "start ECG acquisition" or "write data block to mirocSD® card." With regard to the I/O interface, the driver communicates according to the specifications given by the hardware and involves data management. In general, the driver and I/O layer have a byte-wise, unchecked data exchange.

I/O Layer – Hardware Access: The main task of the I/O layer is to serialize and physically exchange data as defined by implementation protocols, such as UART, SPI, GPIO, etc.

Map – The User Constraints File: The user constraints file maps the logic signals in the FPGA's architecture to I/O pins, which are physically connected to corresponding routes on the PCB. It further defines the signal characteristics so that special internal functions

signals such as clock lines are routed appropriately. The user constraints file is defined in ASArevA_01.ucf.

The following paragraphs describe the driver implementations as shown in the corresponding layer *"Driver"* of Figure 26.

ECG Driver: The EMB3/6 ® daughterboard is connected to the host PCB with two Samtec CLM-107-02-L-D. [66] Two pins are reserved for the communication to the FPGA, which is based on a UART protocol at a data rate of 115.2 kBaud. The EMB3/6® outputs raw and processed data using a proprietary communication protocol. Inbound and outgoing traffic is organized in frames. [66] Incoming sensor data is collected, tagged with meta-information and stored to the module-specific FIFO. The ECG driver is defined in EKG_EMB3.vhd.

PulseOx Driver: The ChipOx® daughterboard is connected to the host PCB with two Samtec CLM-107-02-L-D. [69] Two pins are reserved for the communication to the FPGA, which is based on a UART protocol at a data rate of 9.6 kBaud. The ChipOx® outputs raw and processed data using a proprietary communication protocol. Inbound and outgoing traffic is organized in frames. [69] Incoming sensor data is collected, tagged with meta-information and stored to the module-specific FIFO. The PulseOx driver is defined in CO_ChipOx.vhd.

Temperature Driver: The temperature sensor does not need configuration at startup and outputs the temperature periodically using a proprietary protocol. The mean value is stored to the module-specific FIFO once a second. The temperature driver is defined in TMP_TSIC206.vhd.

ADC Receiver Driver: Once configured, both ADCs continuously transmit digitized samples of each microphone via independent SPI interfaces. Even though SPI is a bus system and a single instance could handle both ADCs, independent implementation was chosen in order to have the highest degree of synchronization and reduce complexity. Inbound samples are collected, sorted in ascending order with respect to the microphone numbering, tagged with meta-information and stored to the module-specific FIFO. The ADC receiver driver is defined in ADC_Receiver.vhd.

ADC Control Driver: A dedicated driver module was introduced to configure both ADCs. After power-up, the driver automatically transmits the default settings via two independently controlled SPI interfaces, but also provides a routine to manually set a different configuration at any time. The ADC control driver is defined in ADC_Control.vhd.

MicroSD® Driver: In order to store a significant amount of sensory data, a microSD® card driver offers storage and recall routines. Even though only 4 Gbyte cards have been tested, the current implementation supports SDHC cards with up to 32 Gbytes. The microSD® card driver is defined in SD_Interface.vhd, SD_Protocol-Controller.vhd, Address_Calculator.vhd and spi_master_SD.vhd.

FPGA Configuration Driver: The FPGA has to be configured after each power-up cycle. This may be accomplished via a common JTAG interface or by loading the configuration from an attached flash memory. Once the flash memory holds the configuration file, a power-up routine can load the configuration from there as part of the FPGA's hardware.

MCU User Interface Driver: Several on-board LEDs and buttons are available in order to set the basic input parameters or read the device status without additional software. The dedicated driver sets or reads the status and provides the information for the sub-level logic.

Wireless Interface Driver: The muRata SN8020 [99] daughterboard establishes a Wi-Fi® connection in order to transmit data wirelessly from the MCU in layer one to the mobile node in layer two as described in chapter 2.1. The driver acts as a simple data relay between the top-level entity and server and does not contain any additional logic. For debugging purposes, the muRata SN8020 was replaced with a wired debug interface. The solution simulates a data relay from the top-level entity to the MATLAB® environment and involves an Opal Kelly XEM6002 board. This allows client-side communication to be established if no server is available.

UART2USB Driver – Tethered Configuration Interface: A dedicated interface was introduced in order to set the basic configuration of the MCU. The communication function uses the existing USB port and is based on a proprietary serial protocol. It is

processed by the top-level entity and the configuration is forwarded to the appropriate modules. The main purpose of this is to allow the settings to be changed easily during runtime as well as enable readout and verification of the hardware settings. The following is a non-exhaustive list of available commands:

1. Startup/power down analog front end, ECG, pulse oximeter, temperature sensor and Wi-Fi® module.

   Each module can be switched on and off individually, e.g., to optimize power consumption. The turn on procedure also includes setting the default configuration and may take up to 300 ms. [66]
2. Enable/disable data output of analog front end, ECG, pulse oximeter and temperature sensor.

   These commands enable the specific selection of active modules. Once activated, they acquire and transmit data.
3. Configuration and control of ADCs.

   Default configuration of Analog Devices AD1974® ADCs is set by the embedded application at each startup or restart of the analog front end. In order to maintain flexibility during development and research, an individual low-level configuration may be sent at any time.
4. Configuration and control of microSD® card.

   Default configuration of the microSD® card is set by the embedded application at each startup. Various commands are available for reading out the status, configuring the card, and reading out or deleting data.
5. Debugging.

   During the development process, various debugging commands have been implemented in order to enable/disable artificial data for verification of the data path, ensure the integrity of each transmission, and perform ADC jitter frequency readouts as well as other actions.
6. Set/read LED status.

   In most use cases, LEDs are set by the embedded application to indicate the active functions, such as “charging”, “low battery”, “acquisition” or “power”.

However, this command was introduced in order to be able to check for proper functionality at any time.

7. Read dip switch status.

   The dip switch status is read out by the embedded application in order to react to user input. However, this command was introduced in order to be able to check for proper functionality at any time.

Clocking Driver: Various clocks are used throughout the design. The driver is sourced from the hardware with 27 MHz and provides 100 MHz, 48 MHz and 12 MHz generated by the Xilinx® digital clock management (DCM).

Power Driver: A dedicated driver was introduced in order to control the circuit's power management. The main functions are to enable charging, read the charging status and shut down the system if the battery is low.

For more information on the embedded application, please refer to the source code, which contains comprehensive detailed documentation on functionality, routines and strategies. [102]

3.2.4.1 Xilinx® Toolchain

Implementation is based on the Xilinx ISE® Design Suite 14.3. [103] The recommended methodology was used throughout the embedded design, which was developed according to the block diagram shown in Figure 27 outlining the steps from design creation, synthesis, simulation, constraints entry, implementation, device configuration to programming. [104]

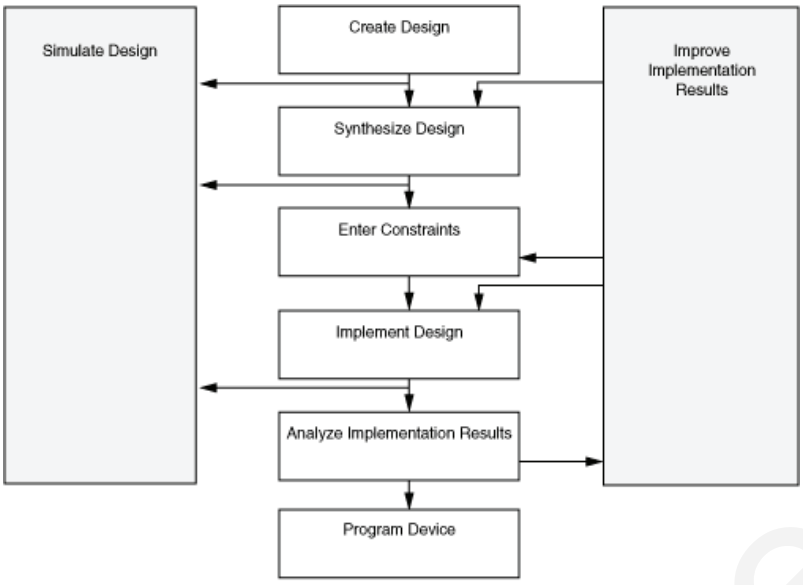

Figure 27: Block diagram for Xilinx ISE design flow. [104]

The code was written in VHDL and the intellectual property (IP) provided by Xilinx® was used if available, e.g., digital clock management (DCM), block ram memory (BRAM) and first-in/first-out memories (FIFOs). As a result of the strict modular approach, the reuse of modules and thus of code greatly accelerated development. For example, the UART and SPI protocols were programmed once and reused three and five times respectively.

3.2.4.2 Communication Methodology

Reliable communication and data transfer is a fundamental requirement for this project. Tethered as well as wireless communication systems are widely used in nearly all industrial and private areas and there are many well-known design patterns available. The most common of these is the Open Systems Interconnection Model (OSI), which is defined in standard ISO/IEC 7498-1:1994. [105] "*The term [...] OSI qualifies standards for the exchange of information among systems [...] and does not imply any particular systems implementation, technology or means of interconnection*" [105] The model introduces seven logical layers, which are broken down horizontally by communication function, as shown in Table 12 below.

OSI Model			
	Data unit	**Layer**	**Function**
Host layers	Data	7. Application	Network process to application
		6. Presentation	Data representation, encryption and decryption, convert machine dependent data to machine independent data
		5. Session	Interhost communication, managing sessions between applications
	Segments	4. Transport	Reliable delivery of packets between points on a network.
Media layers	Packet/Datagram	3. Network	Addressing, routing and (not necessarily reliable) delivery of datagrams between points on a network.
	Bit/Frame	2. Data link	A reliable direct point-to-point data connection.
	Bit	1. Physical	A (not necessarily reliable) direct point-to-point data connection.

Table 12: The 7-layer OSI model. [106]

The **I/O** layer as described in Figure 26 corresponds to the OSI physical layer and involves the electrical and physical implementation. For example, the I/O module serving the ECG driver physically controls and reads the logic states of the outgoing and inbound UART transmit and receive lines. The communication is a direct point-to-point data connection, which is not considered to be secure and does not involve error correction mechanisms.

The **Driver** layer as described in Figure 26 corresponds to the OSI transport and data link layer and does not involve an OSI network layer. The data connection is not open, i.e., it has a point-to-point structure and no addressing or routing is required. The data exchange between the sub-level logic and driver layer is frame wise, whereas the data exchange to the I/O layer is byte wise. Accordingly, the muRata SN8002 wireless hardware implementation would be considered an independent communication system and the MCU a user application in OSI layer 7.

The **Logic** layer with the sub-level logic and top-level entity as described in Figure 26 corresponds to the OSI application layer. The OSI presentation and session layers are not represented here because there is no implementation for session handling, machine independence or encryption.

3.2.4.3 Data Flow

The data communication from the MCUs' sensors to the server or MATLAB® application is divided into two parts. The first part is a proprietary implementation from the sensors to the top-level entity. The second part is from the top-level entity to the server or MATLAB® application.

Figure 28 shows the flow chart for on-board communication and data handling from the sensor to the top-level entity.

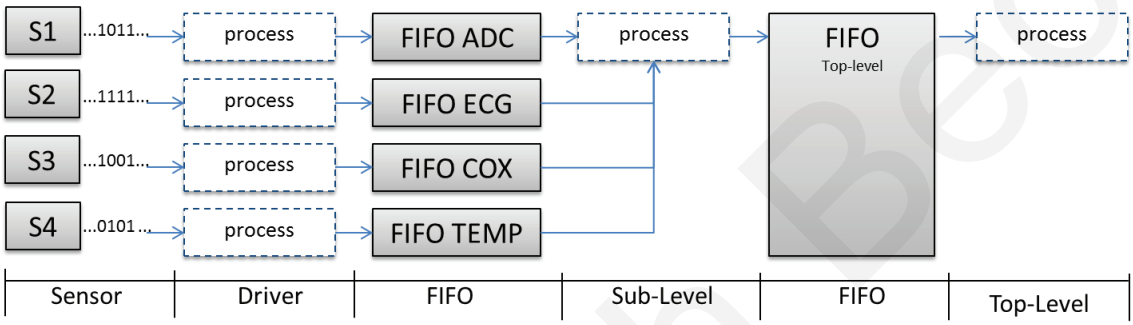

Figure 28: Flow chart for on-board data management.

A generic architecture was chosen in order to meet the highest flexibility with regard to the use of sensors and modularization. First, it allows fast, easy and stepwise implementation. Additional sensors may be added to the system at any time or removed without changing the underlying architecture. Second, it allows a user-defined presence, e.g., for power saving features in cases where individual sensors are switched off. Furthermore, each driver may be revised without the risk of affecting the entire application. The key elements for the approach depicted in Figure 28 are FIFOs with two independent interfaces. They act as connecting components for processes that may even be sourced by different clock speeds.

Each driver controls the communication to its corresponding sensor. The incoming data is either analyzed and stored, or stored directly in a module-specific FIFO together with the information necessary for verification of origin (Frame ID), integrity and completeness according to the OSI model. This involves the compilation of sensor-specific frames as described in Figure 29.

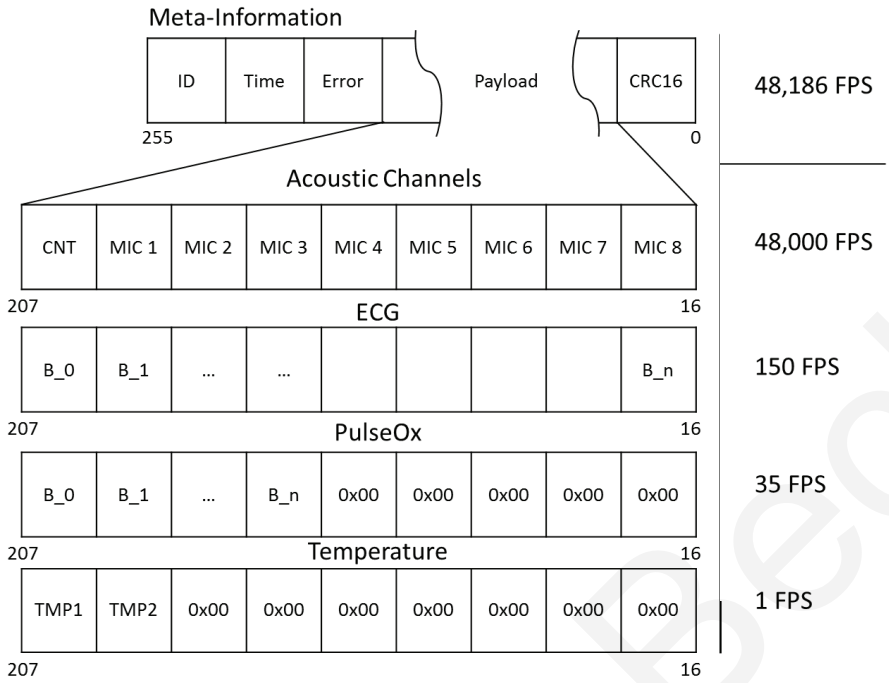

Figure 29: Sensor-specific communication frame data rate defined as frames per second (FPS).

All the frames have a fixed length of 256 bits or 32 bytes accordingly and contain data from just one sensor. *ID* stores the sensor identification number so that any system that is next in line can assign the frame to its origin. Examples of identification numbers for acoustic data are ID 1, ECG ID 2 and pulse oximetry ID 3 to mention just a few. *Time* stores a millisecond time vector that processing routines can use to sort, verify and arrange the data regardless of its reception sequence and allows cross-sensor correlation. *Error* indicates malfunctions in the form of status flags. The data is protected by a *CRC16* in order to ensure integrity.

The *Payload* is sensor specific. For example, the acoustic data starts with a frame counter to verify the incoming order followed by acquired samples from microphones one through eight. The frame definition of EMB3/6 and ChipOx can be found in the corresponding references [66,69].

A process in the sub-level logic collects the data (if available) from the module-specific FIFOs sequentially and stores it in the main FIFO. This pattern illustrates the strict separation and high flexibility of the architecture. Sensors may be switched on or off and even added or removed during runtime, however, the latter is not a deployed use case.

All the FIFOs are held in a reset state until the recording is triggered in order to ensure currentness and prevent buffer overflow in case sensors are enabled without data collection..

The second part is from the top-level entity to the server or MATLAB® application. The block diagram is shown in Figure 30.

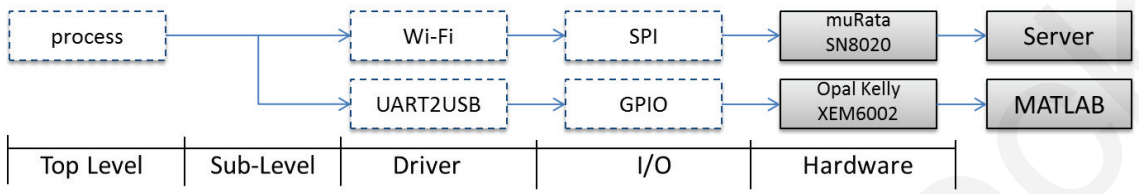

Figure 30: Data flow from top-level entity to server or MATLAB® application.

The top-level entity logic transfers the sensor data to the Wi-Fi® and/or UART2USB driver by sequentially reading the frames from the top-level FIFO. The drivers serialize the incoming frames and transmit the streams to the underlying hardware interface. Both the muRata SN8020 and Opal Kelly XEM6002 modules are treated as black box components. A Wi-Fi® and USB 2.0® stack were implemented in the SN8020 and XEM6002 respectively.

The designated applications compile the incoming streams back to frames and transfer the data to the analysis routines on the target device.

The UART2USB branch was tested up to a transmission speed of 15 Mbits per second without experiencing any major failures. Consequently, recovery and extended failure detection routines have been omitted.

The Wi-Fi® branch was tested in principle; however, there is no server application available at the current state of development and it is not part of this project.

3.2.4.4 Design Pattern for Serial Logic

Communication processes that involve serial logic do not correspond to the concurrent nature of the FPGA's architecture. Nevertheless, special design patterns have to be applied. One well-known and widely used pattern is based on a two-process architecture. First, a register transfer process is carried out to synchronize states, signals

and vectors to the clock signal because their condition may change during readout, assignment or some other action. The second step is an unsynchronized process in which the logic is defined as a finite state machine (FSM). The following source code illustrates a sample FSM fed by a 100 MHz clock with three states.

```
-- Register transfer process ------------------------------------------------------------
-----
register_transfer_process: process (sCLK_100MHZ, sUSER_RESET) is
begin
   -- Reset
        if rising_edge(sCLK_100MHZ) then
                if (sUSER_RESET = '1') then
                        -- reset state register
                else
                        -- state register update
                end if;
        end if;
        -- FFD registers clocked on rising edge, with no reset
        if rising_edge(sCLK_100MHZ) then
                -- signals and vector updat
        end if;
end process register_transfer_process;

-- Next state logic ---------------------------------------------------------------------
-----
next_state_logic: process (…all used signals) is
begin
   -- Assign default or previous signal, value or vector
FSM_state_register_next     <=      FSM_state_register_register
…
case FSM_state_register_register
        when S0 =>
                -- Logic of state S0
        when S1 =>
                -- Logic of state S1
        when S2 =>
                -- Logic of state S2

        when others =>
                -- Rescue state
end case;
end process next_state_logic;
```

The receive process of the ChipOx communication is described in greater detail in order to show the serial logic method in a concurrent architecture. It continuously reads the bytewise incoming data stream, detects frames, adds meta-information and stores it in the module-specific FIFO until each FIFO entry contains one valid frame. Figure 31 shows a simplified diagram of the embedded FSM with the following states: *Init* represents the reset and idle state; *Start* instantiates an internal buffer and adds meta-information; and *Valid* stores the subsequent bytes to the buffer until a frame is completed. Implementation details, such as timing exception, buffer overflow detection, frame errors and recovery from fault state are not shown. The incoming and outgoing signal lines or vectors are represented by the arrows. The input signals on the right-hand side are denoted with the suffix "_i" and the output signals on the right with the suffix "_o." The control signals are not shown.

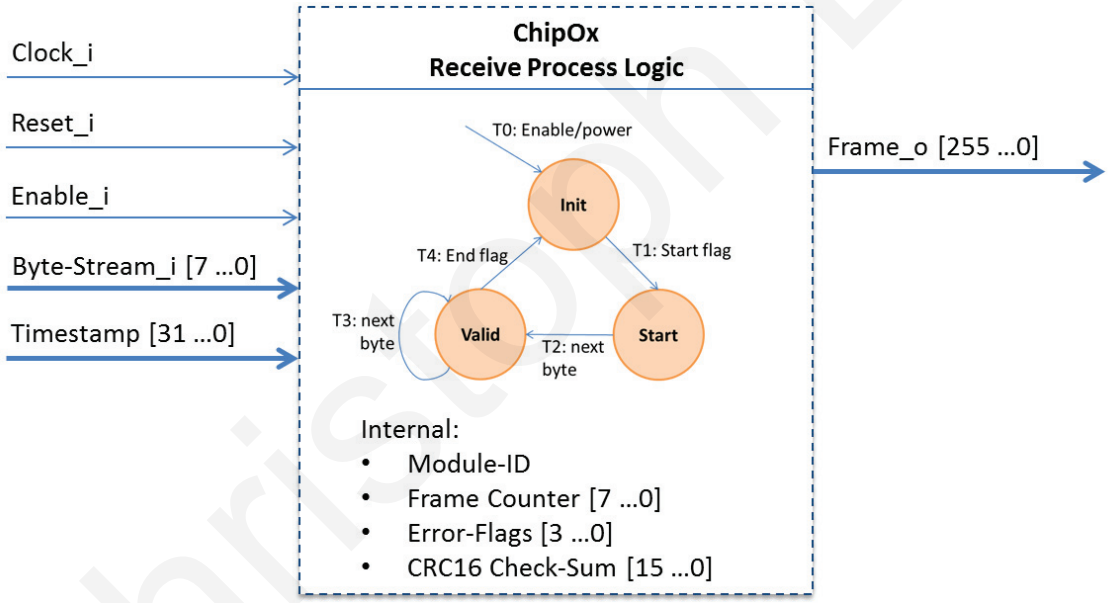

Figure 31: Finite state diagram of receive process of ChipOx module.

According to the ChipOx Technical Integration Manual, each frame starts with a one byte start flag (0xA8) and terminates with a one byte end flag (0xA9). [69] Apart from their respective dedicated purpose, these flags never appear in the communication and may therefore be used as a transition condition. Once enabled or reset, the FSM remains in the Init state and receives continuous incoming bytes. As soon as a start flag is detected, the FSM transits to the Start state, allocates the internal buffer, stores the module ID, timestamp, frame counter, error flags and transits to the Valid state. The FSM stores the

incoming bytes sequentially until an end flag is detected. Finally, the check sum is added to complete the frame and forwarded to the module-specific FIFO as shown in Figure 28. The receive process is part of the CO_ChipOx.vhdl file and takes 119 lines of code.

3.2.4.5 Fact Sheet Embedded Application

The current implementation has a strict modular architecture with 27 modules grouped in 5 horizontal layers. The VHDL logic is organized in 19 files following a top-down approach and comprises approximately 9500 lines of code. The configuration file resulting from the compilation takes about 38% of the resources available on the FPGA. It utilizes 34% of the number of slice registers, 68% of the number of slice LUTs (thereof 1% as memory) and 35% of the available I/O pins. Ten IP core instantiations provided by Xilinx® and two IP core instantiations provided by Opencore.org were used.

3.2.5 Task 9 – MATLAB® Processing and Analysis

A dedicated MATLAB® application was programmed to initiate, receive, analyze and present the human vital signs data recorded with the MCU. Figure 32 shows the General User Interface (GUI), which is arranged by the functional groups "*Recording," "Single Mic Analysis,"* "*Multi Mic Analysis"* and a "*Log"* in order to provide a clear design as well as self-explanatory instructions for the user.

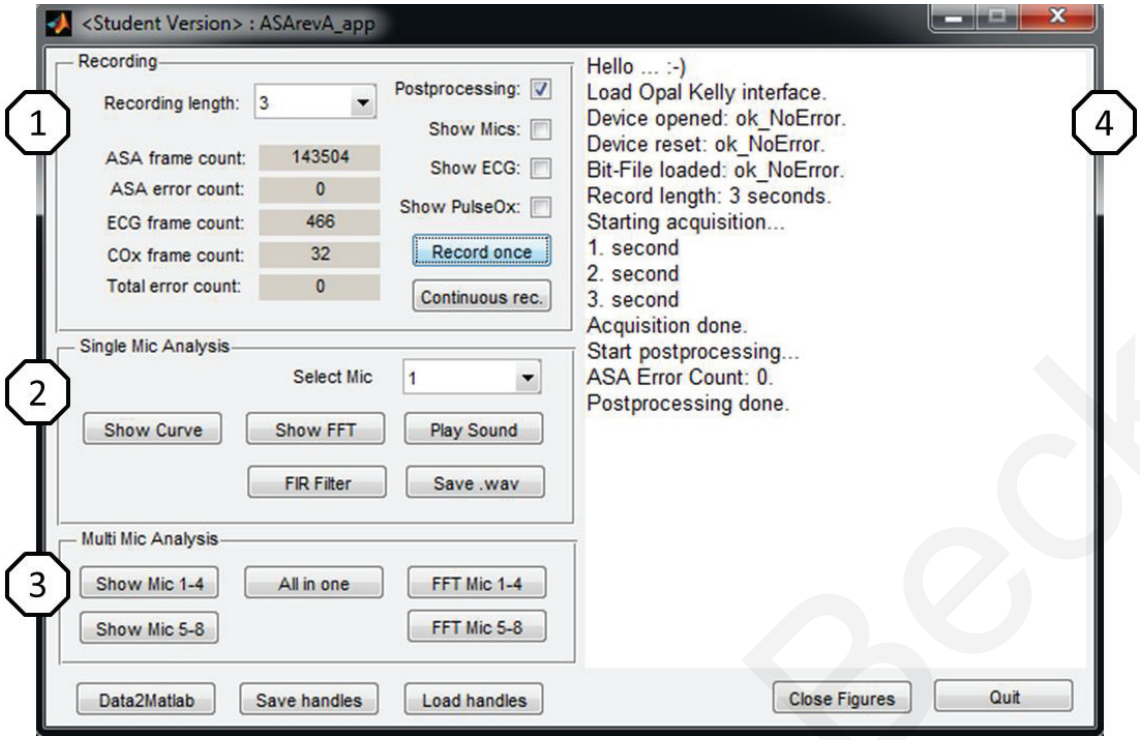

Figure 32: MATLAB® application with functional groups 1) *Recording*, 2) *Single Mic Analysis*, 3) *Multi Mic Analysis* and 4) *Log.*

Function Box 1 – Recording: In the first step, the user can select a recording time from the drop-down selection box "*Recording length*" of 1 to 120 seconds. Pressing the "*Record once*" button initiates a single recording with the selected duration, whereas the "*Continuous rec.*" button initiates continuous acquisition at the selected refresh rate. After completion, an integrity check is performed and the result is displayed in the "*Total error count*" text box. Finally, the protocol parsing routine extracts the frames and sorts the raw sensor data according to its origin, ASA, ECG and CO, and displays the amount of data available in the corresponding text box.

The user can select "*Postprocessing*" to initiate internal processing tasks for extracting sensor information from the raw data and providing it to the GUI. According to the settings the information can now be displayed. A Sensor Overview Figure and ASA Overview Figure were introduced, which allow the user to view the data as a graphical representation. The figures open or update depending on whether the user has selected "*Record once*" or "*Continuous rec.*"

Sensor Overview Figure: The most important graphical representation for a quick overview is shown in Figure 33. Diagram (1) shows one of the three ECG channels.

Diagram (2) shows the plethysmogram, which includes an information box with pulse, blood oxygen and signal quality. Diagram (3) shows one of the eight acoustic channels preselected by the user.

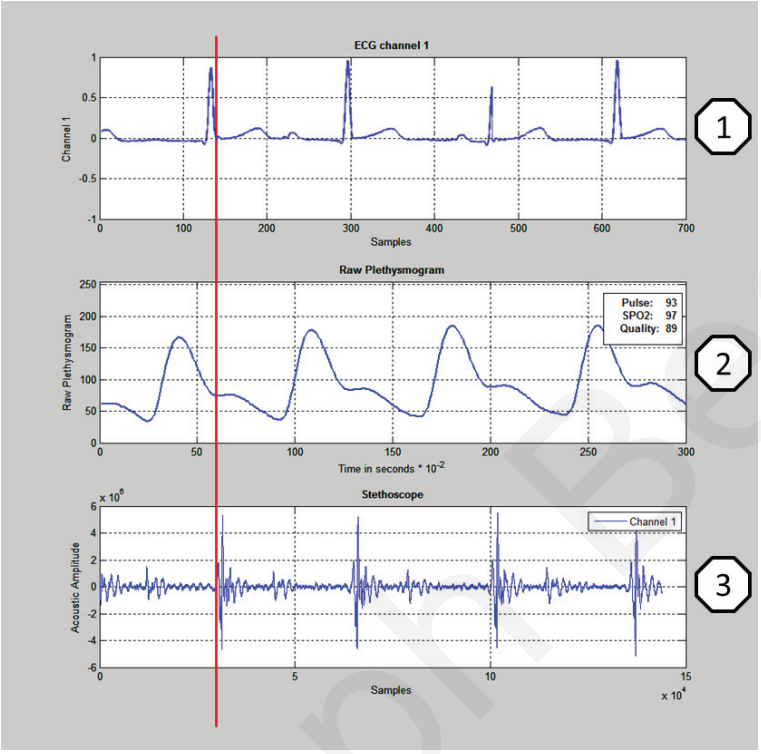

Figure 33: Sensor overview figure: diagram (1) shows one of the three ECG channels, diagram (2) shows the plethysmogram along with an information box with pulse, blood oxygen and signal quality, and diagram (3) shows one of the eight preselected acoustic channels.

ASA Overview Figure: A dedicated diagram was introduced in order to present a quick and reliable overview of all the acoustic channels. In particular, it shows sub-diagrams of the data streams of all the microphones and calculates basic statistical information for each channel, such as peak-to-peak value, mean value, and the percentile values of 5% and 95%. All the curves are displayed in blue under normal conditions and change to red if clipping is detected.

Figure 34 illustrates a three-second recording of six microphones. The frequent bursts represent the S1 acoustic pattern of the heart sounds. The stethoscope heads were applied at different locations on the subject's chest and back, which accounts for the deviating sound patterns of the recordings. Channel two is displayed in red because

clipping was detected. This was done intentionally by tapping the stethoscope's head once.

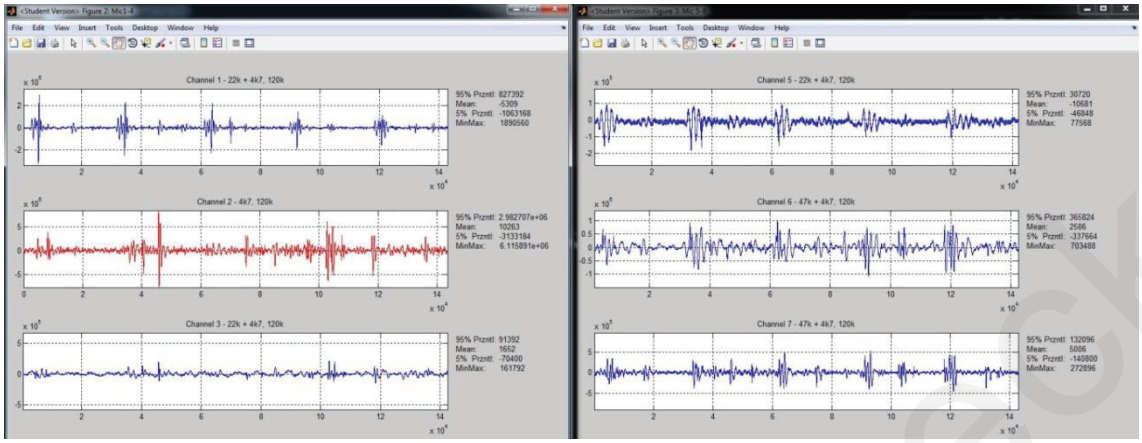

Figure 34: ASA overview figure showing sub-diagrams of the data streams of all the microphones along with basic statistical information for each channel.

Several dedicated diagrams display the information in detail depending on whether *"Show Mics," "Show ECG"* or *"Show PulseOx"* was selected by the user.

Functions Box 2 – Single Mic Analysis: Once the recording is successfully completed, the user can start analyzing a single microphone by pressing the button with the desired functionality. The application provides the following features:

- "Show Curve" draws the selected audio stream in a separate diagram. The user can zoom, measure or mark the data points (e.g., to visually investigate heartbeat patterns).
- "Show FFT" calculates and draws the Fast Fourier Transformation (FFT) of the selected microphone (e.g., to investigate spectral components).
- "FIR Filter" applies a Finite Impulse Response (FIR) filter to the audio stream of the selected microphone. The settings are defined in the corresponding source code and can be changed at any time during runtime.
- "Play Sound" plays back the recording of a single channel for analysis of the audible components. This is suitable for playing back an audio stream, applying an FIR filter and playing it back again. This feature gives a quick first impression of the quality of the system just by listening to it.

- "Save .wav" saves the audio stream to a disk in the widely used .wav file format (e.g., for offline analysis).

Functions Box 3 – Multi Mic Analysis: Special purpose diagrams were introduced in order to quickly verify the acoustic data (e.g., such as during an experiment).

- "Show Mic 1–4" and "Show Mic 5–8" draw either microphones one through four or microphones five through eight in separate diagrams and calculate the important parameters for each channel. In the case of clipping, the normally blue curves are displayed in red. This feature allows the quality of all channels to be assessed quickly and easily.
- "All in one" draws all the acoustic data streams in one diagram to estimate the interchannel time delays or gain differences.
- "FFT Mic 1–4" and "FFT Mic 5–8" calculate and draw the FFT of the data stream of all microphones.

For additional analytical operations not covered by this MATLAB® application, the internal data set can be transferred to the MATLAB® environment by pressing the *"Data2MATLAB"* button. Additional convenient features include the functionality to directly save and recall all internal variables to and from the local disk and simultaneously close all open diagrams at once.

Log: A log was introduced in order to show the status information of the MATLAB® application. The user can follow the application's behavior in real time and quickly troubleshoot any problems if it does not behave as expected.

3.3 Phase 3 – Characterization

Verifying and characterizing the entire system provides a reliable basis for subsequent analysis. The aim of this chapter is to show that every function implemented (e.g., heart sound acquisition, lung sound acquisition, ECG acquisition, etc.) works as intended.

Table 13: Phase 3 of design and implementation

Phase		Task	Status	
Phase 3 Test		Verification	All of the implemented modules have been verified successfully.	100%
		Characterization	The characterization tasks have been completed. The acoustic scene analysis based on this hardware yielded promising results.	100%
		Validation	Validation is completed. All of the required features are available and work as intended.	100%

3.3.1 Test – MCU Hardware

Summary: Five PCBs have been populated and various tests performed. Some corrections and improvements were implemented to address issues regarding initial operation to ensuring hardware reliability. This chapter provides a summary of the major bugs and improvements.

1. **Bug:** The TPS65708 power sequencer for the FPGA has a package with a sixteen-pin ball grid array (BGA). The small dimensions and pin-to-pin distance of just 0.15 mm [98] created fan-out vias for the inside pins. These vias were positioned directly underneath the pins but not filled with lead. As a result, the pins involved either did not connect to the vias or created a short circuit to neighboring ones. This was corrected by replacing all the components and filling the affected vias with lead.
2. **Bug:** The analog and digital ground layers were separated in order to reduce noise in the analog circuit as much as possible. A single TDK MPZ1608S221A ferrite bead [107], which is a common noise reduction solution, was used as a ground connection. Testing revealed that the design principle used did not

achieve the intended function and that multiple direct connections produced less ground noise.

3. **Bug:** The analog part of the circuit is supplied by an ultra-low noise 3.3 V linear dropout regulator (LDO). [108] Its 5.0 V version was accidentally populated providing a too high voltage. As soon as USB power was applied, the voltage stepped up to 5 V and destroyed the analog part of the ADCs. The LDO and affected ADCs were replaced.
4. **Improvement:** The microphones were intentionally placed at defined locations on the PCB in the initial design. The first tests resulted in very difficult, error-prone handling properties as well as significant acoustic noise. First, the stethoscope hoses were rather stiff and the hose-to-PCB connections had to withstand strong forces. Second, any contact to the hoses resulted in significant ambient noise. To remedy this issue, the microphones were placed inside the heads of the stethoscopes, the hoses were replaced by electrical wires and audio jacks were added to each channel. These modifications resulted in the following major improvements: 1) enhanced acoustic properties due to less ambient noise; 2) better handling properties due to the flexible and bendable wires; 3) greater flexibility due to the variable length of the wires; 4) increased adaptability to various settings, such as different stethoscope heads (e.g., for bell mode, diaphragm mode, etc.), due to the new concept involving the use of plugs.

In addition, minor changes and improvements have also been implemented, such as providing the ability to adjust the resistor and capacitor values, as well as change the hardware configuration by adding or removing pull-up or pull-down resistors. The comprehensive step-by-step device change protocol can be found in [109].

Result: A reliable and robust system.

3.3.1.1 Test – Power Supply and Consumption

Scope: The MCU is a mobile unit designed to run on battery. Therefore, the main objective of this test is to obtain the battery life cycle and charge time, which are the two most important parameters.

Test description: The following measurements were carried out in order to achieve the main objective of this test and further characterize the charge/discharge behavior and basic consumption properties of both the MCU and the battery:

1. Total power consumption from the battery at full acquisition
2. Total power consumption from USB at full acquisition
3. Charge current
4. Battery life cycle
5. Charge time

Test setup: A custom board as shown in Figure 35 holding a 0.142 Ohm resistor with 1% tolerance was used to measure the current consumption from the battery. The current was obtained based on the voltage drop over the resistor using Ohm's law.

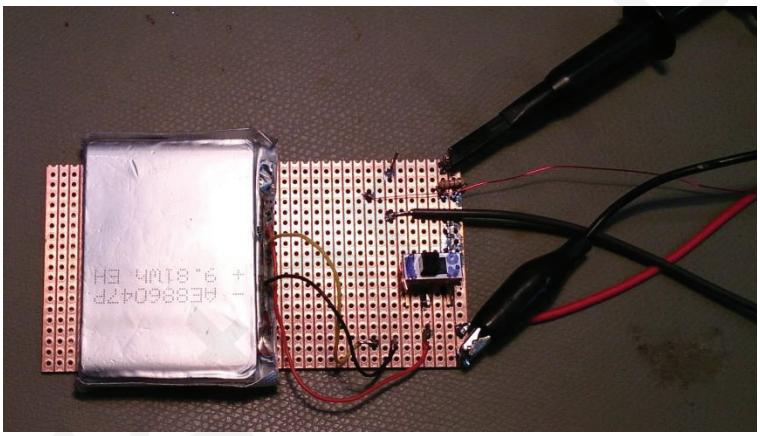

Figure 35: Custom board to measure current and power consumption with a 0.142 Ohm resistor (1% tolerance) between lithium ion battery and PCB.

According to the U/I charging implementation of the PMU, the charge current is kept constant at the maximum level until 4.2 V is reached. [96] Afterwards, the voltage is kept constant by decreasing the current; thus, the maximum charge current can be obtained as long as the voltage potential of the battery is lower than 4.2 V.

Another custom board as shown in Figure 36 holding a 0.142 Ohm resistor with 1% tolerance was used to measure the overall current consumption drawn from the USB supply. The current was obtained based on the voltage drop over the resistor using Ohm's law.

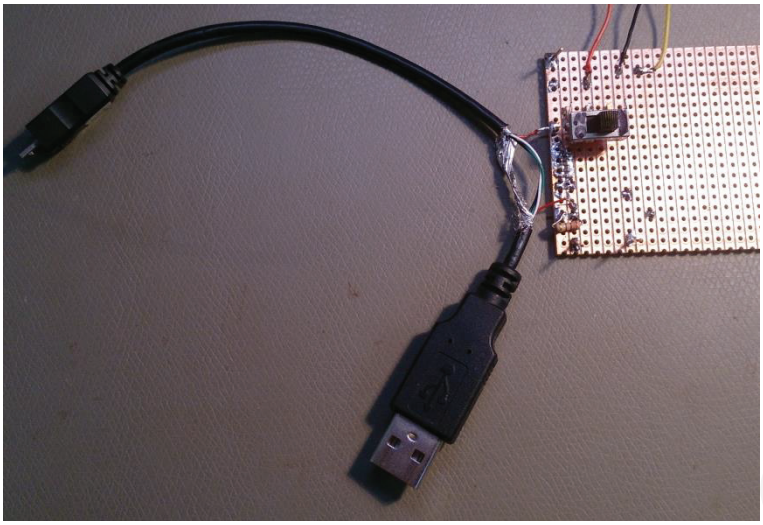

Figure 36: Custom board to measure current and power consumption with a 0.142 Ohm resistor (1% tolerance) between USB 2.0 port and PCB.

Test results: The test was executed according to the description above. All the results were successfully measured or derived and are listed in Table 14.

Table 14: Test objectives and results related to power supply and consumption

Objective	Description	Result
Total power consumption of MCU in battery mode	Current drawn by the MCU at full acquisition from the battery at an average of 3.8 V measured via the voltage drop over a 0.142 Ohm resistor with 1% tolerance	I = 130 mA P= 494 mW
Total power consumption from USB	Current drawn from USB by MCU at full acquisition and charging at 5 V measured via the voltage drop over a 0.142 Ohm resistor with 1% tolerance	I = 240 mA P = 1200 mW
Charge current	Maximum battery charge current from USB by MCU at full acquisition measured via the voltage drop over a 0.142 Ohm resistor with 1% tolerance	I = 185 mA
Battery life cycle	Time until battery is empty and recharge necessary as measured with a stopwatch while the MCU is acquiring data	6:43 h:mm
Charge time	Time of one charge cycle measured with a stopwatch	4:53 h:mm

Discussion: The power consumption of the MCU in battery mode did not include wireless communication, thus it does not give the entire picture. Based on the datasheet, the estimated additional consumption caused by the wireless interface

ranges from 50 mW to 90 mW depending on module selection, traffic and distance. This additional consumption would further decease the battery's charge cycle.

Power consumed from a USB 1.0 host was measured with 1200 mW even though the client should limit it to 1000 mW. This indicates that the existing capabilities were more than exceeded. A proper handshake implementation according to USB 2.0 would increase the allowed consumption to 2500 mW, or even up to 10 W for a custom solution, and provide the highly necessary enhancement. [110]

The system has a lithium polymer battery pack with 1200 mAh at 5 V. The theoretically achievable charge cycle at a given consumption of 130 mA at 3.8 V should last longer than 10 hours. This indicates that the existing capabilities are not fully used yet.

Improving the abovementioned issues would also result in a shorter charge time.

3.3.1.2 Test – Programming and Configuration

Scope: The default settings of the FPGA are defined by the source code. The configuration interface offers commands to reconfigure the various settings in order to preserve flexibility. The MCU is set to the default settings whenever the power supply is interrupted.

Test description: The hardware can be configured using the dedicated configuration interface as described in chapter 3.2.4. All the commands as well as the corresponding acceptance criteria and final results are listed in Table 15.

Test procedure: Table 15 describes the test procedure. Each row represents one command.

Table 15: Test protocol for verification of programming and configuration commands

Test	**P = Procedure** **A = Acceptance criteria**	**Result**
Module: general		
Readout LED status	P: Send command A: Output reflects status of LEDs	**pass**

Test	P = Procedure A = Acceptance criteria	Result
Set LED status	P: Send command to set and reset each LED A: LED status changes according to input	**pass**
Readout dip switch states	P: Send command A: Output reflects status of dip switches	**pass**
Application layer: mirror input data stream (debug command)	P: Send command files: speedtest_16kByte.hex speedtest_32kByte.hex speedtest_64kByte.hex A: Output matches input	**pass**
Physical layer: continuous transmission test	P: Send command files: speedtest_640kByte.hex speedtest_2560kByte.hex A: Transmitted data is similar to received data	**pass**
Module: analog front end		
Power-up analog front end	P: Send command A: Power-up procedure is as follows: Reset ADC1 = low Reset ADC2 = low ADC_MCLK = 12 MHz Default configuration of ADC1 successful Default configuration of ADC2 successful	**pass**
Power-down analog front end	P: Send command A: Power-down procedure is as follows: Reset ADC1 = high Reset ADC2 = high ADC_MCLK = off	**pass**
Enable continuous data acquisition	P: send command A1: Timestamp module starts A2: The following modules start sending data framewise	**pass**

Test	P = Procedure A = Acceptance criteria	Result
Disable continuous data acquisition	P: Send command A1: Timestamp module stops A2: The following modules stop sending data	**pass**
Enable artificial data	P: Send command A1: Continuous data stream w/predefined data A2: Output is similar to predefined data	**pass**
Disable artificial data	P: Send command A: Continuous data stream w/real values	**pass**
New configuration to ADC1	P1: Send command w/new configuration to ADC1 P2: Readout configuration of ADC1 A: Readout similar to sent configuration of ADC1	**pass**
New configuration to ADC2	P1: Send command w/new configuration to ADC2 P2: Readout configuration of ADC2 A: Readout similar to sent configuration of ADC2	**pass**
New configuration to ADC1+2	P1: Send command w/new configuration to ADC1+2 P2: Readout configuration of ADC1+2 A: Readout similar to sent configuration of ADC1+2	**pass**
Module: EMB3/6		
Power-up EMB3/6	P: Send command A: Power-up procedure is as follows: Reset pin of EMB3/6 = low Configuration of EMB3/6 successful Module is in idle state (no acquisition)	**pass**
Power-down EMB3/6	P: Send command A: Power-down procedure is as follows: Reset EMB3/6= high Module is in reset state	**pass**

Test	P = Procedure A = Acceptance criteria	Result
Enable continuous data acquisition	P: Send command A: Enable procedure is as follows: Enable FIFOs Enable Module_Timestamp Transmission according to definition	**pass**
Disable continuous data acquisition	P: Send command A: Disable procedure is as follows: Reset FSM_receive Reset FIFOs Disable Module_Timestamp	**pass**
Enable artificial data	P: Send command A1: Continuous data stream w/predefined data A2: Output is similar to predefined data	**pass**
Module: ChipOx		
Power-up ChipOx	P: Send command A: Power-up procedure is as follows: Reset ChipOx = low Configuration of ChipOx successful Module is in idle state (no acquisition)	**pass**
Power-down ChipOx	P: Send command A: Power-down procedure is as follows: Reset ChipOx = high Module is in reset state	**pass**
Enable continuous data acquisition	P: Send command A: Enable procedure is as follows: Enable FIFOs Enable Module_Timestamp Transmission according to definition	**pass**

Test	**P = Procedure** **A = Acceptance criteria**	**Result**
Disable continuous data acquisition	P: Send command A: Disable procedure is as follows: Reset FSM_receive Reset FIFOs Disable Module_Timestamp	**pass**
Enable artificial data	P: Send command A1: Continuous data stream w/predefined data A2: Output is similar to predefined data	**pass**
Module: TSIC306		
Power-up TSIC306	P: Send command A: Power-up procedure is as follows: Reset TSIC306= low Module is in idle state (no acquisition)	**pass**
Power-down TSIC306	P: Send command A: Power-down procedure is as follows: Reset TSIC306= high Module is in reset state	**pass**
Enable continuous data acquisition	P: Send command A: Enable procedure is as follows: Enable FIFOs Enable Module_Timestamp Transmission according to definition	**pass**
Disable continuous data acquisition	P: Send command A: Disable procedure is as follows: Reset FSM_receive Reset FIFOs Disable Module_Timestamp	**pass**

Test	P = Procedure A = Acceptance criteria	Result
Module: microSD® card		
Reset card (delete content)	P: Send command A: Reset procedure is as follows: Set reset pin Reset module FSM Delete internal variables Set card back to initial state	**pass**
Enable recording	P: Send command Acquired data from analog front end, ECG, PulseOx and temperature sensor will be stored on the card. A: Recorded data is similar to directly transmitted data (via debugging interface)	**pass**
Disable recording	P: Send command A: Acquisition stops	**pass**
Write/read predefined content to card	P1: Write content generated on the FPGA to the card P2: Write content stored on the FPGA to the card P3: Write content transmitted via USB on the FPGA to the card A: Data from source must equal data at destination	**pass**
Readout specific data blocks from card (with given start and end address)	P: Send command Read content from the card from start to end address. A: Content from card must equal received data	**pass**

Test result: All the abovementioned tests were performed successfully. Implementation of the microSD® card required some manual access and dedicated debugging routines because not all of the required functions were available.

Discussion: The successful completion of the tests, which basically covered the hardware functionality of the MCU and communication interface, shows that both components perform very well.

3.3.1.3 Test – Test Setup and Startup Routine

Scope: A default configuration and startup routine was defined and tested in order to have a properly working and reliable system for all tests. The main objective was to provide a system that is compatible with any Windows 7 PC with MATLAB® 2011 or higher and ready for acquisition without any additional configurations once the power supply is established.

Test description: The power supply and communication is realized via a USB 2.0 connection in order to keep handling as simple as possible. The startup routine is defined as follows and sequentially executed once the USB plug is connected:

1. MCU: power FPGA circuit
2. MCU: set global clocking
3. MCU: enable acquisition modules
4. ADC1/2: initialize and set default configuration
5. EMB3/6: initialize and set default configuration
6. ChipOx: initialize and set default configuration
7. TSIC306: initialize and set default configuration

The sequential execution is implemented in the processes *proc_init_reg* and *proc_init_next* in *TOP.vhd*. No additional driver needs to be installed on the host computer.

Test setup: The setup involves a computer with Windows 7® Professional Service Pack 1 running MATLAB® R2013a Student Version with the herein developed script and figure with date code 2014/03/13, MCU with embedded software date code 2014/03/10 and hardware revision A. The hardware was embedded in a robust case in order to protect the MCU and corresponding circuits. As shown in Figure 37 all connectors are pluggable and a 3 m USB 2.0 cable was used to ensure a high degree of mobility.

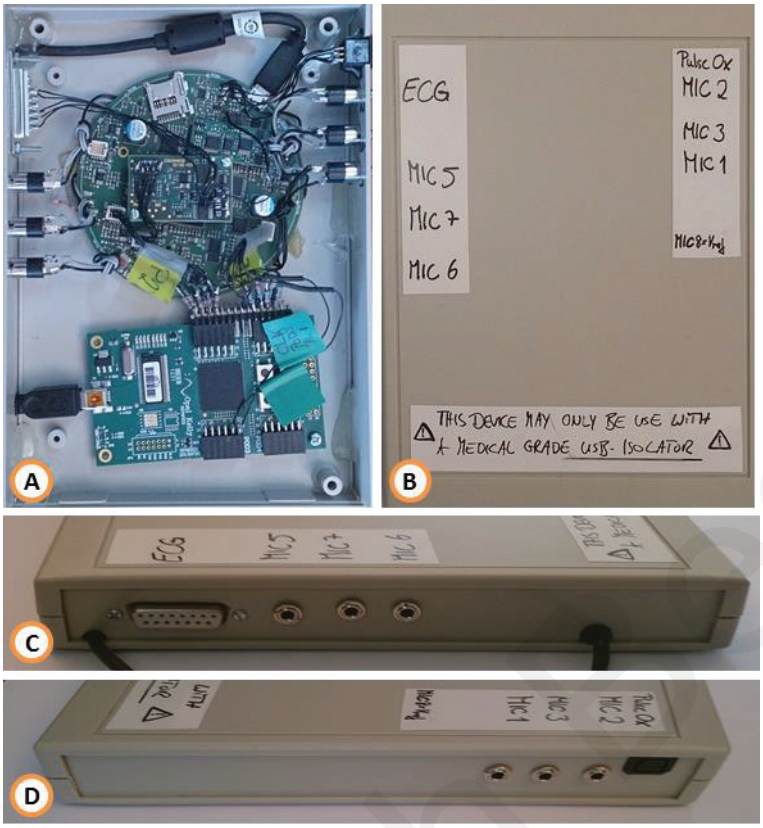

Figure 37: A) MCU and Opal Kelly board embedded in a robust housing; B) front side of the housing with self-explanatory labeling; C) left side with plugs for ECG and channels 5 to 7; D) right side with plugs for PulseOx and channels 1 to 3.

Test procedure: The system is plugged into a PC that fulfills the requirements stated in the scope. Recording is started once the MCU indicates the defined operational state. The recording is considered successful if correct data from all the MCU acquisition units is received. The recordings are repeated with varying durations ranging from 1 to 120 sec. in 10 steps.

Test result: The startup routine and acquisition process were tested successfully. The MCU indicated the defined operational state with a specific LED pattern and there were no failures with the startup routine. The reliability of the recordings decreased as the recording duration increased. While no failure occurred at durations of 1 to 40 sec., one failure occurred at 60 sec. and two at 120 sec. Detailed results are available in the test protocol. [111]

Discussion: During this test no startup errors occurred, thus this routine is highly reliable. The increased communication failure rate at recording with longer durations

indicates that there are timing issues at the USB 2.0 interface, which is controlled by the PC. Once the received data exceeds a certain volume, data handling slows down the PC's processor, which increasingly impedes the acquisition of new data. This behavior greatly depends on the PC's performance. One way to resolve this issue would be to install a multithreading application. With this technique, an independent thread receives the incoming data stream while another stores it sequentially. Unfortunately, the MATLAB® IDE used does not support multithreading.

3.3.1.4 Test – Timing Verification of ADC Samples

Scope: A dedicated test was performed to verify the system's sound acquisition timing behavior with attached patient leads. The main objective was to prove that the implementation samples all the acoustic channels simultaneously and maintains its integrity until the data is displayed in the MATLAB® application. In summary, this involves the analog-to-digital conversion, ADC control, data readout, on-board processing, transmission and finally analysis and display on the computer. The system is expected to perform as intended if the measurements, which are compared to a reference value, result in an error that is smaller than half the sampling period of the MCU.

Test setup: The test setup involved three stethoscope heads placed equidistant from a metronome. The sound waves passed through each stethoscope head and induced responses. The MCU recorded the repeating acoustic stimuli continuously and transmitted it to the MATLAB® application. A scope acquired the voltage potential at the output of the first and third microphones as a reference. Figure 38 illustrates the schematic test setup.

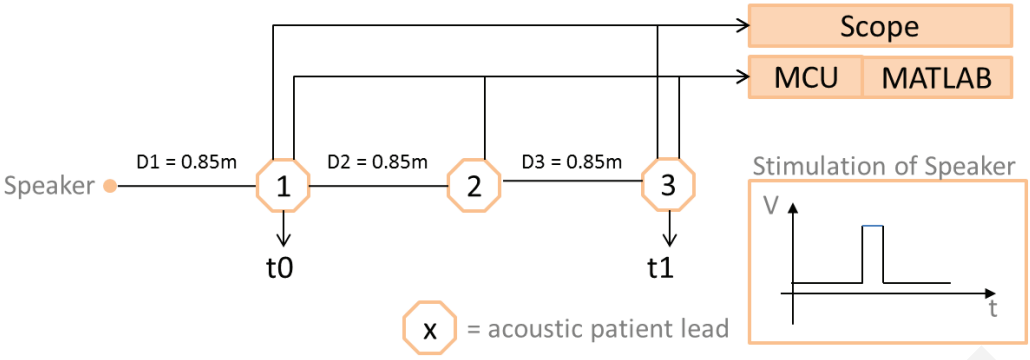

Figure 38: Schematic test setup to verify the MCU's acoustic performance.

Test procedure: The metronome had a clock pulse of 0.5 Hz in order to ensure one complete acoustic stimuli within a one second recording period. Each measurement involved simultaneous recordings performed with the MCU and scope respectively. The first peak of the first complete acoustic stimuli was identified in each channel using the MATLAB® command *max()* and the difference was logged. The scope software Picoscope 6 provided rulers to measure and log the time difference between the two signals. Ten repetitions were performed.

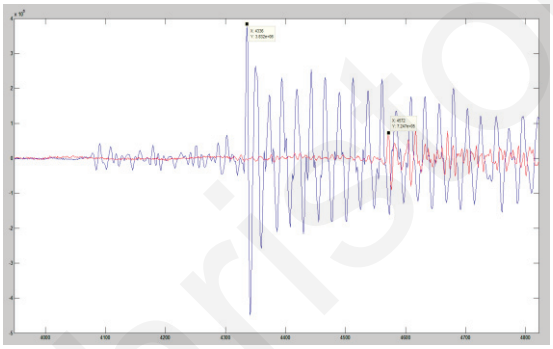

Figure 39: MATLAB® plot of time difference between channel one and three in the sampling period steps recorded by the MCU.

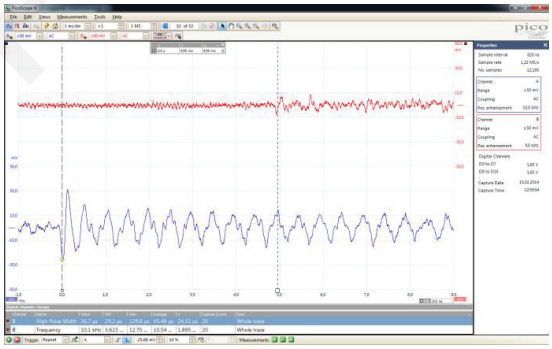

Figure 40: Scope plot of time difference between channel one and three recorded in microseconds with a scope.

Test result: The sound wave of all ten repetitions was successfully acquired with both paths and the first peak was identified in the described manner.

MCU: The first measurement based on the MCU is shown in Figure 39. The blue curve corresponds to channel one (microphone A), whereas the red curve corresponds to channel three (microphone D). The MCU's ADCs sample at 48.000 Hz, thus each

sampling period equals a time period of 20.833 µs. Adding all the ADC counts between t0 and t1 yields a mean value of 235.5 counts and results in a sound wave travel time of 4906.24 µs.

SCOPE: The measurements based on the scope are shown in Figure 40. The blue curve corresponds to microphone A (channel one on MCU), whereas the red curve corresponds to microphone D (channel three on MCU). The measured overall travel time from t0 to t1 yielded a mean value of 4908.8 µs.

The time deviation from MCU to scope is 2.56 µs. The requirement for a successful test was defined as an error smaller than half the sampling period of the MCU, which is 10.416 µs. Since the measured error is below this requirement, it can be concluded that the system works as intended and that all samples are acquired simultaneously.

Discussion: This test focused on verification of the timing requirements of ADCs as the most critical components within the given objective. The performed test did not include all channels even though a comprehensive conclusion is still possible based on the result and the software architecture. Characterizing the system's timing performance to a higher extent would be necessary, if tighter requirements were defined for applications beyond the scope of this project. Since the system's architecture is strictly modular, concurrent extended functionality, such as time error compensation for each channel, is well within the achievable capability of this hardware.

3.3.2 Test – Heart Sounds

Scope: The main objective of this test is to prove the functionality of the system's heart sound recording and allow basic characterization.

Test description: The test was performed with one subject at rest as well as with an increased pulse rate of more than 100 beats per minute. The stethoscope heads were placed on the four locations defined in chapter 2.6.1. Ambient noise was avoided as much as possible in order to ensure reliable results. The system's performance was considered sufficient if the following results were achieved:

1. The pulse rate was recorded 10 times for 30 seconds: 5 times at rest and 5 times at an increased rate of more than 100 beats per minute.
2. The amplitudes of the first heart sounds (S1) were within 30% to 100% of the range of the analog acquisition path.
3. No major artifacts deteriorated the recordings.
4. No major clipping was detected.
5. The first and second heart sounds could be determined through visual inspection.
6. The first and second heart sounds could be audibly determined during playback.

Test setup: The setup involved a computer with Windows 7® Professional Service Pack 1 running MATLAB® R2013a Student Version with the herein developed scripts and figures with date code 2014/03/13, MCU with embedded software date code 2014/03/10 and hardware revision A. Figure 41 depicts the block diagram of the test setup.

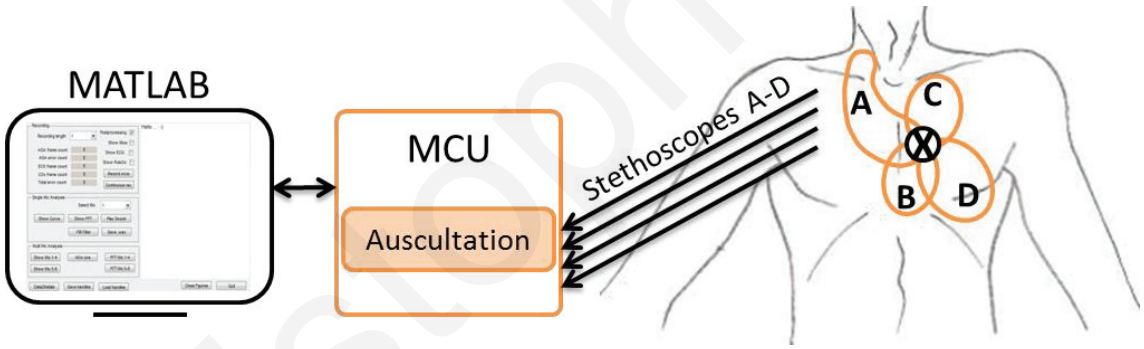

Figure 41: Block diagram of test setup for multichannel heart sound acquisition.

The electronic parts of the MCU were embedded in a robust, shock, dust and splash water resistant housing, which the subject wore at the hip. All the sensors were pluggable and allowed a high degree of mobility during the test procedure. The unit was attached to the PC with a common USB 2.0® connection cable. The stethoscope heads were attached to the chest according to the projection of the heart sounds as shown in Figure 42. The same pattern was used for defining both the labels and locations of the stethoscope heads.

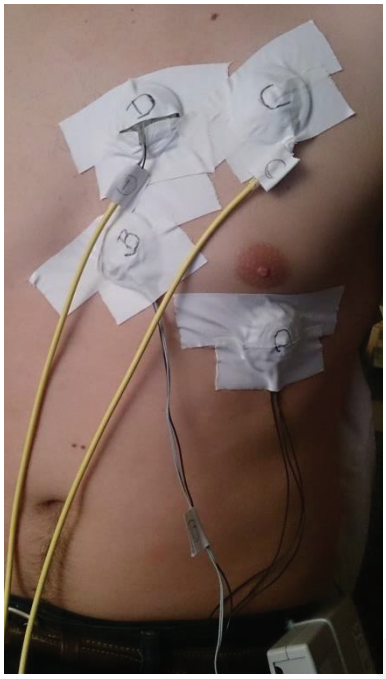

Figure 42: Stethoscope placement according to location definition.

The subject was asked to remain quiet and still during the recording process in order to minimize disturbances due to ambient noise or movement. The subject was then asked to do knee bends, sit-ups and push-ups in order to increase the pulse rate until it reached more than 120 beats per minute.

Test procedure: The recordings were performed as described in the test description according to the following procedure:

1. The subject was attached to a test bench according to the definition.
2. A three-second test recording of the setup was made.
3. The pulse rate was recorded 5 times for 30 seconds while the subject was at rest.
4. The pulse rate was recorded 5 times for 30 seconds at an accelerated rate of more than 100 beats per minute.

The measurements were visually checked for consistency and stored in a local database.

Result: The recordings at rest and after exercising were performed successfully and stored in a local database. Figure 43 shows the parts of a 30-second recording of all stethoscopes placed on the subject at rest.

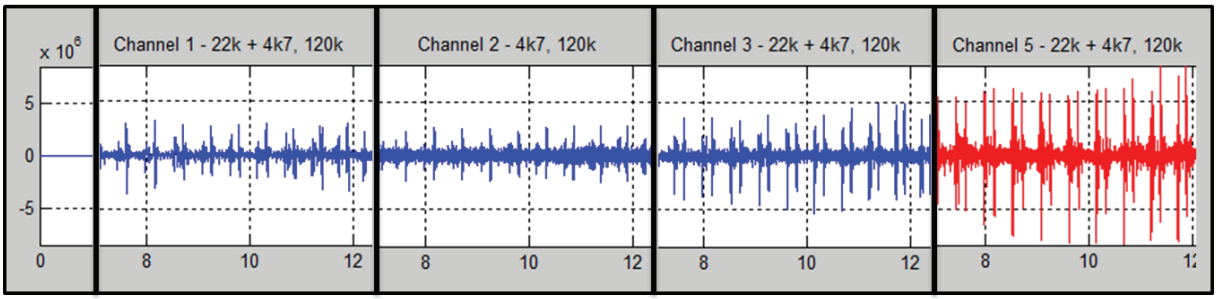

Figure 43: Output of stethoscopes placed at described locations with the following microphone-to-channel mapping: Channel 1 -> Stethoscope B, Channel 2 -> Stethoscope C, Channel 3 -> Stethoscope D, Channel 5 -> Stethoscope A.

The amplitudes of channel one, two and three stayed well within the defined margin while channel five experienced minor clipping. In general, auscultation of the mitral valve at location D produced the loudest results. A slight rise in sound intensity in all channels was experienced when the beats per minute increased. The heart sounds S1 and S2 were visible and audible in all channels. The best results were produced in a silent environment when the subject was still. Major clipping was detected while the subject talked, coughed, touched the stethoscope heads or moved around. If any of the above mentioned situations occurred, the recordings were repeated. In real-world scenarios three countermeasures are possible:

1. In the recent implementation all acoustic channels are connected to custom designed electronic stethoscopes that face the patient. One acoustic channel could be used to record the ambient noise by directing it towards the environment. Today, powerful noise cancelling algorithms exist that can be used to optimize the output.
2. The analysis does not rely on single events rather than on continuous and repeating acoustic phenomena. Thus, sporadic interference does only affect single phenomena and continuous interference does also affect the periods between the phenomena of interest. Therefore it should be possible to identify and filter those adverse sounds.
3. The recent implementation is based on fixed gain amplification. Next generation devices will consider variable gain amplification.

Discussion: The test performed as expected in the laboratory environment. All input requirements were met. In order to cope with an outdoor environment with non-specific ambient noise, an adaptive gain control would be necessary to keep the recordings within the given dynamic range of the system. In addition, the stethoscope heads were placed on the subject using medical tape. The next step has to include a more reliable method of fixation, such as a heads with self-adhesive pads – possibly combined with a temperature sensor and ECG electrodes.

3.3.3 Test – Lung Sounds

Scope: The main objective of this test is to prove the system's lung sound recording functionality based on vesicular sounds and allow basic characterization. It is known from literature that inspiration takes longer than expiration, that there is no gap between inspiration and expiration and that it is heard or recorded best at bases of lungs.

Test description: The test was performed with one subject at rest according to a predefined breathing plan. The recording time chosen was no longer than 10 seconds in order to prevent breathing problems or dizziness of the subject. A single stethoscope head was placed on location "D" (bases of lungs) as defined in chapter 2.6.2.

Ambient noise was avoided as much as possible in order to ensure reliable results. The system's performance was considered sufficient if the following results were achieved:

1. The lung sounds were recorded 5 times for 10 seconds according to a predefined breathing plan.
2. Inhalation and exhalation could be audibly determined during playback.
3. The amplitude of the recorded signal stayed within 30% to 100% of the range of the analog acquisition path.
4. No major artifacts deteriorated the recordings.
5. No major clipping was detected.

The frequency range of inhalation and exhalation is known to be as low as 15 to 40 Hz with very low amplitude and a duration of >1.5 seconds. Thus, unlike heart sounds,

visual identification of the acoustic phenomena associated with lung sounds is not possible.

Test setup: The setup involved a computer with Windows 7® Professional Service Pack 1 running MATLAB® R2013a Student Version with the herein developed scripts and figures with date code 2015/01/20, MCU with embedded software date code 2014/03/10 and hardware revision A. Figure 44 depicts the block diagram of the test setup.

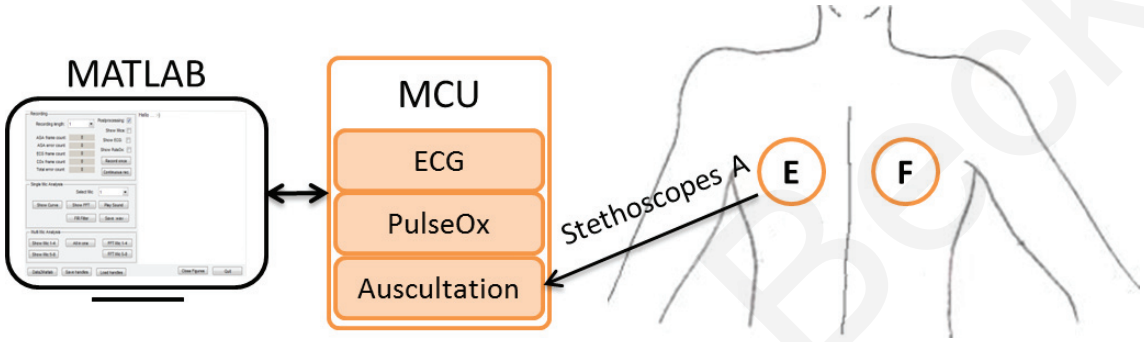

Figure 44: Block diagram of test setup for single channel lung sound acquisition.

The electronic parts of the MCU were embedded in a robust, shock, dust and splash water resistant housing, which the subject wore at the hip. All the sensors were pluggable and allowed a high degree of mobility during the test procedure. The unit was attached to the PC with a common USB 2.0® connection cable. The stethoscope head was attached to the chest according to the projection of lung sounds as discussed in chapter 2.6.2 Lung Sounds. The subject was at rest and asked to remain quiet and still during the recording process in order to minimize disturbances due to heart sounds, ambient noise or movement.

Test procedure: The recordings were performed as described in the test description according to the following procedure:

1. The subject was attached to a test bench according to the definition.
2. A three-second test recording of the setup was made.
3. A ten-second recording was made while the subject followed the predefined breathing plan.
4. A one minute pause was allowed in case the subject experienced breathing problems or dizziness.

5. Steps three and four were repeated until at least five successful measurements were obtained.

Each recording was played back to verify that inhalation and exhalation was audible and then stored in a local database.

Result: The recorded signals were free of clipping or short-term artifacts due to talking, coughing, touching the stethoscope head or moving around. As expected, it was not possible to visually identify any pattern even though the timing was known. Inhalation and exhalation sound patterns have low amplitude, which resulted in a high level of noise on the recordings and partly deteriorated the signal.

A single-sided amplitude spectrum of the complete recording time was calculated for a visual feedback, with the expectation that the dominant frequencies occur at the ranges known from the literature (Figure 45). With the blue curve, which represents the unfiltered spectrum, the dominant components are difficult to identify. The red curve on the other hand, which represents a low-pass filtered signal, provides better insight. It can therefore be assumed that the two dominant frequency components are at around 15 Hz and 37 Hz, which confirms the findings from the literature for normal breathing.

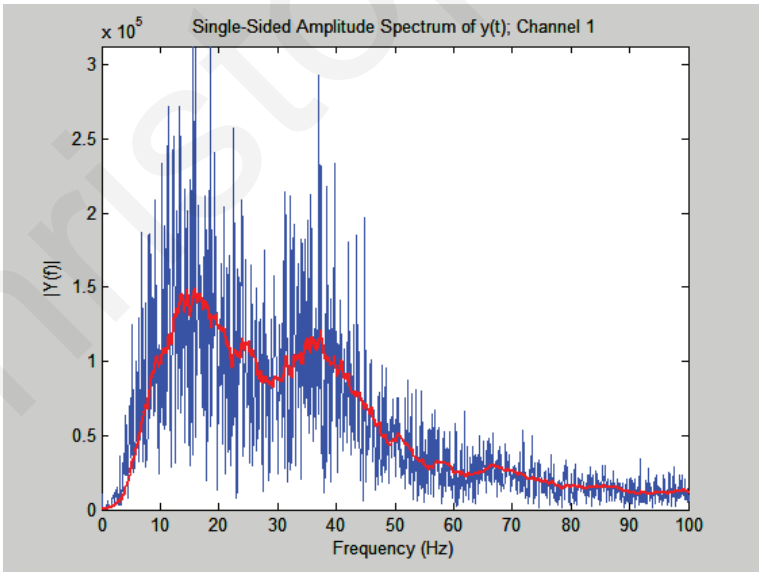

Figure 45: Single-sided amplitude spectrum over a lung sound acquisition period of ten seconds: unfiltered (blue curve) and low-pass filtered (red curve).

Discussion: The test performed as expected in the laboratory environment. All the input requirements were met. Further tests are needed to determine the full capabilities and

limitations of the system not only for vesicular sounds. The R.A.L.E. respiratory sounds database providing various physiological and pathological breath sounds may be one way to carry on further investigations while improving the MCU, e.g., in a second generation project. [112] A systematic review of a computerized lung sound analysis was published by A. Gurung et al., which may be a good starting point for a subsequent algorithm design. [113]

3.3.4 Test – ECG Acquisition

Test description: The purpose of this test was to verify the functionality of the herein developed ECG hardware implementation, data transmission and display. The heart rate and ECG were compared against Corscience's EMB3/6 ECG development kit. Both systems recorded the same subject consecutively using the same electrodes and keeping the subject's condition as constant as possible.

Test setup: Figure 46 depicts the block diagram of the test setup involving the *MCU* part (upper branch), the *Corscience* part (lower branch) and a common part (patient leads).

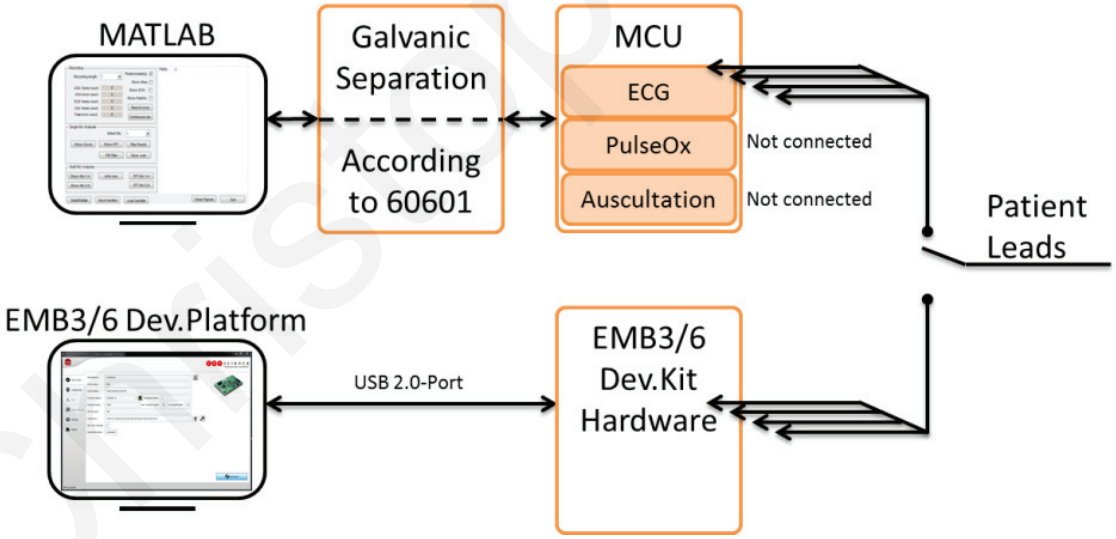

Figure 46: Block diagram of test setup for MCU ECG verification.

The four ECG adhesive pads of each set were cut in half and reassembled with their counterparts using two connectors and carefully making sure that the gel containing sponges touched in order to ensure the same potential at both leads. The custom pads were placed on the locations specified in Corscience's EMB3/6 user manual.

The MCU test setup is shown in Figure 47-1 and involved a computer with Windows 7® Professional Service Pack 1 running MATLAB® R2013a Student Version with the herein developed scripts and figures with date code 2014/03/13, IFTOOLS ISOUSB® (a medical grade galvanic USB separation device), and the herein developed MCU with embedded software date code 2014/03/10 and hardware revision A. The electronic parts were embedded in a robust, shock, dust and splash water resistant housing, which the subject wore at the hip. The sensors were pluggable and allowed a high degree of mobility during the test procedure. To guarantee high bandwidth and a reliable transmission the unit was attached to the PC with a common USB 2.0® connection cable (with galvanic separation). The direct connection simplified the setup in accordance with the experiment's focus. In later experiments the wireless connection can easily be used once transmission is verified, stable and the amount of (raw) data is reduced.

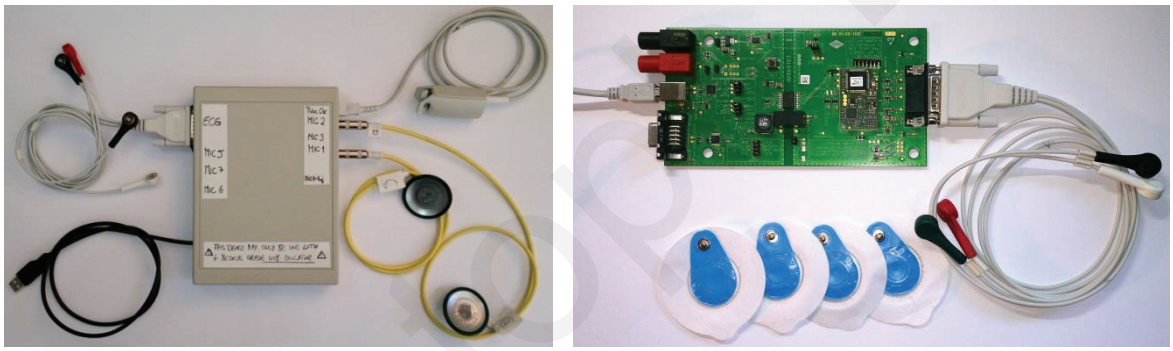

1) 2)

Figure 47: 1) MCU test setup with electronic parts embedded in a robust, shock, dust and splash water resistant housing; 2) Corscience test setup with EMB3/6 development kit with USB 2.0® connection to PC, patient leads and self-adhesive pads.

The Corscience test setup is shown in Figure 47-2 and involved a computer with Windows 7® Professional Service Pack 1 running Corscience's EMB3/6 ECG Development Platform Software Version CS5007C. Corscience's development kit hardware was attached to the PC with a USB 2.0® connection cable.

Measurement: Parallel recordings with both the custom made system and with Corscience's were successfully performed. The recordings were started and stopped manually. The subject was asked to quickly touch a 35 V power supply two times at the beginning of each recording in order to verify signal alignment based on a unique event. The marker is clearly visible in both recordings and thus creates a precise marker. At half

the recording time, the subjects were asked to move for one second to generate minor artifacts.

Both setups were programmed to have the same settings, such as sampling rate, no filters and raw data output, to mention just a few examples. The output was stored and manually imported to MATLAB®.

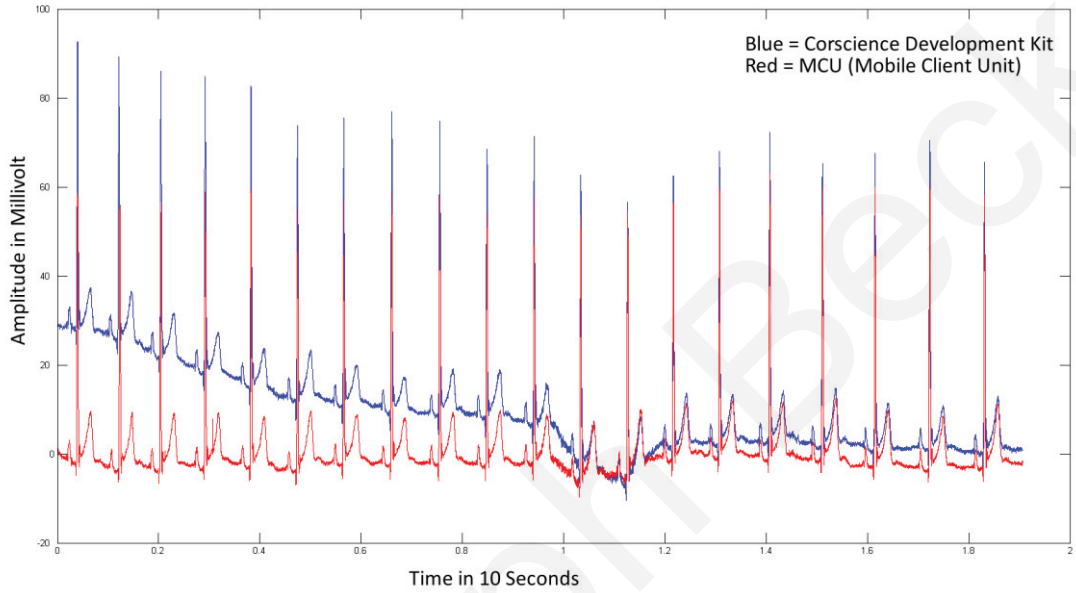

Figure 48: Synchronous recording of ECG with both the Corscience development kit (blue) and MCU (red).

The measurements illustrated in Figure 48 show a high correlation even though the *Corscience* test setup needs about 10 seconds to approach the same level. The artifact is located at second 10 to 12 (1 to 1.2 on the scale).

Result: A comparison showed that both systems were synchronous with respect to timing, amplitude and reaction to an induced movement artifact at 10 to 12 sec., but differed with respect to gain. With respect to the result, the blue signal was preprocessed with the MATLAB® function *"detrend"* to eliminate the offset, whereas the vector was divided into five "linear" parts to yield the best results. Figure 49 illustrates both curves after postprocessing in MATLAB®.

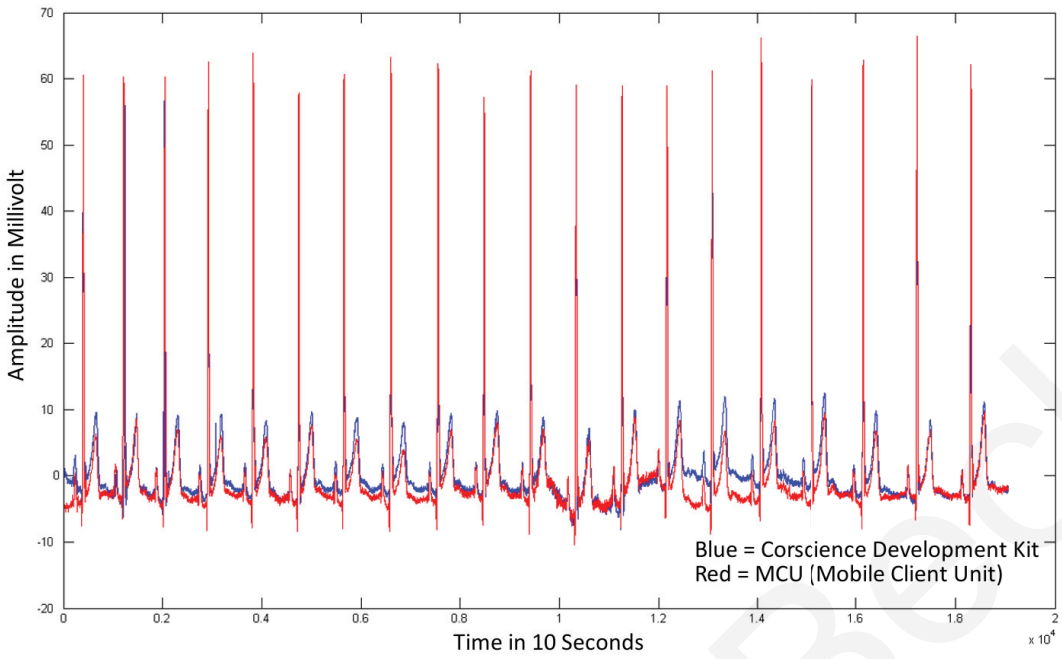

Figure 49: Synchronous recording of ECG with both Corscience development kit (blue) and MCU (red) after postprocessing with MATLAB® "detrend" function.

The correlation of both signals was calculated using the MATLAB® function *"corrcoef"* and resulted in a high correlation of 0.94.

Finally, ten randomly selected single cardiac cycle pairs were compared. The MATLAB® function "corrcoef" was again used, which resulted in an even higher correlation with a mean value of 0.98. Figure 50 visually depicts the high degree of correlation of a single cardiac cycle.

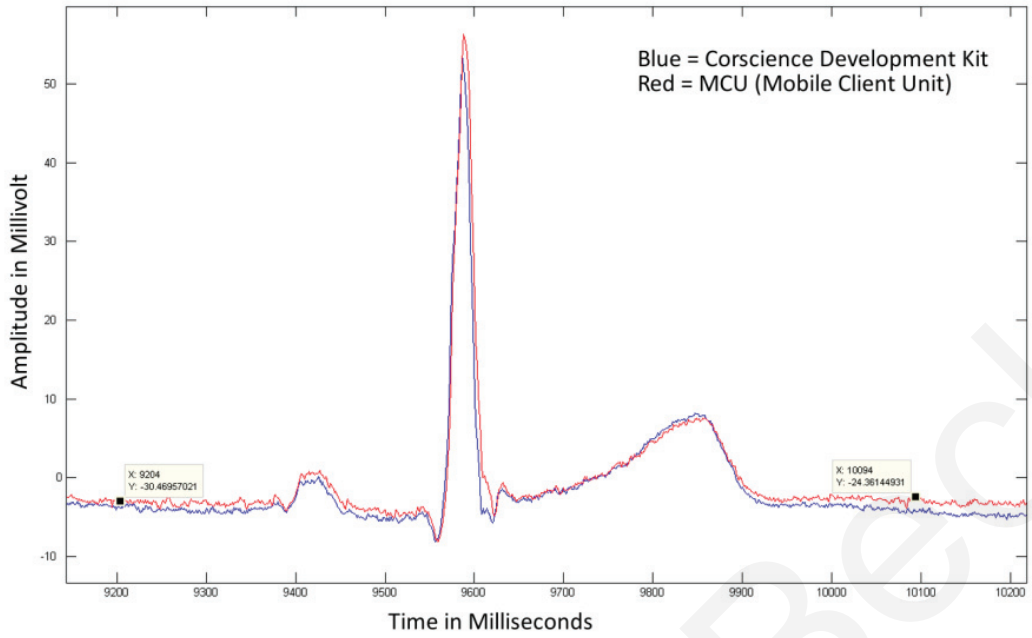

Figure 50: ECG tracing of a single cardiac cycle recorded with the Corscience EMB3/6 development kit (blue) and MCU (red).

3.3.5 Test – Pulse Oximetry

Test description: The purpose of this test was to verify the functionality of the herein developed pulse oximeter hardware implementation, data transmission and display. The heart rate, blood oxygen, signal quality and plethysmogram values were compared against Corscience's ChipOx development kit, which recorded the same subject at the same time.

Test setup: Figure 51 depicts the block diagram of the test setup involving the *MCU* part (upper branch) and *Corscience* part (lower branch). Both systems used Corscience's finger clip sensors CS10299, which were put on the subject's left index and middle finger. The subject was asked to remain still during the recording in order to minimize movement artifacts (except for one dedicated artifact test series).

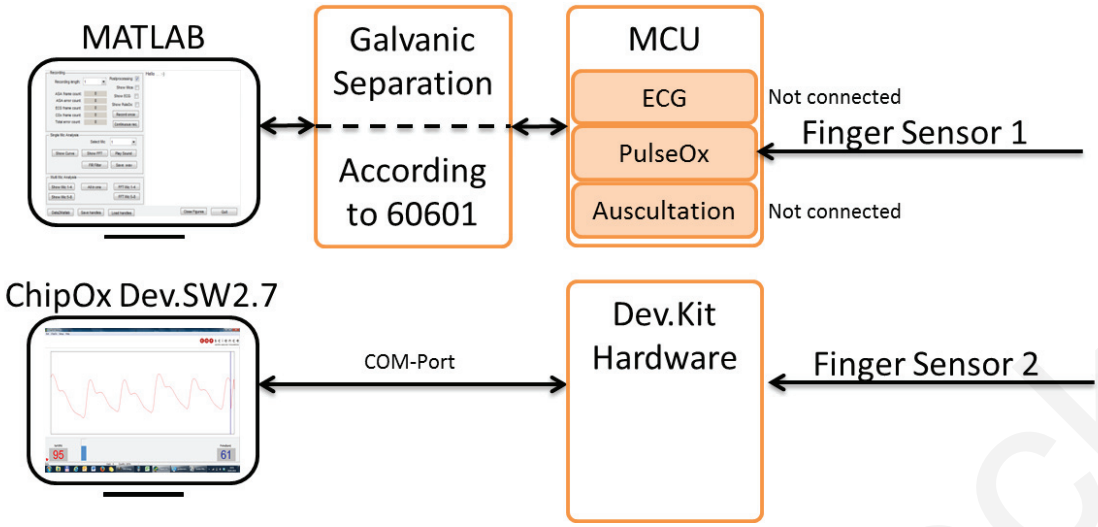

Figure 51: Block diagram of test setup for MCU pulse oximeter verification.

The *MCU* test setup involved a computer with Windows 7® Professional Service Pack 1 running MATLAB® R2013a Student Version with the herein developed scripts and figures with date code 2014/03/13, IFTOOLS ISOUSB® (a medical grade galvanic USB separation device) and the herein developed MCU with embedded software date code 2014/03/10 and hardware revision A.

The electronic parts were embedded in a robust, shock, dust and splash water resistant housing as shown in Figure 52-1, which the subject wore at the hip. The sensors were pluggable and allowed a high degree of mobility during the test procedure. To guarantee high bandwidth and a reliable transmission the unit was attached to the PC with a common USB 2.0® connection cable (with galvanic separation). The direct connection simplified the setup in accordance with the experiment's focus. In later experiments the wireless connection can easily be used once transmission is verified, stable and the amount of (raw) data is reduced.

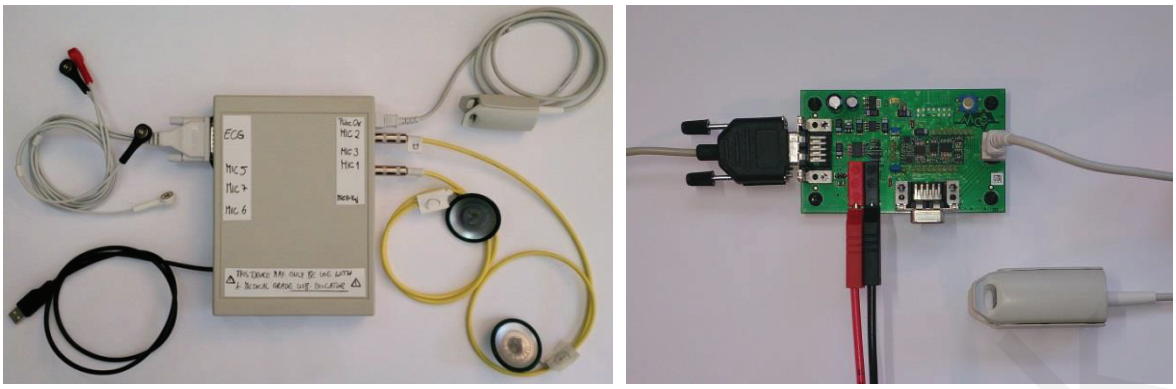

1) 2)

Figure 52: 1) Electronic parts embedded in a robust, shock, dust and splash water resistant housing; 2) Corscience's ChipOx development kit with interface to PC, power supply and finger sensor.

The second test setup involved a computer with Windows 7® Professional Service Pack 1 running Corscience's development kit software version 2.7. Corscience's development kit hardware was attached to the PC with a standard RS-232 connection cable and supplied by a regulated power supply with 7 V. The hardware is shown in Figure 52-2.

Measurement: Parallel recordings were performed successfully even though Corscience's development kit software did not provide the functionality to export raw data streams for a quantitative comparison of the raw plethysmogram. A cross-correlation analysis was not possible. Instead, 10 recordings of 6 seconds with a settling time of at least 30 seconds were performed. Once the recording was performed preprocessed data from *Corscience* and raw data from *MCU* test setup were written to a matrix.

Test Result: Heart rate, blood oxygen and signal quality were compared based on their mean square errors (MSE) according to the following equation:

$$MSE = \frac{1}{n}\sum_{i=1}^{n}(x_i - \bar{x})^2$$

Equation 12: Mean square error. [114]

The analysis showed a high degree of correlation with a very low mean square error as shown in Table 16.

Table 16: Test results for the Corscience and herein developed pulse oximetry systems.

Test Series	Mean Square Error	Description
Heart Rate	0.08	Analysis based on the difference of both measurement vectors applied in Equation 12.
Blood Oxygen	0.18	Analysis based on the difference of both measurement vectors applied in Equation 12.
Signal Quality	0.04	Analysis based on the difference of both measurement vectors applied in Equation 12.

Discussion: The test was performed without problems and results show very high degree of correlation. Most important, the signal characteristics and timing are not affected. The minor differences may be accounted to sensor mismatches, fabrication tolerances and calculations performed by the embedded algorithms. The observed differences on the absolute scale that were eliminated with the *'detrend'* function was due to the floating system principle and different approximation algorithm states of the systems over which the user has no control.

3.4 Vital Signs Acquisition

Scope: The purpose of this test is to establish a database with the human vital signs of ten healthy subjects.

Test description: ECG, oxygen saturation and heart and lung sounds were recorded at rest and at a pulse rate of more than 100 beats per minute for multiple subjects. The database provides input for digital algorithm designs, which can be used for decision making, the separation of heart sounds and other processes.

Test setup: The setup involved a computer with Windows 7® Professional Service Pack 1 running MATLAB® R2013a Student Version with the herein developed script and figure with date code 2014/03/13, IFTOOLS ISOUSB® (a medical grade galvanic USB separation device), and the herein developed MCU with embedded software date code 2014/03/10 and hardware revision A. The subjects were asked to remain quiet and still during recording in order to minimize disturbances due to ambient noise and movement. Figure 53 depicts the block diagram of the test setup.

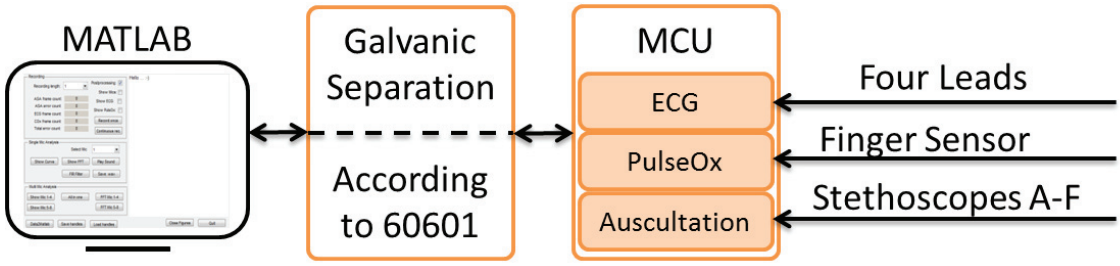

Figure 53: Block diagram of test setup for human vital data acquisition.

The electronic parts were embedded in a robust, shock, dust and splash water resistant housing as shown in Figure 54, which the subject wore at the hip. All of the sensors were pluggable and allowed a high degree of mobility during the test procedure. To guarantee high bandwidth and a reliable transmission the unit was attached to the PC with a common USB 2.0® connection cable (with galvanic separation). The direct connection simplified the setup in accordance with the experiment's focus. In later experiments the wireless connection can easily be used once transmission is verified, stable and the amount of (raw) data is reduced.

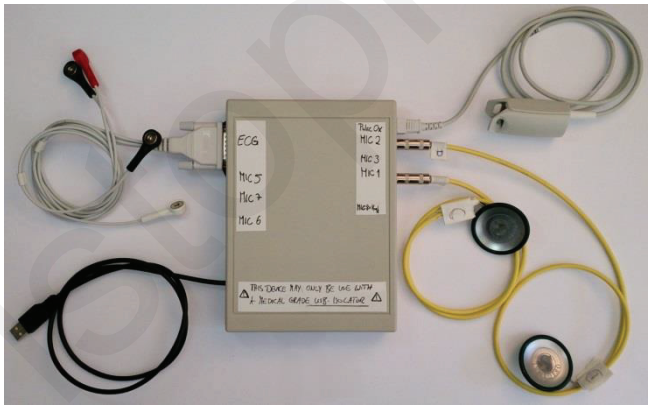

Figure 54: Electronic parts embedded in a robust, shock, dust and splash water resistant housing.

The ECG patient leads were attached to the subject as described in the corresponding instructions for use [66], i.e., RR (right arm), LR (left arm), RL (right leg) and LL (left leg). The finger sensor was attached to the left index finger. The stethoscope heads were attached to the chest (according to the projection of heart sounds described in the literature [60]) and the back (according to the results of the survey in [58]). Figure 55 gives a graphic representation of the locations.

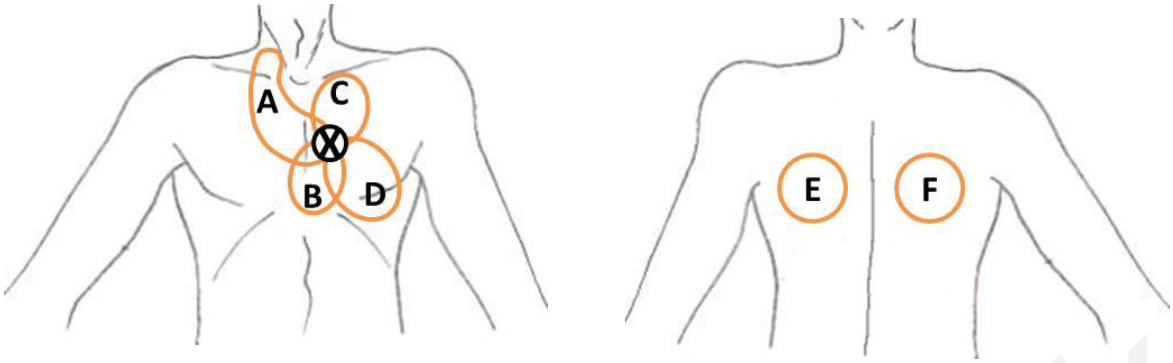

Figure 55: Body locations for stethoscope heads A–D (chest) and E–F (back).

In order to ensure the safety of the subject at all times, the setup has to comply with the safety requirements defined in medical standard EN IEC 60601 [115] and the corresponding documents. Since this test does not aim to provide data for medical diagnosis, consideration may be given to electrical safety, which is accomplished by a medical grade galvanic separation of the subject. The IFTOOLS ISOUSB® is a medical grade USB cable that separates the MCU and subject from the computer and consequently from the mains supply with up to 4000 V for at least 60 seconds.

Test procedure: The recordings were performed with 10 subjects at rest and at an accelerated pulse rate of more than 100 beats per minute. Each of the subjects were attached to the setup one by one, first in a seated position and then on an exercise machine. The duration of each recording was 30 seconds and each setting was repeated three times. The procedure was as follows:

1. The subject was attached to a test bench according to the definition in the test setup [116].
2. Real-time monitoring was carried out for setup verification.
3. The subject was recorded 3 times for 30 seconds while at rest.
4. The subject was recorded 3 times for 30 seconds at an accelerated pulse rate of more than 100 beats per minute.

Test results: The simultaneous acquisition of ECG, blood oxygen, and heart and lung sounds of the ten subjects was successfully recorded according to the test procedure. The test setup showed a high degree of reliability and repeatability. For example, loose sensors were detected during the real-time monitoring phase and immediately

corrected. Each data set was stored in a local database, which and is accessible for off-line analysis and processing.

The ECG and pulse oximeter captured the vital signs at a high quality and without major artifacts. The acoustic recordings also met the necessary requirements. The visual and acoustic inspection showed that all acoustic channels showed a suitable quality. The stethoscope heads were attached to the subjects' chests and backs with medical tape. Some tolerable clicking noise was introduced by the release of tension between the stethoscope head and tape or skin.

The total recording time was 37.5 minutes for the 10 subjects, with 18.5 minutes recorded at rest and 19 minutes while exercising. Six stethoscope heads were attached to each subject, which resulted in a total of 225 minutes of acoustic data, which is available for analysis.

Based on all of the data, the average pulse rate was 92.27 BPM, with 68.56 BPM at rest and 113.11 BPM while exercising.

Discussion: The test was successfully performed without any major problems. The recordings were performed in a quiet but not soundless environment. Some ambient noise was present from a nearby street as well as artifacts from traffic noise. Having ambient noise in the signal was the first step towards recreating a real-life situation and was done intentionally. However, in order to limit the impact, all the recordings were repeated if vehicle movement disturbed the body sounds to an excessive degree. If the signal-to-noise ratio needs to be improved, further recordings could be performed in a soundless chamber.

The current implementation is based on a static gain control with high dynamic range and optimized on the acoustic phenomena of interest. This focused approach increases robustness and reduces complexity at the expense of clipping in the case of stronger acoustic stimulation. A dynamic gain control would allow reliable recordings in a louder environment in order to further adapt the system to real-life conditions. The acoustic phenomena of interest would probably disappear in the noise but may still be a valid part for analysis depending on the digital algorithm.

3.5 Automated Alarm

The device continuously analyzes incoming vital data streams in order to assist medical personnel during an MCI. Specific minimum and maximum thresholds are set for each vital sign. If the measured data deviates from the defined margin, an alarm is triggered. The appearance and prominence of these alarms may differ quite significantly. To show the proof of concept of this system, two medically related and two technically related parameters are monitored and an alarm is triggered if the values deviate from the defined margin. Table 17 lists the selected parameters:

Table 17: Monitored parameters that trigger an alarm if values deviate from the defined margin.

Parameter	Valid Range	Alarm
Heart rate	50 – 210 BPM	Visual alarm box
Oxygen saturation	Changes of > 5 percent points per minute	Visual alarm box
Signal quality at finger sensor	75% – 100%	Visual alarm box
Valid acoustic bandwidth of all incoming acoustic streams	0 – 224 bit	Varying color of curve: blue = within margin red = clipping

The **pulse rate** is a continuously updated value and derived from both the EMB1/3 and ChipOx. It has a value of between 50 and 210 BPM according to the technical specifications. Internally, it may be set to any threshold in order to adapt it to any medical case. Once the pulse rate deviates from the defined margin, the implementation triggers an alarm and displays a text box in red in the plethysmogram as shown in Figure 56. For example, the pulse rate shown in the text box on the left and right is below and above the defined thresholds respectively, while the text box in the center shows a normal rate.

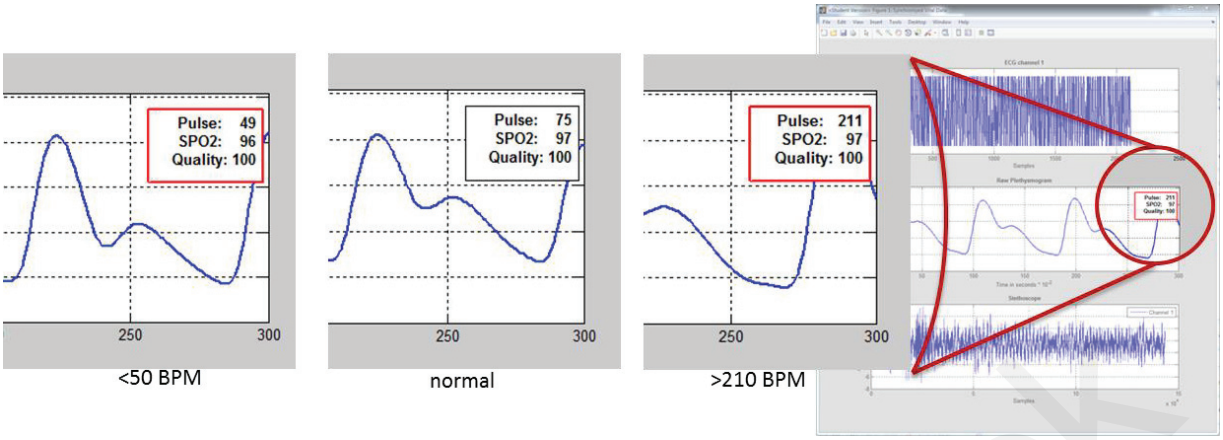

Figure 56: Alarm indication if heart rate deviates from defined margin of 50 to 210 BPM.

The patient's **oxygenation** level is derived from the finger sensor and expressed in percent. The oxygenation is constant under normal conditions. A drop would indicate that the patient is in danger. The edge detection is set to decrease by more than 5 percentage points per minute. The triggered alarm displays a message box indicating that the patient's oxygenation has dropped by 5 percentage points.

The **signal quality** derived from the finger sensor is provided by the ChipOx module and is expressed in percent. If no finger is detected in the sensor or if the level of continuous movement reaches a certain intensity, the signal quality drops down to 0%. With little movement, the signal quality usually reaches 95% to 100%. On the exercise machine the system shows reliable values with signal qualities of greater than 75% and responds quickly to changing heart rates. If the signal quality is below 75%, it is considered an artifact if it is temporary and corrupted if it lasts longer. The triggered alarm implementation is displayed as a red curve.

The fixed gain amplification of the **analog front end** is adjusted to the acoustic phenomena of interest and may clip in louder situations. During the test, these situations were caused by coughing, talking or touching the stethoscope head. Processing algorithms rely on high-quality signals and are sensitive to clipping. The acoustic streams are continuously checked and an alarm is triggered once clipping is detected in order to allow proper recording.

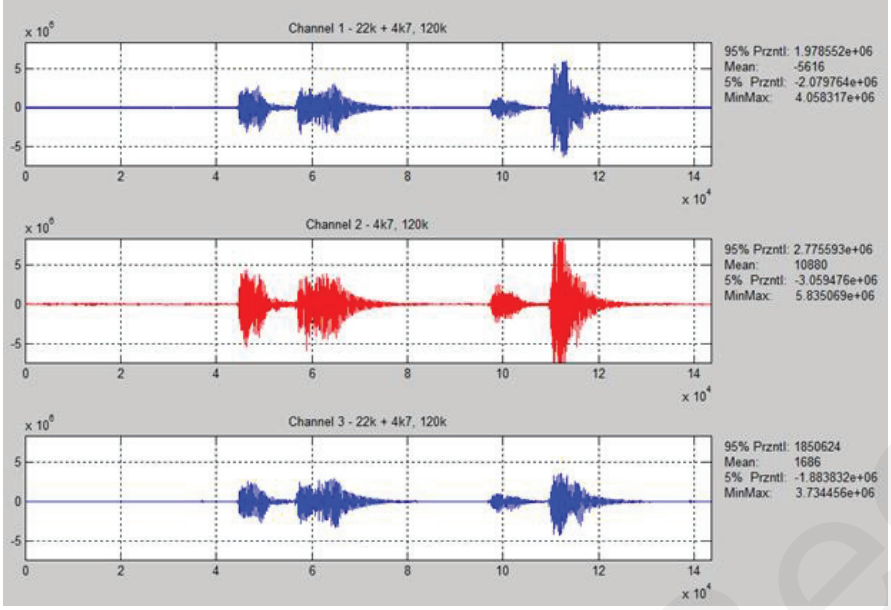

Figure 57: Simultaneous auscultation of the heart with channel one (top) to three (bottom). Clipping was experienced at channel two (middle) which is indicated in red.

Figure 57 illustrates simultaneous auscultation of the heart with three channels. While channel one and three are displayed in blue indicating that the signal is well within the range, channel two is displayed in red to indicate clipping.

Additional tests would help the user to quickly estimate whether the system is functioning properly and prompt a message if an error is detected with respect to the connection state of the device, data integrity for each incoming frame, battery filling level or proper programming after each startup, to mention just a few examples.

3.6 Sound Source Localization

A great deal of information can be extracted by listening to the sound sources in the body such as whether the heart is beating normally and the person is normally or has a punctured lung, pneumothorax, or else. But having a system with eight similar acoustic channels also opens additional opportunities such as sound source localization. Localization within the body is a very complex and challenging exercise and exceeds the possibilities of this project, but sound source localization of a nearby ambulance could add a great contribution to this project. To examine the capabilities of the system a bio-inspired feasibility study was set up. A considerable amount of work has been done in recent years in the design and implementation of bearing angle estimation systems, or

so- called Acoustic Surveillance Units (ASU), and various localization methods have been introduced. Based on the idea to realize a bio-inspired approach and the fact that sand scorpions use their eight legs to sense their environment and this system has eight acoustic channels it seemed appropriate to investigate in that direction.

Scorpions belong to the most ancient groups of terrestrial animals. Based on the findings of preserved fossils it is believed that the species is more than 430 million years old. Most scorpions are nocturnal and seek shelter in the morning for protection from predators and predominately live in sandy or rocky subsoil close to the ground in the tropics, subtropics, semi-deserts or deserts.

The outer anatomy basically consists of the anterior part of the body (Prosoma), posterior part of the body (Mesosoma), tail with sting (Metasoma), eight legs, claws (Pedipalbs) and pincers (Chelae).

Some subspecies like the sand scorpion perceive their environment by a unique and fascinating method – they sense ground waves with their basitarsal compound slit sensilla (BCSS), located just above the joint of the foot (Tarsus). Due to the anatomy and the very high sensitivity organs the scorpions can detect ground waves with less than 0.1nm amplitude, what is around the size of an atom.

By measuring the time delay, between the waves arriving at each of its feet, the scorpion can calculate the precise direction and distance to e.g. a threat, a predator, a prospective prey, or even a mate.

And the ability to perceive the environment based on vibrations is something we humans share with scorpions. While they sense ground waves, we detect vibrations in the air – sound. Based on this link we propose an approach that adapts a sand scorpion inspired neuronal model to human audible sound.

Julian et al. compared four different algorithms for sound localization using MEMS microphones and signals recorded in a natural environment. [117] The spatial-gradient algorithm (SGA) showed the best accuracy results and its implementation requires a sampled data analog architecture that is able to solve a standard least means square (LMS) problem adaptively. The performance of a system with a low-power CMOS VLSI

design gives an error margin of the order of 1° and a similar standard deviation of the bearing angle estimation. [118–120] A very low-power implementation for an interaural time delay (ITD) estimation without delay lines with the same ASU unit is reported by Chacon-Rodriguez et al. with an estimation error of a couple degrees. [121]

Masson et al. used a data fusion algorithm to perform a position estimation based on the measurements from five nodes with four MEMS microphones each. [122] The measurement is made with a unique fixed source emitting a 1kHz signal.

Zhang et al. used a cross correlation of the signals received and a zero crossing point to estimate the bearing angles of moving vehicles. [123] The hardware was an ASU with four MEMS microphones.

The reported algorithms have demonstrated good results but seem computationally hungry in comparison to using a neural network approach. The advantages of neural network computations over other digital algorithms is discussed in [124,125].

A consensual theory of ITD-based localization did not exist until Benichoux et al. recently proposed a unifying model of the function of binaural cells in mammals that explains both behavioral and neural data. [126] However, neuromorphic implementations, such as the neuromorphic sound localizer introduced by Van Schaik et al., have been proposed. In this application, two MEMS microphones are connected to two analog neuromorphic cochlea. It uses a low-power system and the average standard deviation of the estimated azimuth is 4.5°. [127,128] The system bases its azimuth estimation on the interaural delay between the two “ears.”

A considerable model was created by Stürzl et al. and is adapted to the mechanism a nocturnal sand scorpion perceives its environment. [129] It senses ground waves through its eight legs. The sense organ of each leg, located just above the joint of the foot (tarsus), is compressed as a transverse wave passes through it and is sensitive to the mentioned movements of less than 0.1 nm. Each one of the eight legs is connected to one command neuron and three inhibitory partner neurons (illustrated in black and grey respectively in Figure 58). The reaction mechanism creates an excitatory spike at the command neuron corresponding to this leg. It also creates an excitatory spike at the

three inhibitory partner neurons connected to the leg, which project their inhibitory spike to the command neurons of the opposite legs. In nature, the scorpion has a 13° to 15° error on the localization of acoustic stimuli. [130]

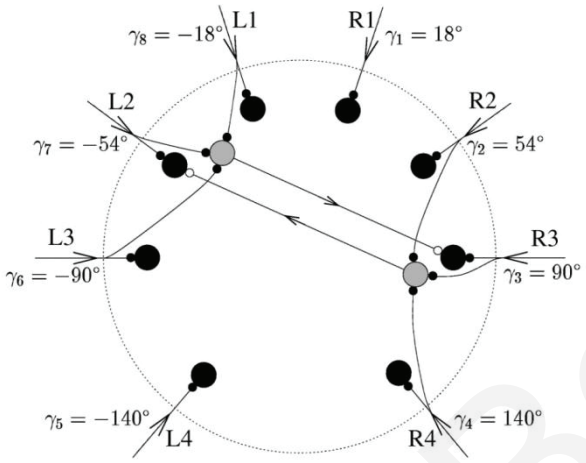

Figure 58: Original spiking neuron model developed for the sand scorpion by Stürzl et al. [129] The eight command neurons are shown in black. For two of them, k = 3 and k = 7 = $\overline{3}$, which corresponds to R3 and L2 respectively. The inhibitory partner neurons are shown in grey. The triad of R3 consists of L1, L2 and L3.

This model has been implemented on a Brian spiking neural simulator [131,132] and takes eight input streams, which perfectly matches the MCU with its eight channels. The spiking neural simulator was expanded to sound waves and adapted to the herein designed and developed MCU hardware in cooperation with Guillaume Garreau (University of Cyprus). The recorded data needed some processing (e.g., normalization and format adaption) to satisfy the simulator's input requirements.

The MCU was placed 45 cm above a table with the microphones facing upwards for the data collection. Acquisition was initiated by the MATLAB® application described in chapter 3.2.5. A Gallo Acoustics A'Diva omnidirectional speaker was used for the sound source. It was attached to a function generator for producing various frequencies, sweeps and wave shapes. The speaker was placed at a distance of 50 cm to 93 cm from the center of the MCU on the same horizontal plane. The distance was kept constant during one recording, but sometimes changed for the others. One position was defined as 0° with a counterclockwise rotation. The MCU was rotated either continuously or stepwise around its center. An arrow pointing to the angular rotation of the MCU used the previously defined 0° position as a reference. A camera continuously recorded the data collection in order to have a ground truth of the location of the speaker compared

with the reference on the MCU, and a time reference was also included. The data acquisition setup is shown in Figure 59.

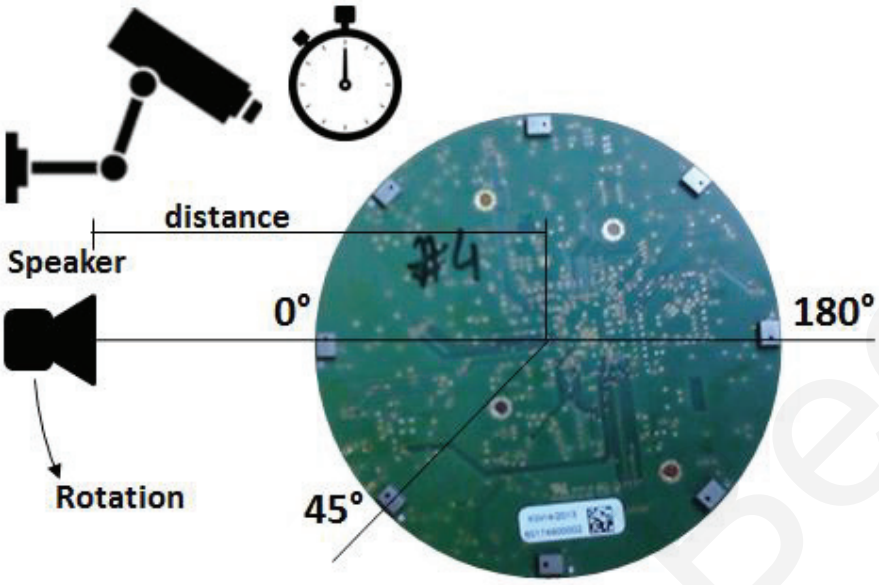

Figure 59: schematic setup with video and time surveillance and the speaker placed in the same horizontal plane as the microphones rotating counterclockwise.

To first test single or muli-microphone set-up, a simple sine wave was recorded and displayed in diagrams with amplitude over time, where the schematic illustration in Figure 60-1 shows the switch on behavior, Figure 60-2 a recording with equal microphones to speaker distance and Figure 60-3 a recording with varying microphones to speaker distance

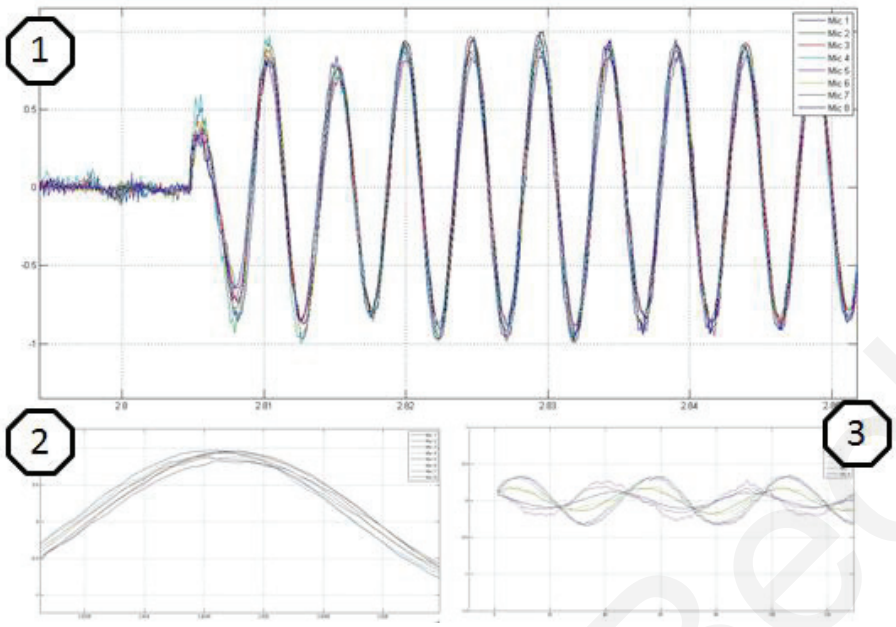

Figure 60: sine wave recordings illustrated in diagrams, amplitude over time, where 1 shows the switch on behavior, 2 a recording with equal microphones to speaker distance and 3 a recording with varying microphones to speaker distance.

Finally two scenarios were explored with the described test setup in order to be able to characterize the neural network based localization system and compare its accuracy based on measurements taken with real scorpions found in nature. [132]

For the first scenario, a continuous 1kHz sine wave was used as an acoustic stimulus while the sound source was moved from 0° to 360° in steps of 45° using premarked locations. The sound source was kept at each position for approximately two seconds and then moved to the next one.

For the second scenario, a continuous 1 kHz sine wave was used as a stimulus while the sound source was moved from 0° to 360° in 20 seconds at an approximately constant speed.

Several recordings of each scenario were made at a distance of 50 cm, 64 cm and 93 cm between the speaker and ASA. In total, the data collected comprised 15 recordings.

The bearing angle of the sound source could be identified and compared by feeding a modified, spiking neural network model of the scorpion with normalized raw data. In nature, the scorpion has a 13° to 15° error on the localization of acoustic stimuli.

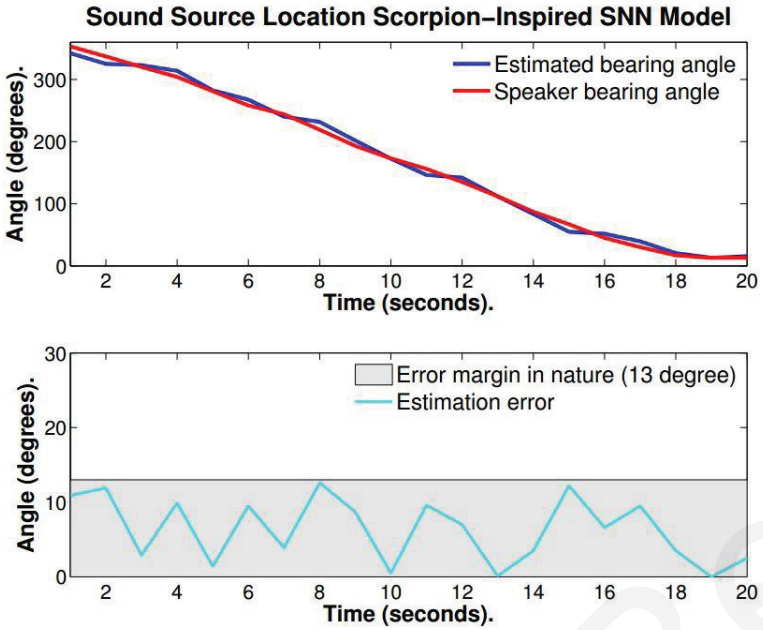

Figure 61: Plots of the speaker bearing angle (red), the estimated bearing angle (blue) and the estimation error (cyan). The average error reported was 6.34° ± 4.36°.

Figure 61 illustrates the continuously moving source scenario. In the top graph, the red curve is the bearing angle of the source of sound (speaker) and the blue curve is the estimated bearing angle of the source calculated with the SNN model. The estimation error is given in the bottom graph. In this example, the average estimation error is 6.34° ± 4.36°. If we take all the trials into account, the average estimation error is 9.6° ± 7.6°, which is better than the margin found in nature (13° to 15°).

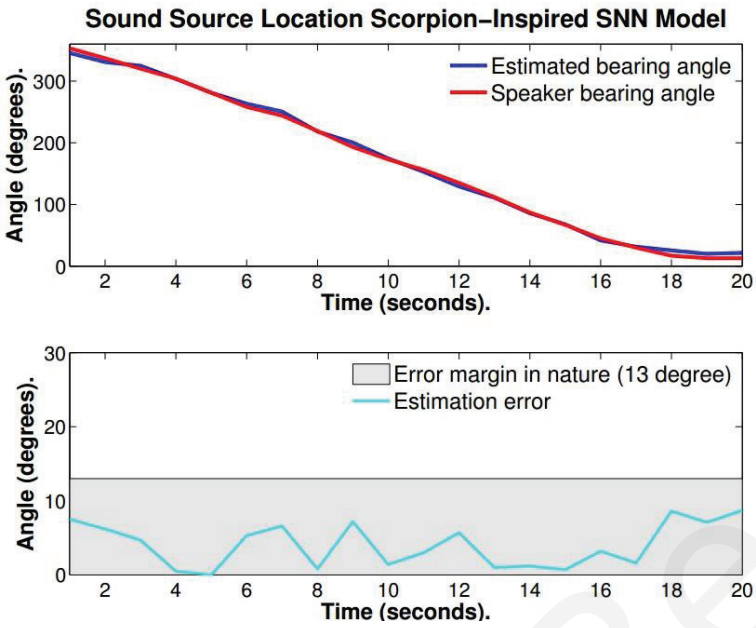

Figure 62: Plots of the speaker bearing angle (red), the estimated bearing angle (blue) and the estimation error (cyan). The average error reported was 4.05° ± 3.01°.

Figure 62 illustrates the same example as in Figure 61 with an increase of 15% for the refractory period. In the top graph, the red curve is the bearing angle of the source of sound (speaker) and the blue curve is the estimated bearing angle of the source calculated with the SNN model. The estimation error is given in the bottom graph. In this example, the average estimation error is 4.05° ± 3.01°. This is almost 25% of the error observed in nature.

Discussion: in this test, a sound source localization test was performed with the eight MEMS microphones from the MCU and a bioinspired spiking neuron model of the scorpion. The merge showed some very promising results indicating that the proposed approach is feasible and since the neural network is very simple, implementation in the MCU is expected to be viable. Hence it is estimated that the feature supports first responders at an emergency scene in localizing subjects.

3.7 ECG Time-Based Heart Sound Analysis

Heart sounds reflect the physical condition of the heart and provide valuable information to a practitioner during a medical examination.

Heart sound segmentation, the process of identifying and dividing the signal according to its acoustic phenomena, is the first step in automated heart sound analysis. Once the segments are available, analysis and categorization algorithms evaluate and extract the medical information that leads to a diagnosis.

There has been ongoing research on the various challenges that make it difficult to develop algorithms with acceptable performance, such as large signal variability, the complex nature of acoustic signals, low signal-to-noise ratio and noise sensitivity. A positive development in this area is the continuously increasing computational power of electronic systems that allow more comprehensive and complex techniques.

Bahekar et al. discuss different segmentation techniques in a small survey. They concluded that segmentation using a discrete wavelet transform (DWT) in conjunction with the Shannon entropy provides a useful tool. However, they also indicated that none of the solutions achieved optimum performance. [41]

Malarvili et al. presented an algorithm with input from an ECG and a single channel stethoscope to detect S1 and S2. In the first step, they calculated the instantaneous energy of the ECG and mapped the time vector to the acoustic stream. The team acquired data from 15 subjects and concluded that this approach is feasible and could serve as input for further development of an automated heart diagnosis. [25]

Debbal and Bereksi-Reguig analyzed and compared techniques for separating S1 and S2 as well as their internal components. These included a short-time Fourier transform, Wigner distribution and wavelet transform techniques. *"The continuous wavelet transform is found to be the most successful technique for the analysis based on the fact that the signals are characterized by transients and fast changes in frequency as time progresses."* [45]

A current project of the University of Coimbra, Portugal is investigating the design and development of algorithms using a multichannel heart sound auscultation system that can be applied in long-term home monitoring. The project started in 2013 and is scheduled to continue until mid-2016. [133]

Scope: The aim of this experiment is to design and develop a heart sound separation algorithm to determine S1 by taking full advantage of the unique feature set of the MCU with highly synchronized ECG and multichannel heart sound acquisition.

Test description: The S1 acoustic phenomenon acquired as described in chapter 2.6.1 occurs during the ECG R-wave to S-wave transition. This process is used to evaluate S1 without having to run high-performance algorithms to analyze complex acoustic signals in the first step. A custom ECG R-wave identification algorithm determines the heartbeats in order to create a time vector, which is then mapped to the highly synchronized acoustic streams. Finally, a customized algorithm separates S1 and creates a vector containing all the phenomena for further processing and analysis.

Test setup: The test setup involved the data from eight subjects from the local database created in the experiment described in chapter 3.4 Vital Signs Acquisition. Custom algorithms were written in the MATLAB® environment with a script and figure with date code 2015/03/14 [134] and the analysis was visualized using MATLAB® GUI elements. The test log containing the raw data and analysis was stored in the corresponding record. [135]

Test procedure: All of the subjects were investigated at rest and with a pulse rate of more than 100 beats per minute. Two of the three 30-second data sets with the highest quality were identified for each subject. In each data set, the best out of six channels were selected for analysis. The script was started manually and performed individually for each subject. The resulting graphs were visualized and inspected manually to identify the quality of separation. The final result was logged in the corresponding test record. [135]

Analysis: The segmentation algorithm takes full advantage of the unique acquisition modalities that the MCU provides, which include a highly synchronized ECG and multichannel auscultation. All of the data was normalized to increase comparability, especially the amplitude trends, even though it was not necessary to do this prior to subsequent processing. The ECG signal was then analyzed for R-waves and the corresponding time was added to a vector for each occurrence. This time information gave the approximate moments of occurrence of the S1s but not the duration.

Therefore, an envelope was calculated over the acoustic data utilizing a low-pass Butterworth filter with a 15 Hz cutoff frequency. The ECG time vector was then mapped to the envelope and the corresponding maximum determined for each entry. In order to evaluate the duration, the minima on both sides of the peaks were identified. The time period between the two minima was then mapped to the acoustic stream and the resulting signal part copied to a dedicated vector.

Test results: In total, 1361 ECG R-waves from eight subjects were identified, with two recordings performed at rest and two at an accelerated pulse rate, using a recording length of ten seconds in each case. The number of S1s that were successfully identified and separated from the acoustic streams came to 1353. This corresponds to a success rate of 99.41%. Identification of eight of the S1 phenomena failed due to a time deviation between the ECG and acoustic stream with an unknown root cause. During this artifact, two successive S1s were fully compromised and the system required six additional S1s to recover.

In 4 of the 16 cases, the average pulse rate was under 100 beats per minute. Although the pulse rate was approximately 120 beats per minute at the beginning of the recording period, it dropped during the recording time so the resulting average fell below the target threshold. However, this is not expected to compromise the results and the objective of covering a wide pulse rate range was still achieved.

Figure 63 illustrates the visual output of the algorithm. Diagram 1 shows the combined, synchronous and normalized data over time, where the blue vertical lines mark the ECG R-waves and the black dots the corresponding amplitudes, the red curve marks the acoustic stream, the purple curve the acoustic stream's envelope, and the black dots the maxima and minima around S1. Diagram 2 depicts a single heart cycle in which the R-wave, S1 and even S2 are prominent.

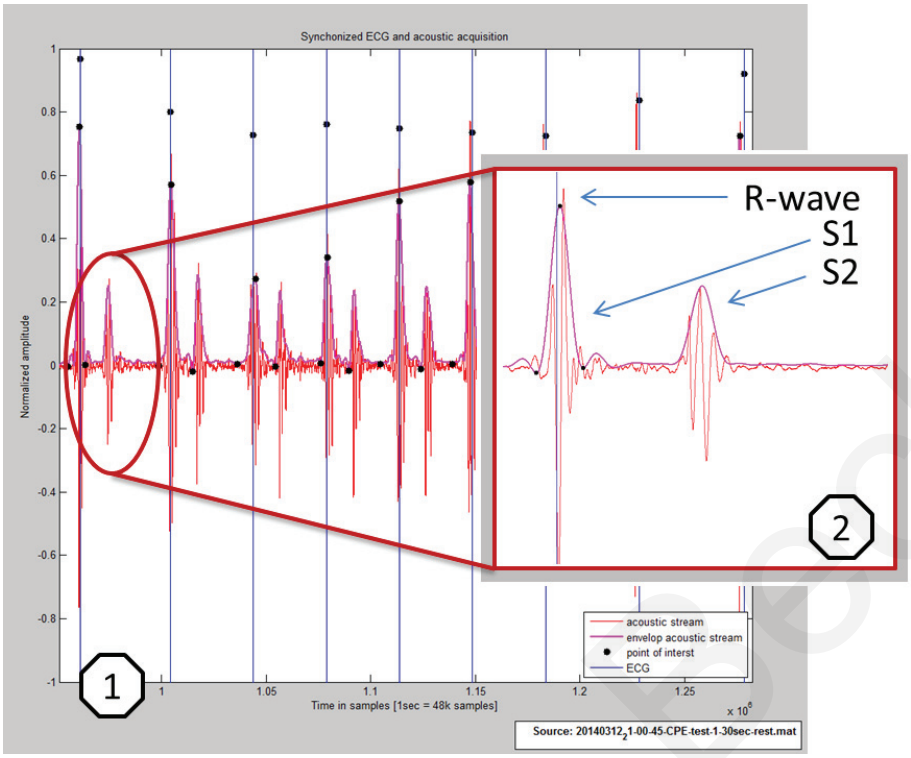

Figure 63: 1) Combined, synchronous and normalized ECG and auscultation over time; 2) A single heart cycle with prominent R-wave, S1 and S2.

All of the samples between the enclosed black dots in diagram 2 were taken as an S1 and added to a vector. In order to test the capabilities of the S1 vector, a sample recording of the subject CPE was taken at rest. Calculation of a mean S1 over the entire S1 vector results in the curve shown in Figure 64. This phenomenon lasts approximately 160 milliseconds.

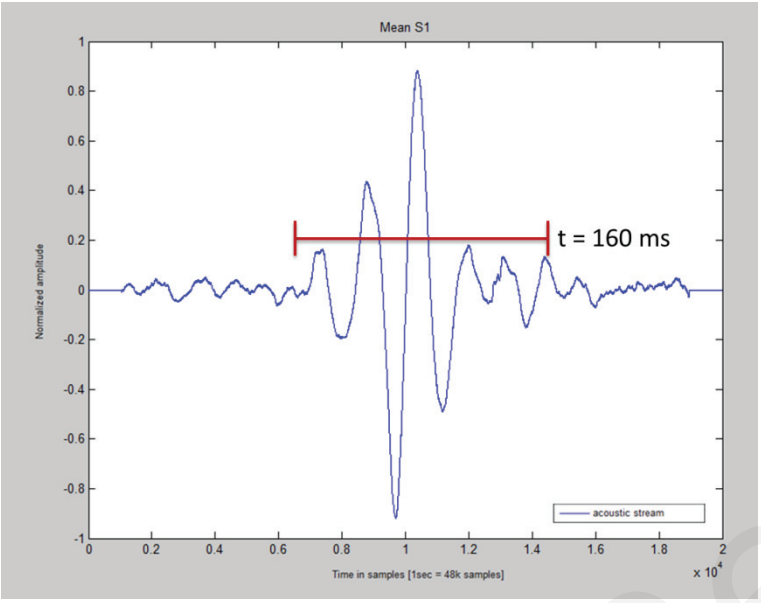

Figure 64: Calculation of a mean S1 over the S1 vector with 30 entries for subject CPE at rest.

The S1 vector as well as the mean S1 provide a solid basis for more comprehensive analysis in the future.

Discussion: In this experiment, the successful identification of S1 phenomena based on the ECG R-wave time vector was shown. In particular, low-performance algorithms suitable for mobile systems with power constraints were used for evaluating the potential of a system with synchronized data acquisition. Calculation of the mean S1 represents just one of the innumerable opportunities for subsequent analysis. The vector could also be used to identify basic characteristics, detect acoustic artifacts by comparing new S1 to mean S1, detect artifacts on other acquisition paths (ECG, PulseOx) since most artifacts occur in only one domain, identify characteristic changes over time, identify and categorize abnormal sounds, and train neuronal networks. Other areas of application could include beam shapes and localization and using it in combination with additional vital signs provided by the MCU.

4 Contributions

In this one-person project, a unique human vital sign acquisition research platform was developed to acquire ECG, blood oxygen, body temperature and up to eight acoustic streams for heart and lung sound auscultation. The custom-designed human wearable MCU is the first device to provide highly synchronized acquisition modalities as well as multichannel auscultation. The new and unique set of continuously acquired data opens up new ways of analysis by taking advantage of the time correlation between different vital signs. It is a lightweight battery powered embedded system designed for mobile operation.

The research platform for human vital sign acquisition is a multidisciplinary work that serves as a linking element to various research areas. Therefore, it is designed to allow maximum flexibility for expansion in every possible direction. The MCU's hardware provides generic interfaces to add or remove sensors or interfaces at any time as required by the research. The embedded VHDL application is also capable of controlling additional hardware as well as executing high-performance on-board analysis. The associated MATLAB® application has access to raw data in order to provide algorithm design options in a high-level language before optimizing for use in embedded systems.

The system's architecture is designed for emergency scenes trying to assist medical resources in overwhelming environments. It is the only known platform that transmits other vital signs such as heart and lung sounds to central nodes that are independent from the acquisition location. The central node simulated with the herein developed MATLAB® application is capable of analyzing, monitoring, making basic decisions and visualizing in real time as well as performing offline analysis.

Custom-designed algorithms extract and visualize the medically relevant information from the input streams, such as ECG, heart rate, blood oxygenation, body temperature and S1. Dedicated experiments with dedicated algorithms analyze S1 and continuously monitor and trigger an alarm if there is a deviation from the predefined ranges. The work with Guillaume Garreau proved the very low time error in acquisition of the

acoustic input streams. An experiment performed to locate a sound source moving around the MCU in a circular fashion yielded very promising results.

In this project, a database was created comprising the vital signs of ten healthy male subjects at rest and with an accelerated pulse rate of more than 100 beats per minute. The unique data set provides the opportunity for researchers to access highly synchronized values for ECG and blood oxygenation as well as four heart sound channels and two lung sound channels.

5 Conclusion

The accident and emergency center intelligent monitoring system is organized according to a three-tier architecture. The MCU, which is the main part of this project, was successfully designed and developed. Comparable systems do not exist to date. The project involved a PCB with ~430 components, an embedded VHDL application comprising ~9500 lines of code, 7 interfaces and a robust housing. In addition, a MATLAB® application with ~5100 lines of code and user-friendly GUI was successfully designed and developed to receive raw data from the MCU, interpret, analyze, and visualize in real time.

The system was continuously adapted to new findings during the design process, such as the modifications made based on the first measurements. The microphones were located on the PCB and connected to the stethoscope hoses, which produced significant noise when they were touched and reduced usability due to their lack of flexibility. Incorporating the microphones in the stethoscope heads dramatically improved the signal quality and handling properties. Finally, the design of two prototypes was finalized and one prototype served as the MCU for all experiments.

Characterization of the MCU in various experiments showed promising results. All hardware modules, additional hardware functions, embedded software, MATLAB® application and their interaction with one another performed as expected. The experiments with lung sounds showed that additional work on the hardware is necessary because device-based noise and lung sounds share a frequency range that compromises the signal. The combination of ECG and heart sounds allowed the design of a low-performance heart sound separation algorithm and subsequent analysis of S1. The experiments on the acquisition of other human vital signs yielded satisfying results, i.e., ECG, heart rate, blood oxygenation, body temperature and heart sounds were successfully recorded. A database was created comprising the vital signs of ten healthy male subjects at rest and with an accelerated pulse rate of more than 100 beats per minute. The design and development of a neuronal network-based sound source localization setup carried out in a partner project yielded very satisfying results.

In conclusion, the aim of this project was to introduce a new and unique human vital signs acquisition platform that brings together various fields of research. This objective was successfully achieved and the first generation of the Accident and Emergency Center Intelligent Acquisition Unit has been completed.

As a result of the generic and modular approach that was maintained during the design process the system offers great flexibility. This opens up the opportunity to spread the use of this monitor prototype to other application areas with relatively little effort, such as:

- A heart valve monitor for chronically ill patients in the home care market.
- A generic multi-channel stethoscope for the primary care practitioner that comes with recording capabilities and thus allows comparison.

5.1 Future Work

This project provides a solid basis to act as an integration platform for various research areas by providing capabilities for algorithm designs optimized for embedded systems, vital sign analysis and interpretation, synchronous multiple input for vital sign analysis and interpretation, and human wearables for MCIs, to mention just a few. Some specific operations for further investigation could include the following:

- Heart and lung sound separation
- Heart sound categorization
- Lung sound categorization
- Pulse transit time evaluation
- Heart rate variability analysis
- Vital sign artifact identification based on multiple independent sources
- Embedded algorithms for decision making based on vital signs
- Usability and handling properties for human wearables in MCIs
- Architecture design for MCIs

Special consideration should be given to the following aspects within the scope of extending or developing a successful second generation of the project:

Server-based application: A server-based application with a real-time data display is highly recommended in order to create a full feature set of a decentralized multipatient monitoring system. All the detected/connected units could be displayed in a brief overview showing only the most important data or a quick summary of each patient in descending priority. The selection of a single patient could show a full detailed view while hiding the data of the other patients.

Decision-making algorithms: A patient priority as list in the server-based application could be set by algorithms analyzing the incoming data according to predefined criteria.

Alarm system: The aforementioned algorithms could also be used to monitor all incoming human vital signs and trigger an alarm if they deviate from a predefined margin.

Blood pressure: A blood pressure measuring unit is recommended in order to complete the emergency human vital signs set so that it can be easily accessed by automated electronic systems. Depending on the required measurement setup, this implementation will either use up considerable space and power or result in a stand-alone product.

Housing: A proper solid, water and dust resistant case is recommended. It should have an IP54 rating and be shock resistant since it will be used in harsh environments. The connectors should be especially safeguarded against movement artifacts.

Ambient noise cancellation: A dedicated microphone could record the ambient noise and provide an additional, valuable input for digital postprocessing algorithms for noise cancellation in order to further increase the sound quality.

Regulatory affairs: Once the basic research phase of this project is completed, it is recommended that research be done on the applicable standards based on medical devices directive 93/42/EWG (CE) such as EN IEC 60601-1 and the accompanying documents to identify additional safety requirements.

6 References

[1] EM-DAT. The International Disaster Database; 2014. Available from: http://www.emdat.be.

[2] Beck C. Research on active EU projects on emergency situations. Freiburg, Deutschland; 2014.

[3] Davoli E, Righi F. Emergency Medical Services Systems in the European Union. Copenhagen, Denmark; 2008.

[4] Jakubowski E, Busse R. HEALTH CARE SYSTEMS IN THE EU. Luxembourg; 1998.

[5] Leaning J, Guha-Sapir D. Natural disasters, armed conflict, and public health. N. Engl. J. Med. 2013;369(19):1836–42, doi:10.1056/NEJMra1109877.

[6] Guha-Sapir D, Vos F, Below R. Annual disaster statistical review 2011: the numbers and trends. In: Brussels: Center for Research. p. 1–52.

[7] Guha-Sapir D, D'Aoust O. DEMOGRAPHIC AND HEALTH CONSEQUENCES OF CIVIL CONFLICT. World Development Report 2011;2011:1–47.

[8] EM-DAT. The OFDA/CRED International Disaster Database – www.emdat.be – Université catholique de Louvain – Brussels – Belgium.: Information on complex, natural and technical disasters in the period 2010 to 2014.

[9] EM-DAT. The OFDA/CRED International Disaster Database – www.emdat.be – Université catholique de Louvain – Brussels – Belgium.: Information on earthquake 2010 in Haiti.

[10] EM-DAT. The OFDA/CRED International Disaster Database – www.emdat.be – Université catholique de Louvain – Brussels – Belgium.: Information on earthquake 2011 in Japan.

[11] E-Triage. Forschungsprojekt Elektronische Betroffenenerfassung in Katastrophenfällen e-Triage. Available from: http://www.e-triage.de/.

[12] Gebhart ME, Pence R. START Triage: Does It Work? Disaster Management & Response 2007;5(3):68–73, doi:10.1016/j.dmr.2007.05.002.

[13] Blöss T. Katastrophenmedizin: Zwang zur Selektion; 2004. Available from: http://www.aerzteblatt.de/archiv/42936/Katastrophenmedizin-Zwang-zur-Selektion.

[14] Howland SA, editor. Steamboat Disasters and Railroad Accidents in the United States: Accounts of recent shipwrecks, fires at sea, thrilling incidents, & co. Massachusetts; 1840.

[15] Koekemoer HL, Scheffer C. Heart sound and electrocardiogram recording devices for telemedicine environments. In: 2008 30th Annual International Conference of the IEEE Engineering in Medicine and Biology Society. p. 4867–4870.

[16] Iftikhar M, Singh HMP, Arifianto MS. Telecardiology for e-Diagnosis and e-Learning in Rural Area of Sabah, Malaysia: A Novel Approach for Cardiac Services in Rural Medicine. p. 83–88.

[17] Alqudah YA, AlQaralleh EA. A cloud based web analysis and reporting of vital signs. p. 185–189.

[18] Yuenyong S. Automatic heart sound analysis for tele-cardiac auscultation; 2009.

[19] Beck C. IEEE Xplore search - heart sounds in general; 2013.

[20] Beck C. Research on IEEE Xplore - stethoscopes in monitors; 2013.

[21] Grundlehner B. 2011 International Conference on Body Sensor Networks: Proceedings Dallas, Texas, 23-25 May 2011. Los Alamitos, Calif: IEEE Computer Society; 2011.

[22] McKee A, Goubran R. Sound Localization in the Human Thorax. p. 117–122.

[23] Geethu R, George SN, Kumar MK. A Proposal for Source Separation of Heartbeat Sounds and Its FPGA Implementation. p. 755–758.

[24] Khan AK, Onoue T, Hashiodani K, Fukumizu Y, Yamauchi H. Signal and noise separation in medical diagnostic system based on independent component analysis. p. 812–815.

[25] Malarvili M, Kamarulafizam I, Hussain S, Helmi D. Heart sound segmentation algorithm based on instantaneous energy of electrocardiogram. p. 327–330.

[26] McKee A, Goubran R. Beam shape, focus index, and localization error for performance evaluation of a multisensor stethoscope beamformer. p. 2062–2065.

[27] McKee A, Goubran R. Chest Sound Pick-Up Using a Multisensor Array. In: Sensors, 2005 IEEE. p. 780–783.

[28] Spadaccini A. Performance Evaluation of Heart Sounds Biometry Systems in an Open Dataset 2011:1–6.

[29] Ye X, Cai Q, Chen Y. Noninvasive detection of coronary artery disease based on heart sounds. p. 1546–1548.

[30] Ausen D. About BRIDGE; 2011. Available from: http://www.bridgeproject.eu/en/about-bridge.

[31] Horn G. Bridging Resources and Agencies in Large-Scale Emergency Management. Internet; 2011.

[32] Dag Ausen. Bridgeproject.eu; 2014. Available from: http://www.bridgeproject.eu.

[33] Dag Ausen. Bridgeproject.eu; 2014. Available from: http://www.bridgeproject.eu.

[34] Security Research Conference. Proceedings: 5th Security Research Conference, Berlin, September 7th - 9th, 2010. Stuttgart: Fraunhofer Verlag; 2010.

[35] Tia Gao, Massey T, Selavo L, Crawford D, Borrong Chen, Lorincz K, Shnayder V, Hauenstein L, Dabiri F, Jeng J, Chanmugam A, White D, Sarrafzadeh M, Welsh M. The Advanced Health and Disaster Aid Network: A Light-Weight Wireless Medical System for Triage. IEEE Trans. Biomed. Circuits Syst. 2007;1(3):203–16, doi:10.1109/TBCAS.2007.910901.

[36] Pantelopoulos A, Bourbakis NG. A Survey on Wearable Sensor-Based Systems for Health Monitoring and Prognosis. IEEE Trans. Syst., Man, Cybern. C 2010;40(1):1–12, doi:10.1109/TSMCC.2009.2032660.

[37] Sakanushi K, Hieda T, Shiraishi T, Ode Y, Takeuchi Y, Imai M, Higashino T, Tanaka H. Electronic Triage System: Casualties Monitoring System in the Disaster Scene. In: 2011 International Conference on P2P, Parallel, Grid, Cloud and Internet Computing. p. 317–322.

[38] M.Vishwanath Shervegar, Ganesh.V.Bhat,Raghavendra M Shetty K. Phonocardiography–the future of cardiac auscultation. International Journal of Scientific & Engineering Research 2011;2(10):1–12.

[39] Bravo-Zanoguera ME, Medrano ZY, Reyna-Carranza MA, Lopez-Avitia R, Arriola H. Simultaneous capture and display of electrocardiogram and multi-site phonocardiogram. In: 2009 Pan American Health Care Exchanges. p. 26–28.

[40] Chien JC, Tai C. A New Wireless-Type Physiological Signal Measuring System Using a PDA and the Bluetooth Technology. In: 2006 IEEE International Conference on Industrial Technology. p. 3026–3031.

[41] Baherkar L, Misal, Abhishek, Sinha, G.R. Heart Sound Segmentation Techniques: A Survey. In: OSR Journal of Electrical and Electronics Engineering. p. 46–49.

[42] Quiceno AF, Delgado E, Vallverd M, Matijasevic AM, Castellanos-Domnguez G. Effective phonocardiogram segmentation using nonlinear dynamic analysis and high-frequency decomposition. In: 2008 35th Annual Computers in Cardiology Conference. p. 161–164.

[43] Gupta CN, Palaniappan R, Swaminathan S. Classification of Homomorphic Segmented PhonocardiogramSignals Using Grow and Learn Network. In: Proceedings of the 2005 IEEE. p. 1–4.

[44] Liang H, Lukkarinen S, Hartimo I. Heart sound segmentation algorithm based on heart sound envelogram. In: Computers in Cardiology 1997. p. 105–108.

[45] Debbal SM, Bereksi-Reguig F. Time-frequency analysis of the first and the second heartbeat sounds. Applied Mathematics and Computation 2007;184(2):1041–52, doi:10.1016/j.amc.2006.07.005.

[46] Erne P. Beyond auscultation--acoustic cardiography in the diagnosis and assessment of cardiac disease. Swiss Med Wkly 2008;138(31-32):439–52.

[47] Robertson-Steel I. Evolution of triage systems. Emerg Med J 2006;23(2):154–55, doi:10.1136/emj.2005.030270.

[48] Blair J. Nikolai Ivanovich Pirogov (1810-1881). Journal of the Royal Army Medical Corps 2002;148(3):303, doi:10.1136/jramc-148-03-18.

[49] Weyrich P, Christ M, Celebi N, Riessen R. Triagesysteme in der Notaufnahme. Med Klin Intensivmed Notfmed 2012;107(1):67-78; quiz 79, doi:10.1007/s00063-011-0075-9.

[50] Lerner EB, Schwartz RB, Coule PL, Weinstein ES, Cone DC, Hunt RC, Sasser SM, Liu JM, Nudell NG, Wedmore IS, Hammond J, Bulger EM, Salomone JP, Sanddal TL, Markenson D, O'Connor RE. Mass casualty triage: an evaluation of the data and development of a proposed national guideline. Disaster Med Public Health Prep 2008;2 Suppl 1:S25-34, doi:10.1097/DMP.0b013e318182194e.

[51] Aghababian R. Essentials of emergency medicine. 2nd ed. Sudbury, Mass.: Jones and Bartlett Publishers; 2011.

[52] Schellein O, Ludwig-Pistor F, Bremerich DH. \"Manchester Triage System\". Prozessoptimierung in der interdisziplinären Notaufnahme. Anaesthesist 2009;58(2):163–70, doi:10.1007/s00101-008-1477-9.

[53] Telemedicine. What is telemedicine?; 2013. Available from: http://www.telemedicine.com/whatis.html.

[54] Paja WA, Wilamowski BM. 2013 6th International Conference on Human System Interactions (HSI): June 06-08, 2013, Gdańsk, Sopot, Poland.

[55] La Torre I de, Martinez B, Lopez-Coronado M. A review of applications for the improvement of the life quality in patients with mental disorders. In: 2013 IEEE 15th International Conference on e-Health Networking, Applications and Services (Healthcom 2013). p. 182–187.

[56] Smith Welsh T. ORGANIZATIONAL STRUCTURE OF TELEHEALTH CARE: AN EXAMINATION OF FOUR TYPES OF TELEMEDICINE SYSTEMS. University of Tennessee, Knoxville, Tennessee; 2002.

[57] Beck C. General discussion about ECG, pulse oximetry, auscultation, heart failure, heart insufficiency and modalities how to combine acquired vital signs for advantageous analysis. Phone; 2014.

[58] Beck C. Questionnaire referring to auscultating the lung. Strategy and Effort; 2011.

[59] Wartak J. Phonocardiology; integrated study of heart sounds and murmurs. 1st ed. Hagerstown, Md: Medical Dept., Harper & Row; 1972.

[60] Gahl K, Holldack K. Auskultation und Perkussion: Inspektion und Palpation ; [inklusive CD mit Auskultationsbeispielen]. Stuttgart [u.a.]: Thieme.

[61] Beck C. Research on IEEE Xplore - heart sound algorithms; 2014.

[62] National Heart, Lung, and Blood Institute. Your Heart's Electrical System; 2011. Available from: http://www.nhlbi.nih.gov/health/health-topics/topics/hhw/electrical.html.

[63] National Heart, Lung, and Blood Institute. What Is an Electrocardiogram?; 2011. Available from: http://www.nhlbi.nih.gov/health/health-topics/topics/ekg/.

[64] Rockmann F. Taschenbuch Monitoring Intensivmedizin. 2nd ed. Berlin: MWV Medizinisch Wissenschaftliche Verlagsgesellschaft; 2011.

[65] Carr JJ, Brown JM. Introduction to biomedical equipment technology. 4th ed. Upper Saddle River, N.J.: Prentice Hall; 2001.

[66] Corscience. Technical Integration Instruction for EMB1, EMB3/6. Erlangen, Germany; 2011.

[67] Webster JG. Design of pulse oximeters. Medical science series. Bristol, Philadelphia: Institute of Physics Pub; 1997.

[68] Webster JG, Clark JW. Medical instrumentation: Application and design. 4th ed. Hoboken, NJ: John Wiley & Sons; 2010.

[69] Corscience. Technical Integration Instruction for digital pulse oximeter module ChipOX. Erlangen, Germany; 2010.

[70] Harvard Health Publications. Normal Body Temperature Rethinking the normal human body temperature; 2006. Available from: http://www.health.harvard.edu/press_releases/normal_body_temperature.

[71] WebMD. First Aid & Emergencies - Body Temperature; 2013. Available from:

http://www.webmd.com/first-aid/body-temperature.

[72] Corscience GmbH & Co. KG. Miniature OEM module for blood pressure measurement - NiBP2010 5V. 60095th ed. Internet; 2010.

[73] PR Newswire. FDA Clears New Continuous Blood Pressure Technology From Sotera Wireless. San Diego: PR Newswire; 2013.

[74] Safara F, Doraisamy S, Azman A, Jantan A, Abdullah Ramaiah, Asri Ranga. Multi-level basis selection of wavelet packet decomposition tree for heart sound classification. Computers in biology and medicine 2013;43(10):1407–14, doi:10.1016/j.compbiomed.2013.06.016.

[75] Shashikiran. Respiratory Auscultation; 2010. Available from: http://www.mediscuss.org/respiratory-auscultation-tips-audio-mp3-examples-71.html.

[76] NIH. Picture of the thorax. Available from: http://www.nlm.nih.gov/research/visible/image/thorax.jpg.

[77] Onmeda. Bronchoskopie; 2013. Available from: http://www.onmeda.de/arztbesuch/untersuchung_behandlung/lungenspiegelung.html.

[78] Phonocardiograph System Overview; 2010. Available from: http://www.stethographics.com/main/products_phono.html.

[79] Gavriely N, Palti Y, Alroy G. Spectral characteristics of normal breath sounds. Journal of applied physiology: respiratory, environmental and exercise physiology 1981;50(2):307–14.

[80] Pasterkamp H, Kraman SS, Wodicka GR. Respiratory sounds. Advances beyond the stethoscope. American journal of respiratory and critical care medicine 1997;156(3 Pt 1):974–87, doi:10.1164/ajrccm.156.3.9701115.

[81] Littman. Stethoscope 3200 Instruction Manual; 2009.

[82] DIN EN. DIN EN 13402. 3rd ed;13402(13402). Internet: Beuth.de; 2014. Available from: http://www.beuth.de/de/norm/din-en-13402-3/179167681.

[83] National Physics Laboratory. Technical Guides - Speed of Sound in Sea-Water. Available from: http://resource.npl.co.uk/acoustics/techguides/soundseawater/.

[84] Pohlmann KC. Principles of digital audio. 6th ed. Digital video/audio. New York: McGraw-Hill; 2011.

[85] Lee EA. Structure and interpretation of signals and systems. 2nd ed. [S.l.]: LeeVaraiya.org; 2011.

[86] Maxfield C. FPGAs. Amsterdam, Boston: Newnes/Elsevier; 2009.

[87] Seeber B. Handbook of applied superconductivity. Bristol: Institute of Physics Publishing; 1998.

[88] Bin Le, Rondeau TW, Reed JH, Bostian CW. Analog-to-digital converters. IEEE Signal Process. Mag. 2005;22(6):69–77, doi:10.1109/MSP.2005.1550190.

[89] de la Rosa, José M. Sigma-Delta Modulators: Tutorial Overview, Design Guide, and State-of-the-Art Survey. IEEE Trans. Circuits Syst. I 2011;58(1):1–21, doi:10.1109/TCSI.2010.2097652.

[90] Peter Bishop. A tradeoff between microcontroller, DSP, FPGA and ASIC technologies; 2009. Available from: http://www.eetimes.com/document.asp?doc_id=1275272.

[91] Flik T. Mikroprozessortechnik: CISC, RISC, Systemaufbau, Assembler und C. 6th ed. Berlin [u.a.]: Springer; 2001.

[92] Xilinx Inc. Applications. Available from: http://www.xilinx.com/applications.html.

[93] Frank Riemenschneider. Xilinx erhöht Profitabilität; 2014. Available from: http://www.elektroniknet.de/halbleiter/programmierbare-logik/artikel/113694/.

[94] Xilinx, editor. xCell - The quaterly journal for Xilinx programmble logic users, 1. Internet: Xilinx; 1998.

[95] Xilinx. Spartan-6 Family Overview. 160th ed. Internet; 2011.

[96] Texas Instruments. User Guide - A Single-Chip Li-Ion and Li-Polymer Charge Management IC; 2010.

[97] Buchmann I. Battery University; 2003. Available from: http://batteryuniversity.com/.

[98] Texas Instruments. TPS65708 - PMU for Embedded Camera Module. www.ti.com; 2011.

[99] Murata Electronics. SN820X Wi-Fi Network Controller - Module Family Data Sheet. 2nd ed. Kyoto, Japan; 2013.

[100] Murata Electronics. SN820X Wi-Fi Network Controller - Module Family User Manual. 2nd ed. Kyoto, Japan; 2013.

[101] Beck C. Schematics; 2013.

[102] Beck C. Source code for MCU embedded application: 20141101_VHDL_Sources_ASArevA_01.zip; 2014.

[103] Xilinx. Xilinx ISE Design Suite: Xilinx; 2013.

[104] Xilinx. ISE Design Suite Help. Software Manual; 2013.

[105] ISO, IEC. Information technology - Open Systems Interconnection. 1st ed.(ISO/IEC 7498-1). Internet: EMAC Interantional; 1994. Available from: http://www.ecma-international.org/.

[106] Kbrose, Guy Harris, Dgtsyb. OSI model; 2014. Available from: http://en.wikipedia.org/wiki/OSI_model.

[107] TDK. Chip Beads for power line - MPZseries; 2013.

[108] Texas Instruments. ULTRALOW-NOISE, HIGH-PSRR, FAST RF 200-mA LOW-DROPOUT LINEAR REGULATORS; 2013.

[109] Beck C. D5.10.3 Presentation - Accident and Emergency Center Intelligent Monitoring System. Nicosia, Cyprus; 2013.

[110] USB.org. USB 2.0 Specification. Internet: USB.org; 2000. Available from: http://www.usb.org/developers/docs/usb20_docs/#usb20spec.

[111] Beck C. Test Record - Test Setup and Startup Routine. 1st ed; 2014.

[112] Palaniappan R, Sundaraj K, Sundaraj S. A comparative study of the SVM and K-nn machine learning algorithms for the diagnosis of respiratory pathologies using pulmonary acoustic signals. BMC bioinformatics 2014;15:223, doi:10.1186/1471-2105-15-223.

[113] Gurung A, Scrafford CG, Tielsch JM, Levine OS, Checkley W. Computerized lung sound analysis as diagnostic aid for the detection of abnormal lung sounds: a systematic review and meta-analysis. Respiratory medicine 2011;105(9):1396–403, doi:10.1016/j.rmed.2011.05.007.

[114] Stöcker H. Taschenbuch der Physik: Formeln, Tabellen, Übersichten. 4th ed. Thun, Frankfurt am Main: Deutsch; 2000.

[115] Subcommittee 62A. EN IEC 60601-1;CEI/IEC 60601-1:2005(3). Internet: www.beuth.de; 2005.

[116] Beck C. Test Record - Human vital sign acquisition; 2014.

[117] Julian P, Andreou AG, Riddle L, Shamma S, Goldberg DH, Cauwenberghs G. A Comparative Study of Sound Localization Algorithms for Energy Aware Sensor Network Nodes. IEEE Trans. Circuits Syst. I 2004;51(4):640–48, doi:10.1109/TCSI.2004.826205.

[118] Andreou A, Cauwenberghs G, West J, Stanacevic M, Celik A, Julian P, Teixeira T. A Miniature, Low-Power, Intelligent Sensor Node for Persistent Acoustic Surveillance. Proceedings of the SPIE 2005;5796:294–305.

[119] Julian P, Andreou AG, Goldberg DH. A low-power correlation-derivative CMOS VLSI circuit for bearing estimation. IEEE Trans. VLSI Syst. 2006;14(2):207–12, doi:10.1109/TVLSI.2005.863740.

[120] Pirchio FNM, Sañudo S, Gutierrez H, Julián P. AN ACOUSTIC SURVEILLANCE UNIT FOR ENERGY AWARE SENSOR AN ACOUSTIC SURVEILLANCE UNIT FOR ENERGY AWARE SENSOR. XII Taller IBERCHIP 2006;12:1–6.

[121] Chacon-Rodriguez A, Martin-Pirchio F, Sanudo S, Julian P. A Low-Power Integrated Circuit for Interaural Time Delay Estimation Without Delay Lines. IEEE Trans. Circuits Syst. II 2009;56(7):575–79, doi:10.1109/TCSII.2009.2023281.

[122] Masson F, Puschini D, Julian P, Crocce P, Arlenghi L, Mandolesi PS, Andreou AG. Hybrid Sensor Network And Fusion Algorithm For

Sound Source Localization. In: 2005 IEEE International Symposium on Circuits and Systems. p. 2763–2766.

[123] Zhang Z, Andreou AG. Slow Moving Vehicles Using the Microphone Arrays in the Hopkins Acoustic Surveillance Unit: Close Range Bearing Estimation and Tracking. Argentine School of Micro-Nanoelectronics, Technology and Application 2008(EAMTA 2008):140–43.

[124] ORPONEN P. Computational complexity of neural networks: a survey. Nordic J. of Computing 1994;1(1):94–110.

[125] Goutte C. Some computational complexity aspects of neural network training 1996:1–3.

[126] Benichoux V, Stimberg M, Fontaine B, Brette R. A unifying theory of ITD-based sound azimuth localization at the behavioral and neural levels. BMC Neurosci 2013;14(Suppl 1):P39, doi:10.1186/1471-2202-14-S1-P39.

[127] van Schaik A, Shamma S. A neuromorphic sound localizer for a smart MEMS system. In: ISCAS 2003. International Symposium on Circuits and Systems. p. IV-864.

[128] van Schaik A, Shamma S. A Neuromorphic Sound Localizer for a Smart MEMS System. Analog Integrated Circuits and Signal Processing 2004;39(3):267–73, doi:10.1023/B:ALOG.0000029662.37528.c7.

[129] Sturzl W, Kempter R, van Hemmen, J L. Theory of arachnid prey localization. Phys Rev Lett 2000;84(24):5668–71.

[130] Brownell P, Farley RD. Prey-localizing behaviour of the noc-turnal desert scorpion, paruroctonus mesaensis: Orientation to substrate vibrations. Animal Behaviour 1979;27(27):185–93.

[131] Goodman D. Brian: a simulator for spiking neural networks in Python. Front. Neuroinform. 2008;2, doi:10.3389/neuro.11.005.2008.

[132] Brette R, Goodman D. Brian: a simple and flexible simulator for spiking neural networks. Institute of Neuromorphic Engineering (INE) 2009;July:1–2.

[133] Carvalho Pd. HeartSafe: Assessing Heart Function for Unsupervised Homecare Applications through Multi-Channel Auscultation; 2013. Available from: https://www.cisuc.uc.pt/projects/show/152.

[134] Beck C. heartSoundAnalysis.m. MATLAB script: Beck, Christoph.

[135] Beck C. Test record - S1 identification based on ECG r-peak vector; 2015.

7 Appendix A – Publications

The following publications are planned in relation to this project:

1. System Design and Implementation (submitted, in review)
   Journal: Emerald – Disaster Prevention and Management
2. A body-worn multi-parameter monitoring platform for human vital signs acquisition (accepted)
   Conference: MEDICON 2016
3. A Wearable, Multimodal, Vitals Acquisition Unit for Intelligent Field Triage (accepted)
   Conference: ISCAS 2016
4. Sound Source Localization Through 8 MEMS Microphones Array Using a Sand-Scorpion Inspired Spiking Neural Network (submitted, in review)
   Journal: Frontiers - Neuroscience, section Neuromorphic Engineering
5. Open database with synchronized human vital signs of ten healthy male subjects (pending)
   Society contribution: PhysioBank at Physionet.org
6. Medical value of a multi-parameter emergency monitoring system including body sounds (pending)
   Journal: TBIOCAS

8 Appendix B – Schematics

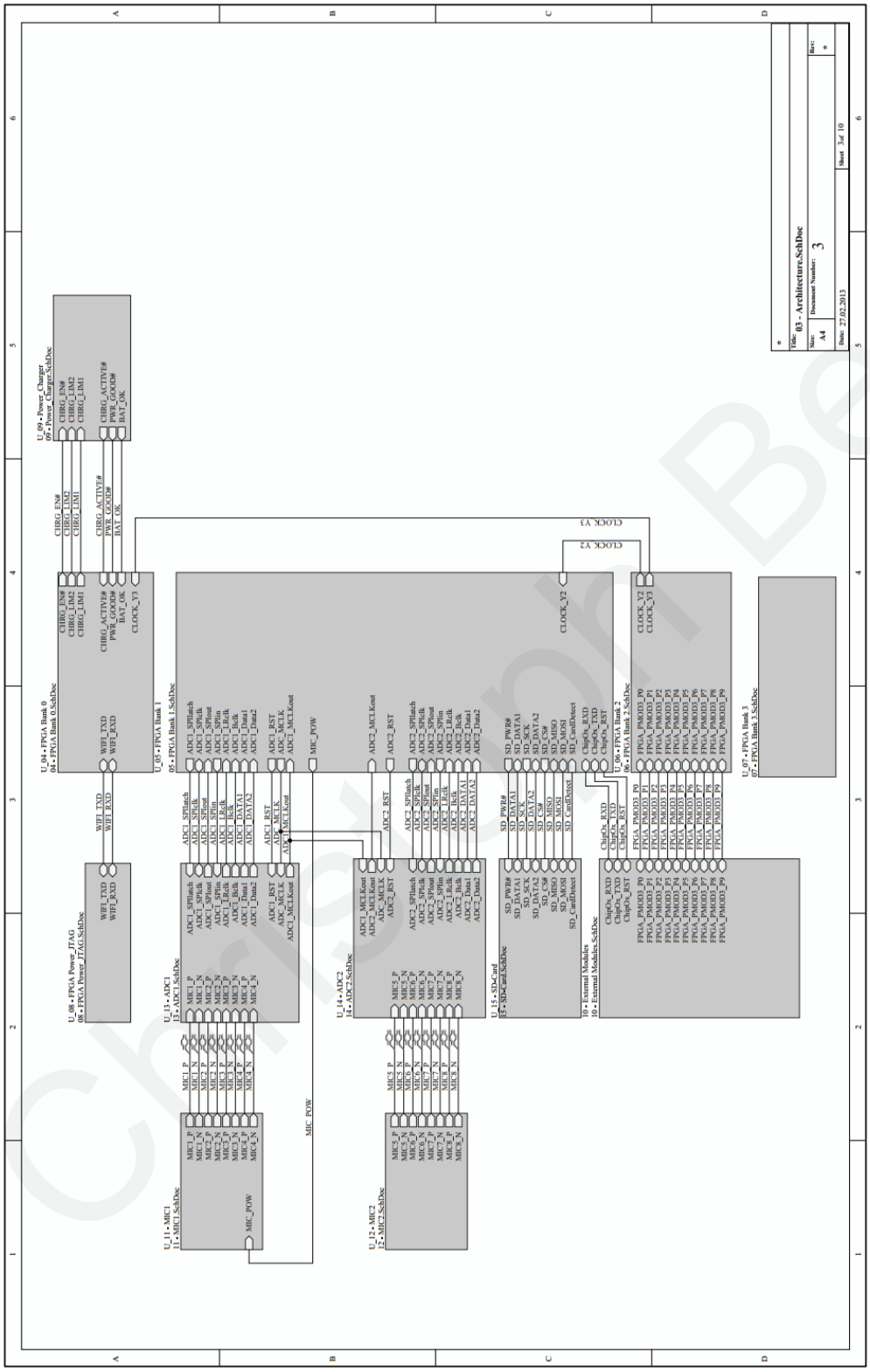

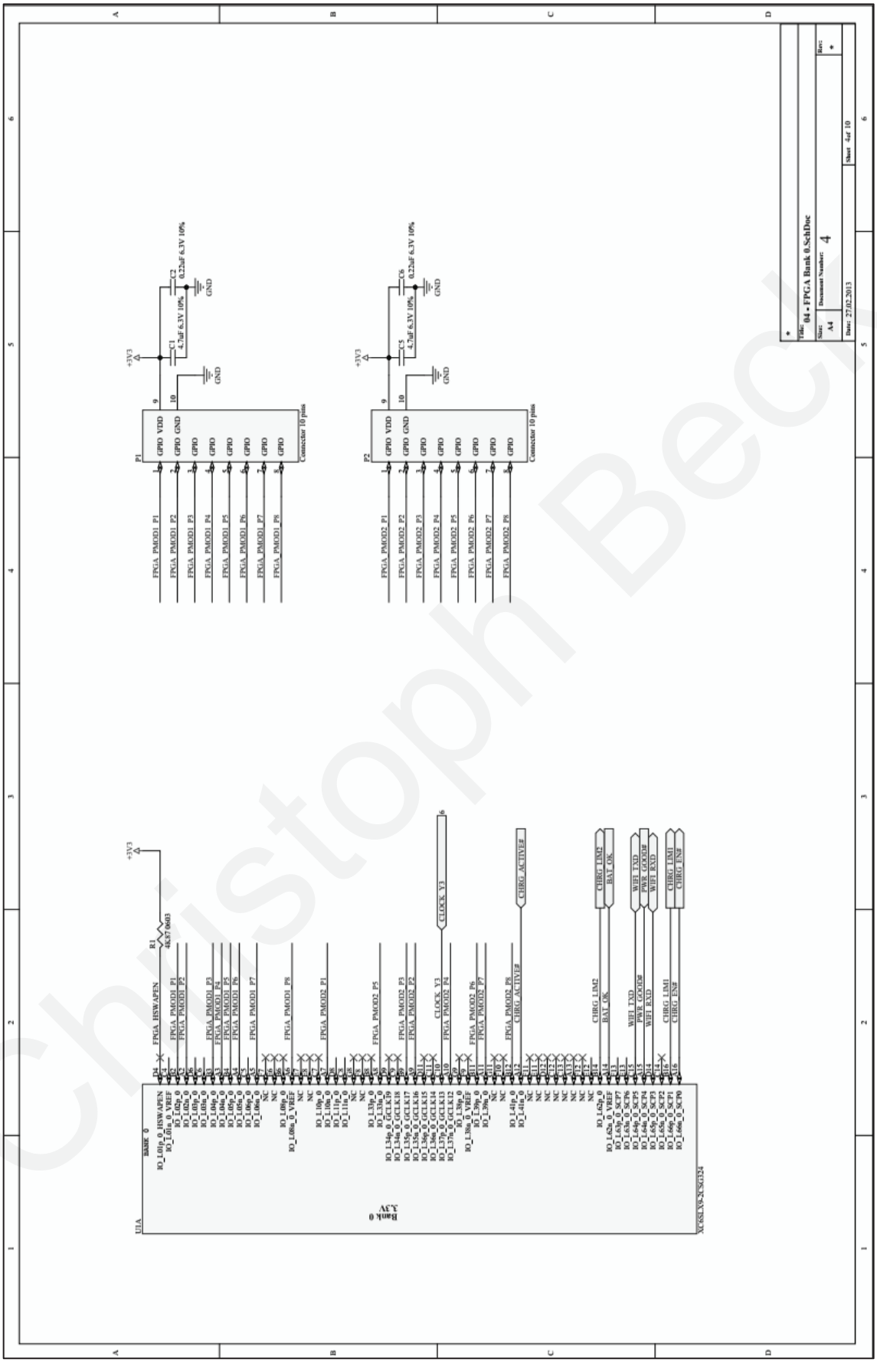

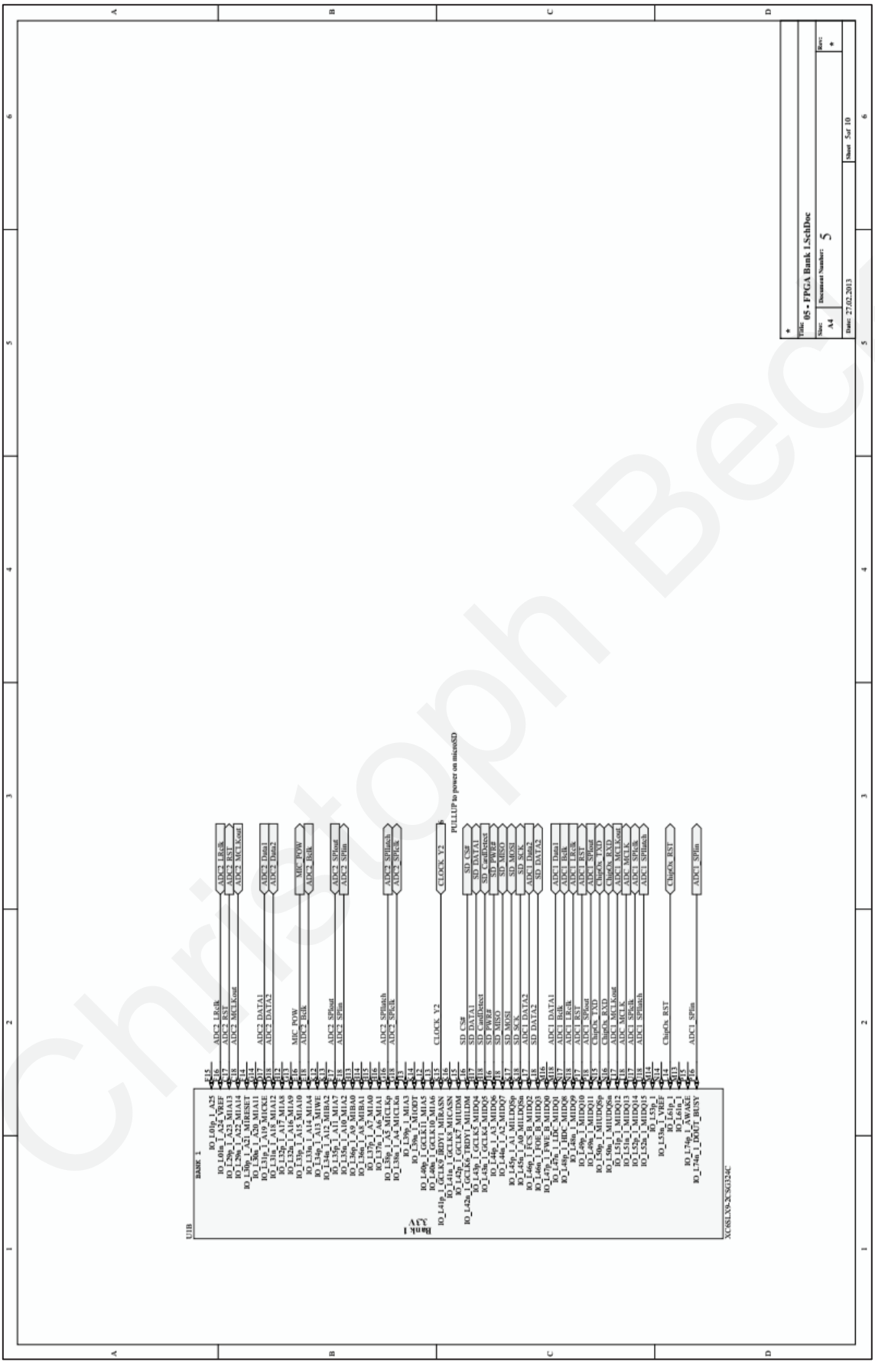

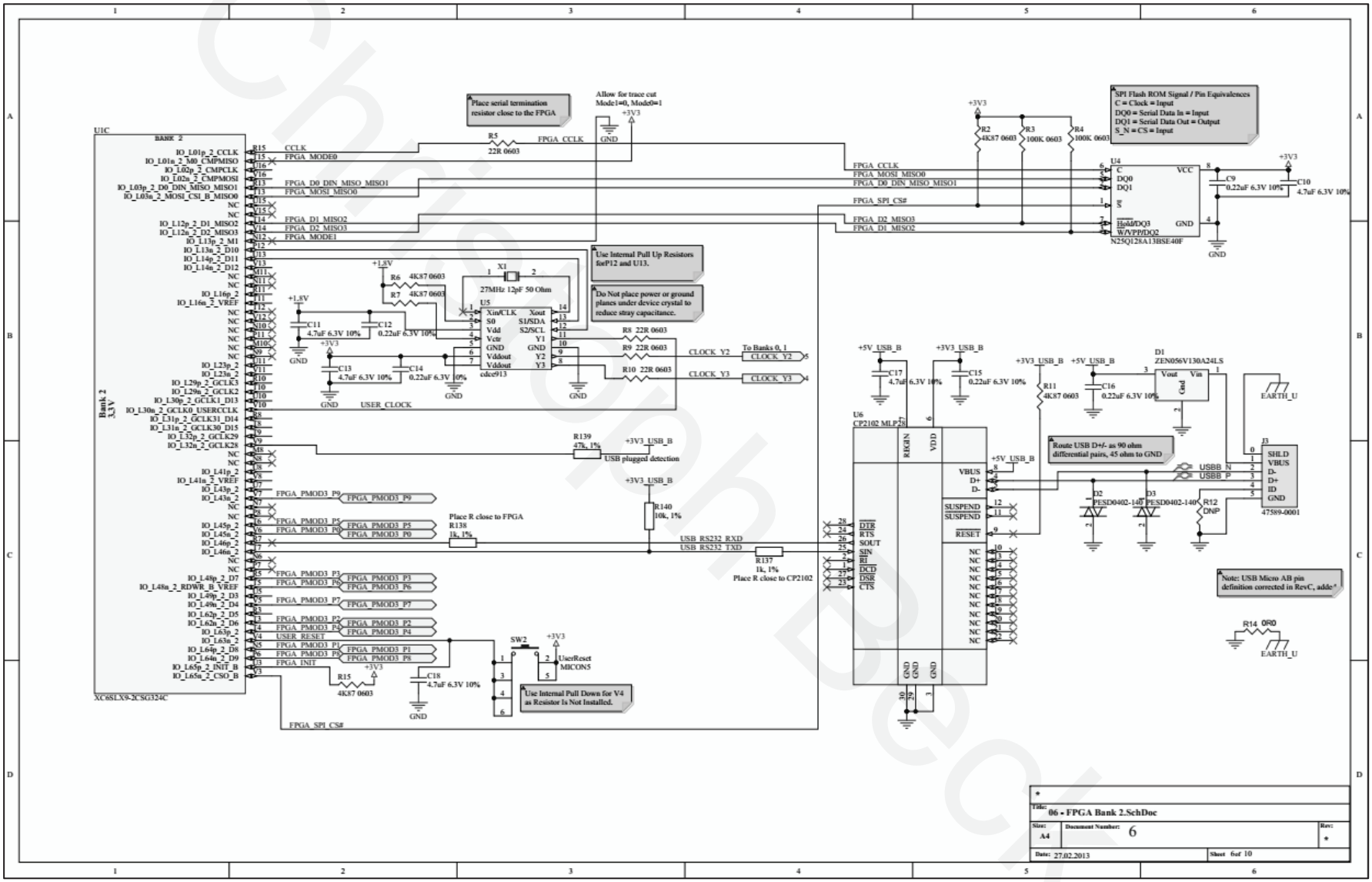
Place serial termination resistor close to the FPGA
Allow for trace cut Mode1=0, Mode0=1
SPI Flash ROM Signal / Pin Equivalences
C = Clock = Input
DQ0 = Serial Data In = Input
DQ1 = Serial Data Out = Output
S_N = CS = Input
Use Internal Pull Up Resistors forP12 and U13.
Do Not place power or ground planes under device crystal to reduce stray capacitance.
Route USB D+/- as 90 ohm differential pairs, 45 ohm to GND
Note: USB Micro AB pin definition corrected in RevC, adde
Use Internal Pull Down for V4 as Resistor Is Not Installed.
USB plugged detection
Place R close to FPGA
Place R close to CP2102
To Banks 0, 1
N25Q128A13BSE40F
CP2102 MLP28
XC6SLX9-2CSG324C
06 - FPGA Bank 2.SchDoc
Document Number: 6
Date: 27.02.2013
Sheet 6of 10